LEVEL III ①

STREAM CHANNEL STABILITY

APPENDIX I

SINGLE EVENT NUMERICAL MODEL FOR ROUTING WATER AND SEDIMENT ON SMALL CATCHMENTS

Project Objective 4

by

D. K. Borah, C. V. Alonso
and S. N. Prasad

USDA Sedimentation Laboratory
Oxford, Mississippi

April 1981

Prepared for
US Army Corps of Engineers, Vicksburg District
Vicksburg, Mississippi

Under
Section 32 Program, Work Unit 7

DTIC
SELECTED
JUL 1 5 1981
H

81 7 14 098

STREAM CHANNEL STABILITY.

APPENDIX I.

SINGLE EVENT NUMERICAL MODEL FOR ROUTING WATER

AND SEDIMENT ON SMALL CATCHMENTS

Project Objective 4

by

D. K. Borah[1], C. V. Alonso[2], and S. N. Prasad[3]

USDA Sedimentation Laboratory

Oxford, Mississippi

April 1981

Prepared for

US Army Corps of Engineers, Vicksburg District
Vicksburg, Mississippi

Under

Section 32 Program, Work Unit 7

[1] Research Associate, Department of Civil Engineering, The University of Mississippi, University, MS.

[2] Research Hydraulic Engineer, Sediment Transport and Deposition Research Unit, USDA Sedimentation Laboratory, Oxford, MS.

[3] Professor, Department of Civil Engineering, The University of Mississippi, University, MS.

PREFACE

The main objective of this study is to develop a numerical model for routing water and sediment on small agricultural catchments. Part 2 of this report presents a detailed description of the model. The model is developed on a general basis so that it may be applied to any agricultural catchment, and it can be used to simulate the effect of different land uses on the water and sediment yields from the modeled catchment. Part 3 presents results from validations of the model using several data sets including data from natural catchments. Input data and computer coding details are given in the Addendum to this report.
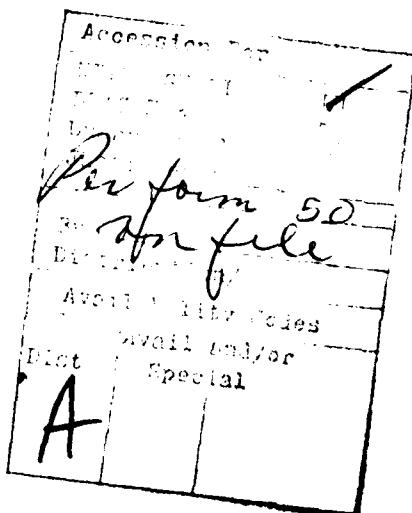
TABLE OF CONTENTS

LIST OF TABLES

LIST OF FIGURES

U.S. CUSTOMARY TO S.I.-UNITS CONVERSION FACTORS

To convert	To	Multiply by
inches (in.)	millimeters (mm)	25.4
feet (ft)	meters (m)	0.305
yards (yd)	meters (m)	0.914
miles (miles)	kilometers (km)	1.61
square inches (sq. in.)	square millimeters (mm^2)	645
square feet (sq ft)	square meters (m^2)	0.093
square yards (sq yd)	square meters (m^2)	0.836
square miles (sq miles)	square kilometers (km^2)	2.59
acres (acre)	hectares (ha)	0.405
cubic inches (cu in.)	cubic millimeters (mm^2)	16,400
cubic feet (cu ft)	cubic meters (m^3)	0.028
cubic yards (cu yd)	cubic meters (m^3)	0.765
pounds (lb) mass	kilograms (kg)	0.453
tons (ton) mass	kilograms (kg)	907
pound force (lbf)	newtons (N)	4.45
kilogram force (kgf)	newtons (N)	9.81
pounds per square foot (psf)	pascals (Pa)	47.9
pounds per square inch (psi)	kilopascals (kPa)	6.89
U.S. gallons (gal)	liters (L)	3.79
acre-feet (acre-ft)	cubic meters (m^3)	1,233

1   INTRODUCTION

Alluvial streams are dynamic systems that continuously change their configuration and state in response to either changes in the natural environment, or perturbations introduced by man's activity. Frequently, these changes conduce to alteration of the stream-channel stability, which often results in channel migration and shoaling.

Among the leading causes of channel instability are several that are intimately associated with land-management and conservation practices carried out on the upland areas. They are (a) clearing of land that removes the soil-protective and flow-retardant ground cover, which in turn leads to increased erosion and flood peaks; (b) installation of reservoirs for flood protection and irrigation control, which upset the water-sediment equilibrium downstream of those structures; and (c) excessive soil erosion resulting from uncontrolled sources. The combined effect is an aggregate flow of water and sediment coming from a variety of point and non-point sources within the upstream catchments. This aggregate yield acts as a time and space dependent loading on the streams draining the catchments. If this loading becomes quite different from that which the streams have adjusted to, the result is a breakdown in the stability of the channel system.

The catchments contributing to the loading of any given channel system exhibit in general a great variety of soils, vegetation, and land uses. In order to effectively assess the impact of these catchments on the loading of the channel system, it is necessary to develop improved methods for predicting the effects of alternative land managements of those catchments. There is, therefore, a need for the development of mathematical models so that the hydrology of a catchment can be simulated and the effects of various management practices understood and predicted. In response to this need, the goal of the present study is the development of a prediction model for estimating sediment yield from agricultural catchments. In developing the model, the following specific objectives were considered: (i) estimate the amount of soil loss from specified soil-source units with homogeneous characteristics; (ii) estimate the amount of water and sediment transported out of the catchments through the principal drainage networks; and (iii) estimate the rate of channel aggradation and degradation along the flow system. The model is oriented towards the needs of the Corps of

Engineers for better means of assessing the impact of land-management practices on stream channel behavior.

Many hundreds of papers have been written concerning studies on various aspects of hydrology. For this reason it is quite impossible to summarize the previous work that has led to the current understanding of the hydrologic cycle. Reference can be made to some of the existing comprehensive hydrology books (i.e., Chow, 1964), and to a number of American Society of Agronomy Monographs (Luthin, 1957; Van Shilfgaarde, 1974; Hagan, Haise and Edminster, 1967) and reports (Pierre et al., 1966; Neilsen, Jackson, Cary, and Evans, 1972) that discuss current knowledge of soil-water-plant system. Excellent reviews of the progress made during recent years in several hydrologic subjects have been presented by Schaake (1975), Amerman et al. (1975), Johnson and Meyer (1975), and Nordin (1975). Only because of this accumulated knowledge is the proposed project even feasible. As a better understanding of the hydrologic cycle and the basic physical laws governing it have evolved, they have been synthesized into more rational and physically based models. Finally, the accessibility to high-speed digital computers has made possible the development of detailed comprehensive hydrologic models.

Because the physical processes governing catchment behavior are very complicated, many past studies have utilized regression models. However, it is difficult to predict the response of a catchment to different land-management activities using regressional methods, because these methods are based on the assumption of time and space invariability. This assumption almost always fails to be valid in the case of natural catchments.

A second type of models includes lumped parametric simulation methods, such as the TVA Continuous Daily-Streamflow Model (TVA, 1972). These models simulate the response of a given catchment by adjusting a number of coefficients, with little physical significance, using data collected under certain environmental conditions. The impossibility of relating those coefficients to a different set of environmental conditions, seriously restrict the use of these models for predicting the response of ungaged catchments.

A different class of models embodies the distributed process simulation methods. These techniques use mathematical descriptions of the

basic hydrologic processes being modeled, and their interaction. In addition, this approach tends to minimize the number of adjustable parameters and, whenever possible, relates them to physical quantities that can be readily measured in the field.

The Stanford model (Crawford and Linsley, 1966) was one of the first general models developed to simulate runoff from a catchment. It is basically a lumped-parameter model, although large, heterogeneous catchments can be subdivided into subcatchments if sufficient data are available to define model parameters. The model has gained widespread use and as a result has undergone numerous modifications. Holtan and Lopez (1970) have described the USDAHL-70 model of catchment hydrology. Although this model is basically lumped, a heterogeneous catchment can be broken down into smaller homogeneous areas. An attempt is made to incorporate spatial variability by dividing the catchment into land capabilities classes that correspond to uplands, hillslopes, and bottom lands. Dawdy et al. (1972) reported on a lumped-system model similar to the Stanford model which describes surface runoff from small catchments. TVA (1972) recently described a lumped daily-streamflow model with sixteen parameters, five of which require optimization. This model has been reasonably successful in predicting daily streamflows.

A continuous distributed model is not yet available. However, several single-event distributed models that include part of the hydrologic cycle have been introduced since the pioneering works of Wooding (1965) and Woolhiser and Liggett (1967). Since then, a cascade of various sizes and slopes (Brakensiek, 1967; Kibbler and Woolhiser, 1970) or converging inverted cone-shaped surfaces (Woolhiser, 1969) have been used for geometric representation of complex topographies. The works of these and other investigators have let to the acceptance of the kinematic-wave approximation as an adequate model of shallow overland flow and flow in channels. The reductionist approach to watershed simulation was introduced by Huggins and Monke (1970). They employed a square grid for decomposing a complex catchment into elemental surface units. Most physically-based overland flow models used simplified lumped-system infiltration models. Smith and Woolhiser (1971) were the first to introduce a distributed infiltration model, derived from soil moisture flow theory, to calculate point infiltration rate, and therefore rainfall excess rate. The foregoing

concepts have been incorporated, in one way or another, into more detailed models recently reported by Simons et al. (1975) and Smith (1976). These models use flow routing techniques based on the kinematic-wave approximation of the flow governing equations. Since its formulation by Lighthill and Whitham (1955), the kinematic wave approximation has received extensive application to catchment runoff modeling. This approximation is restricted by the assumption that the friction slope equals the stream bed slope, but it has been found to be applicable in many stream flows and in most overland flow situations. In addition, the kinematic-wave formulation admits an analytical solution by the method of characteristics (Eagleson, 1970; Kibler and Woolhiser, 1970; Li et al., 1975b; Singh, 1975). This analytical solution has two main advantages over other numerical solutions. It eliminates the wave-celerity-damping and phase lag usually induced by numerical schemes; and, in addition, results in faster computational procedures. In spite of these advantages, applications of this analytical solution have been restricted in the past to catchment models with a high degree of geometric abstraction. The reason is the formation of kinematic shock waves (Lighthill and Whitham, 1955; Kibler and Woolhiser, 1970; Harley et al., 1970; Whitham, 1974). Formally, innumerable shock waves can be generated during the routing process, as a result of the time and spatial discretization of precipitation and the physical characteristics of the catchment. In the past, the existence of these shocks has frequently been ignored by using approximate numerical techniques. This practice, however, may not be considered as valid particularly when the foundation and the physical relevance of the kinematic wave approximation is under investigation. It is well known that shock formation is intrinsic to the hyperbolic equation governing kinematic theory. Further, they are considered to be the manifestations of higher order effects such as formation of monoclinal flood waves, bores, etc. These discontinuities play important roles in the dynamics of hydraulic systems and an ad hoc smoothing by numerical means does not necessarily make the theory look better. The model described in the present report introduces a new solution to the kinematic approximation, which retains the dynamic effects of the shocks by routing the discontinuities as they appear. Certain simplifying assumptions are made which permit closed form solutions and an efficient numerical algorithm, based on the method of characteristics. The

I.9

resulting procedure, called an approximate shock fitting scheme, preserves the effect of the shocks without the usual computational complications and compares favorably with existing finite difference solutions (Borah et. al., 1980).

Different types of sediment production models have appeared widely dispersed in the technical literature. Reference can be made to a recent review presented by Heinemann and Piest (1975) and to a publication of the Agricultural Research Service (1975). Several regression equations for predicting gross soil erosion have been proposed. The most commonly used among these is the so-called universal soil loss equation (USLE) proposed by Wischmeier and Smith (1965). Other equations of similar nature have been developed by Musgrave (1947), and Gottschalk and Brune (1950). In these equations, the soil loss rate is correlated with storm, land, and vegetation characteristics. Such equations are applicable on seasonal basis or longer. Also, they do not take advantage of the physical processes occurring within the catchments; hence, it is not possible to use them on large, complex basins. Williams (1972) modified the USLE to make it applicable for predicting storm sediment yields. Onstad and Foster (1975) combined a different modification of the USLE with the USDAHL-70 catchment model to predict sediment yield for single storms. They applied their model to two small catchments with limited success.

The first physically-based sediment yield model was reported by Negev (1967). This model uses the Stanford model for the water phase, and takes into consideration rainfall soil splash, entrainment by overland flow, and rilling and gullying, along with separate channel transport of fine and coarse sediment. Sediment production is evaluated in terms of power functions of water discharge containing a number of parameters that must be calibrated. A modified version of Negev's model has been incorporated in the Agricultural Runoff Management (ARM) model recently reported by Donigian and Crawford (1976). The aforementioned models of Simons et al. (1975) and Smith (1976) also incorporate the capability of describing sediment movement on a catchment as a time and space distributed process. The structures of these two models are similar; however, there are differences in numerical techniques and functional relationships. The sediment movement is described by linking the excess-rainfall flow equations to the sediment continuity equation, with relations describing

I.10

sediment detachment and transport capacity at any point on the surface or in a channel. A similar structure has been incorporated in the erosion and sedimentation component of the present model. In addition, sediment is routed using a sediment characteristic scheme that takes advantage of the efficient analytical solution mentioned above.

Part 2 of this report provides a detailed description of the model. Part 3 discusses the validation of the model on sets of laboratory and field data. Input data and coding details are given in Addendum 1. This report is based on material presented in an earlier study by Borah (1979).

The model basically consists of two intertwined models: one describing the hydrology of the basin; the other describing the associated erosion and sedimentation processes. It simulates the movement of water and sediment as a time and space distributed process, and it has the ability of distinguishing between overland and channel flows. The catchment is regarded as consisting of a mosaic of individual subcatchments interconnected by channel reaches. The model can thus be regarded as a cascading process in which the output of one or more subcatchments becomes the input to another subcatchment or channel reach. In mimicking the overland movement of water and sediment, the model simulates processes of interception, infiltration, runoff, detachment, transport, and deposition of sediment. The water and sediment reaching the streams are then routed through the channel system, and the rates of channel aggradation and degradation are computed. The basic structure of the model is graphically illustrated in Fig. 1. The details of the model components are given in the following sections. The applicability of the model is restricted to catchments where the streamflows are ephemeral, the subsurface flow and ground water movement are not significant, and the kinematic wave approximation for flow routing is valid. The computer program has been written assuming a uniform distribution of rainfall. However, the program can be easily modified to accomodate any other aerial rainfall distribution.

The catchment is segmented into subcatchment and channel reaches to account for the lack of uniformity in terrain, soil, and land use characteristics in most natural catchments. Within each of the segments these characteristics are treated as being uniform. The subcatchments are replaced by sloping rectangular areas with representative length, slope, width, soil, and vegetative characteristics. The channel segments are described by representative cross-sectional shape, slope, length, and roughness. Gravity flow logic is used to determine the computational sequence as explained in Appendix 1. The input data required by the model includes storm characteristics, geometry data, vegetative cover data, soil data, and water and sediment routing data. Details on input data preparation are given in Addendum 1.
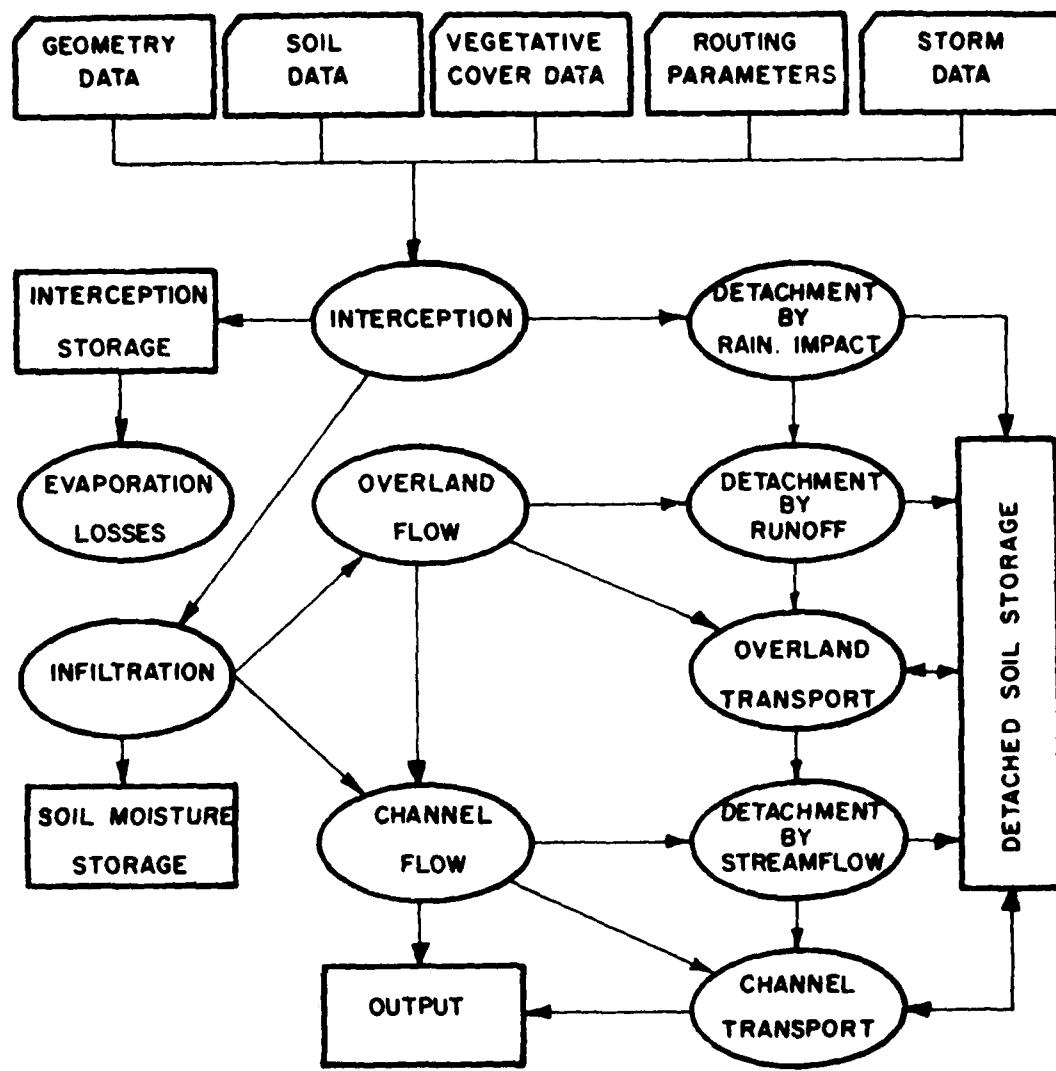
Fig. 1. Structure of the model

I.13

2.1   INTERCEPTION. NET RAINFALL RATE

The rainfall excess is the rainfall contributing to the water flowing over the surface of an overland unit. This is the resultant *rainfall after* incurring the losses due to interception, evaporation, transpiration and infiltration. At the beginning of a rainfall event, some rainfall is lost due to interception at the canopy and ground covers and thus interception is the first concern in computing rainfall excess. The interception component adopted in this model is based upon the approach proposed by Simons, et al. (1975).

The canopy cover and the ground cover are the two major features which influence the motion of raindrops before reaching the ground surface. The canopy cover and the ground cover are represented by the canopy cover density and the ground cover density, respectively. The canopy cover density, D_c, is defined as the ratio of the area covered by trees to the total area, and the ground cover density, D_g, is the ratio of the ground area covered with litter, rock, grass, etc., to the total area. The canopy cover and the ground cover densities are assumed uniform on a flow unit.

Net rainfall is the quantity of rainfall reaching the ground after passing through those covers. Without any obstruction like canopy cover or ground cover, the rain reaches the ground surface at the same intensity without any recognizable loss. In the presence of trees, a portion of the rainfall is stored in the canopy and the remainder passes through the trees as throughfall and stemflow (Zinke, 1965). In the presence of ground cover, a portion of the throughfall is intercepted and the remainder finally reaches the ground as net rainfall.

Let I be the rainfall rate (or intensity) at time t at a level above the tree canopy as shown in Fig. 2. Let I_c be the rate at which rain is being stored in the canopy at time t. Then, the rainfall rate under the tree canopy is reduced to the throughfall rate and the weighted average throughfall rate is

$$I_o = I - D_c I_c, \qquad . \tag{1}$$

where stemflow has been neglected. Similarly, let I_g be the rate at which rain is being stored in the ground cover at time t. Then the weighted average net rainfall rate reaching the ground is

$$I_n = I_o - D_g I_g \qquad . \tag{2}$$
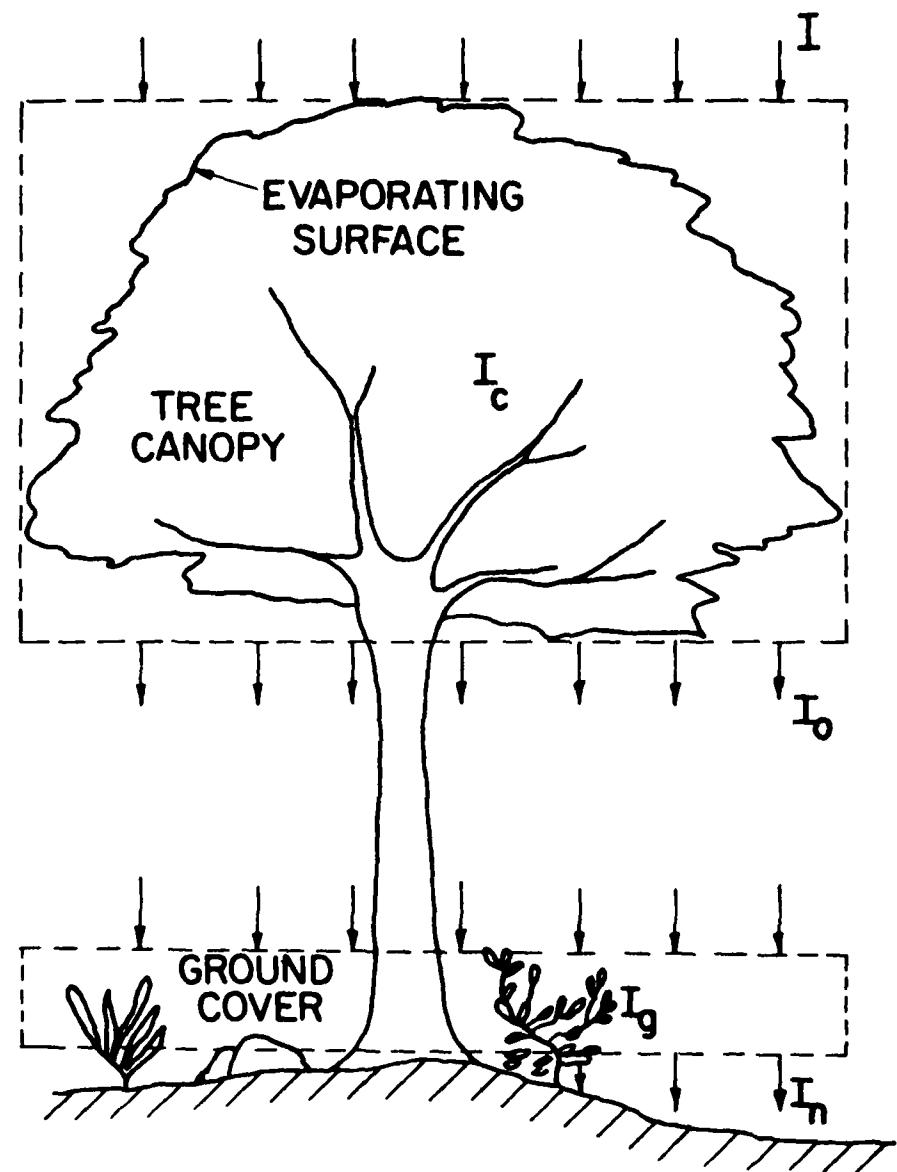
Fig. 2 Control volumes for tree canopy and ground cover

According to Horton (1919), the total interception equals leaf storage capacity plus evaporation loss during the storm. Zinke (1965) indicated that ". . . usually for a storm, there is an initial period during which the vegetation cover is wetted and a so-called interception storage capacity is satisfied. This is followed by loss from this storage, and the loss is dependent upon the evaporation opportunity during the remainder of the storm."

Let V_c be the interception storage capacity of a tree canopy per unit area of tree canopy, V_g the interception storage capacity of the ground cover per unit area of ground cover, E the mean evaporation rate form the interception storages, S_c and S_g the ratios of the evaporating surface area to the horizontal projected area for a tree canopy and for a typical ground cover, respectively, and I_s the initial interception storage content which is defined as the ratio of the initial storage to the interception storage capacity. Accordingly,

$$I_c = I, \text{ if }, \int_o^t I(\tau)d_\tau \leq (1 - I_s) V_c \quad , \tag{3}$$

and

$$I_c = ES_c \text{ , if }, \int_o^t I(\tau)d\tau > (1 - I_s) V_c \quad . \tag{4}$$

Similarly,

$$I_g = I_o \text{ , if }, \int_o^t I_o(\tau)d \leq (1 - I_s) V_g \quad , \tag{5}$$

$$I_g = E S_g \text{ , if }, \int_o^t I_o(\tau)d\tau > (1 - I_s) V_g \quad . \tag{6}$$

I.16

For easy handling of data, a parameter r_v is introduced, defined as the ration of the interception storage capacity of a typical canopy cover to that of the ground cover. Therefore,

$$V_c = r_v V_g \quad ,$$

and

$$S_c = r_v S_g \quad .$$

Eqns. 3 and 4 can be rewritten in the discrete form as

$$I_c = I \ , \ \text{if} \ \Sigma \ I\Delta t \leq (1-I_s) r_v V_g \quad , \tag{7}$$

$$I_c = E \ R_v S_g \ , \ \text{if} \ \Sigma \ I\Delta t > (1-I_s) r_v V_g \quad . \tag{8}$$

Similarly, one obtains

$$I_g = I_o \ , \ \text{if} \ \Sigma \ I_o \Delta t \leq (1-I_s) V_g \quad , \tag{7'}$$

$$I_g = E \ S_g \ , \ \text{if} \ \Sigma \ I_o \Delta t > (1-I_s) V_g \quad . \tag{8'}$$

Eqns. 1, 2, 7, 8, 7' and 8' are used to compute the discretized net rainfall rate.

2.2   INFILTRATION. RAINFALL EXCESS RATE

Water reaching the ground surface at the beginning of a storm passes through into the soil because in nearly all cases the initial infiltration capacity rate is greater than the initial net rainfall rate. In that case, the infiltration rate is equal to the net rainfall rate and there is no runoff. Once the net rainfall rate exceeds the infiltration rate, the excess rainfall either runs off or is stored on the ground surface as depression storage and thus ponding takes place. The time elapsed until the beginning of excess rainfall is known as the ponding time.

It is very difficult to describe mathematically the process of runoff originating from rainfall excess, because, very little is known concerning the magnitude of depression storage. Meaningful observation of depression storages are not easily obtained. Thus, depression storage is usually combined with interception and treated as an initial loss with respect to storm runoff (Linsley et al. 1958). For simplicity, the depression storage is omitted in this model, but implicitly is included in the interception storage capacity described in the previous section.

Thus, the water balance equation at the ground surface is

$$I_e = I_n - f_i \tag{9}$$

in which I_e is the rainfall excess rate, I_n is the net rainfall rate, and f_i is the infiltration rate.

The ponding time and the infiltration rate are computed from the infiltration model developed by Smith and Parlange (1978). The model was developed from a simplified solution of the equation for one dimensional diffusion of water under gravity, by imposing the rainfall pattern as flux-type boundary condition. The equation and the general initial and boundary conditions are

$$\frac{\partial \theta}{\partial t} = \frac{\partial}{\partial z} \left(D \frac{\partial \theta}{\partial z} \right) + \frac{\partial k}{\partial z} \quad , \tag{10}$$

and,

$$t = 0, \ z > 0, \ \theta = \theta_i \quad ; \tag{11a}$$

$$0 < t \leq t_p, \ z = 0, \ K - D \frac{\partial \theta}{\partial z} = I_n(t) \quad , \tag{11b}$$

where θ is the soil water content; z is the vertical distance from the soil surface; D is the moisture diffusivity; K is the hydraulic conductivity; t_p is the ponding time; and $I_n(t)$ is time-varying net rainfall intensity pattern. Eq. (10) is also generally written as

$$\frac{\partial z}{\partial t} + \frac{\partial}{\partial \theta} \left(D \frac{\partial \theta}{\partial z} \right) = \frac{dK}{d\theta} \tag{12}$$

by using an elementary identity of differentials. The primary assumption used in the derivations is that D varies rapidly with θ, which implies that

water flux within the soil varies little with relative position. Integrating Eq. 12 with the condition 11b, and using an expression of conservation of mass, Smith and Parlange (1978) obtained the solution

$$\int_o^t I_n dt = \int_{\theta_i}^{\theta_1} (\theta - \theta_i) \frac{D(\theta)}{I_n - K(\theta)} d\theta \quad , \tag{13}$$

where the subscript 1 refers to conditions at the surface, and i refers to initial conditions. When ponding occurs $\theta_1 = \theta_s$ (saturated water content), and the left-integral upper limit becomes $t = t_p$.

By further assuming that K varies slowly in the region near θ_s, or if K is much larger than I_n, Eq. 13 may be approximated by

$$\int_o^{t_p} r dt = B(\theta_i) (I_{np} - K_s)^{-1} \quad , \tag{14}$$

where I_{np} is the net rainfall rate at ponding time, and $B(\theta_i)$ is a parameter dependent only on soil type and θ_i. B is theoretically identified as a function of sorptivity and it can be roughly estimated from $B \cong S^2/2$, where S is the soil sorptivity. Eq. 14 is used in estimating the ponding time, t_p. Where $I_n(t)$ is a continuously differentiable expression, an analytical expression for t_p results from Eq. 14. Engineering use of this expression is quite simple. As a rain pattern progresses, the value of $\int_o^t I_n dt$ is calculated and compared with the value of the right hand side of Eq. 14, with $I_{np} = I_n$. This expression is an inequality only up to the time at which ponding occurs.

For the same conditions on K given above, the expression for the decay of infiltration capacity for $t > t_p$ was derived as was the expression for ponding time. A more general expression for surface conditions related to Eq. (13), which reduced to Eq. 14, is

$$A \int_{\Psi_i}^o \frac{(\theta - \theta_i)K}{I_n - K} d\Psi = \int_\Psi^o (\theta - \theta_i)K d\Psi \int_o^t I_n dt \quad . \tag{15}$$

Here, the variable of integration is Ψ, rather than θ. This expression applies for all times. The value of Ψ at the surface is taken equal to zero for $t > t_p$, although a surface depth could be taken into account if desired, the effect of which is, in fact, small.

I.19

Differentiating Eq. 15 with respect to t yields

$$- \frac{A}{I_n} \frac{dI_n}{dt} \int_{\Psi_i}^{o} (\theta-\theta_i) \frac{K}{(I_n-K)^2} d\Psi = \int_{\Psi_i}^{o} (\theta-\theta_i)Kd\Psi \qquad (16)$$

Taking $t > t_p$, the surface flux is $f(t) < I_n(t)$, and integrating from t_p to t yields

$$A \int_{\Psi_i}^{o} \{\frac{(\theta-\theta_i)}{K} \ln [\frac{I_{np}(f-K)}{f(I_{np}-K)}] + \frac{K}{f-K} - \frac{K}{I_{np}-K}\} d\Psi =$$

$$(t-t_p) \int_{\Psi_i}^{o} (\theta-\theta_i)Kd\Psi \qquad . \qquad (17)$$

Here A depends slightly on the rainfall rate pattern. From Eq. 14

$$A \cong B = (I_{np}-K_s) \int_{o}^{t_p} I_n dt \qquad . \qquad (18)$$

The function of K in the left integrand of Eq. 17 can be replaced by its value at saturation, K_s, and combined with Eq. 18 to eliminate A, yielding

$$K_s (t-t_p) = \int_{o}^{t_p} r dt \{\frac{I_{np}-f}{f-K_s} - \frac{I_{np}-K_s}{K_s} \ln [\frac{(I_{np}-K_s)f}{(f-K_s)I_{np}}]\} \qquad (19)$$

Eq. 19 is solved numerically to compute the infiltration decay, $f(t)$ for $t > t_p$. In this model, Newton's method is applied and according to this method, the infiltration rate at the ith time interval and kth iteration step is

$$f_{i,k} = f_{i,k-1} - \frac{F(f_{i,k-1})}{F'(f_{i,k-1})} \qquad . \qquad (20)$$

The function $F(f)$ and its derivative, $F'(f)$, are

$$F(f) = K_s(t-t_p) - \int_{o}^{t_p} I_n dt \{\frac{I_{np}-f}{f-K_s} - \frac{I_{np}-K_s}{K_s} \ln (\frac{I_{np}-K_s}{I_{np}} \frac{f}{f-K_s})\} = 0, \qquad (21)$$

and,

$$F'(f) \simeq \frac{\int_0^{t_p} I_n dt \ (I_{np} - K_s)}{(f - K_s)^2} \ (1 - \frac{f - K_s}{f}) \quad . \tag{22}$$

To start the computation, the following initial values are assumed:

$$f_{o,o} = f(t_p) = I_{np} \quad , \tag{23a}$$

$$f_{i,o} = f_{i-1} \quad . \tag{23b}$$

Due to the lack of infiltrometer data in most of the catchments, the parameter B in Eq. 14 is presently estimated from the results presented by Smith and Parlange (1978), Fig. 3. For simplicity, the results for Colby S. L. (swelling) were used in the tests discussed in this report. With the known information of initial soil moisture deficit, $(\theta_s - \theta_i)$ and the saturated hydraulic conductivity K_s (cm/sec), the value of $B = S^2/2$ (cm²/sec) is estimated from the quasi-linear functions plotted in Fig. 2.

2.3   WATER ROUTING

The motion of water moving either as overland flow or channel flow, is governed by the equations of mass continuity, momentum balance, and flow resistance. The flow routing scheme described in this report is based on the kinematic-wave approximation to the general equations of motion. The following sections present the basic assumptions underlying the kinematic-wave theory, along with the essential points of the analytical solution. This solution is then used to investigate the conditions under which kinematic shock waves may be expected. Subsequently, procedures for proper shock fitting are discussed. Simplifying approximations are made which allow closed form solutions and preserve the effects of the shocks. The resulting approximate shock fitting scheme is compared with an existing implicit finite difference solution. The accuracy and efficiency of the new scheme are illustrated in Part 3 by computing a variety of unsteady flows, ranging from simple cascades to complex natural catchments.
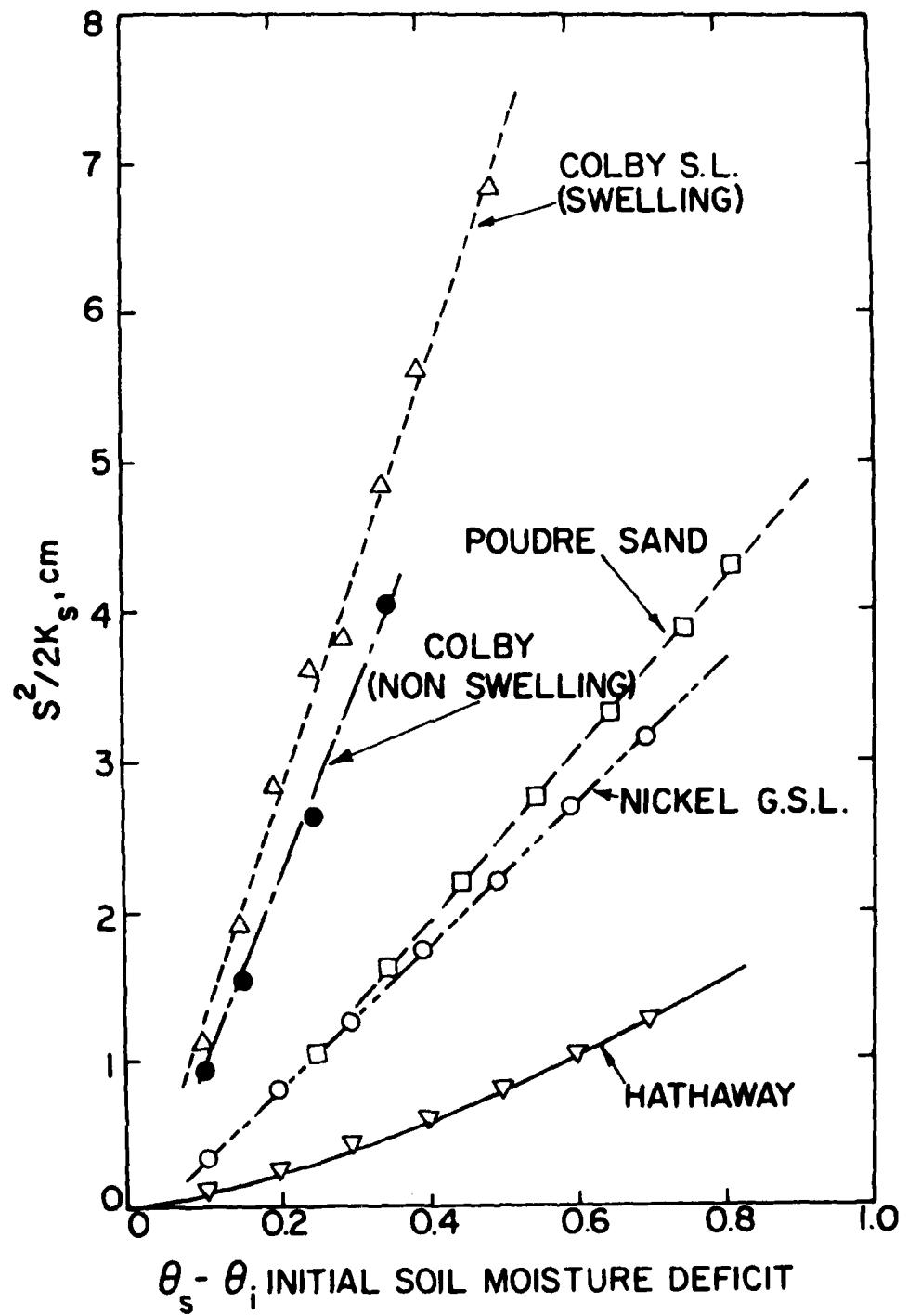
Fig. 3 Quasi-linear relation of the second power of soil sorptivity to initial moisture deficit (after Smith and Parlange, 1978)

I.22

2.3.1   Kinematic Wave Approximation

This approximation is based on a simplification of the Saint-Venant or shallow-water equations governing unsteady free-surface flows. The underlying assumption is that energy gradients due to local and convective accelerations are negligible in comparison with gravitational and frictional effects. The momentum equation thus become:

$$S_0 \cong S_f \tag{24}$$

where S_0 and S_f are the bed slope and friction slope, respectively. The continuity equation for water is as usual:

$$\frac{\partial A}{\partial t} + \frac{\partial Q}{\partial x} = q_\ell \tag{25}$$

in which A is the flow cross sectional area, Q is the flow rate of discharge, x is the downslope position, t is time, and q_ℓ is the rate of lateral inflow or outflow per unit length of stream.

Any suitable law of flow resistance can be used to express Eq. 24 as a parametric function of the stream hydraulic parameters. A widely used expression is as follows:

$$Q = \alpha A^n \tag{26}$$

where α and n are parameters related to channel (or plane) roughness and geometry. Obviously, α and n are functions of time and position. The space dependence can be removed by making the stream hydraulic properties and the lateral inflow piece-wise uniform in space (Fig. 4). The flow region is segmented into a network of different elements with properties remaining constant within each element, but varying from element to element. This approach, known as a kinematic cascade, was introduced by Brakensiek (1967b) and latter elaborated upon by Kibler and Woolhiser (1970). Similarly, the time dependence of those coefficients and the lateral discharge can be eliminated by assuming each piece-wise constant in time (Fig. 5). Then Eq. 25 and Eq. 26 can be solved for each cascade element subject to given initial and upstream boundary conditions (i.e., upstream inflow rate, Q_U). The subscripts U and D will be used to indicate upstream and downstream conditions, respectively.
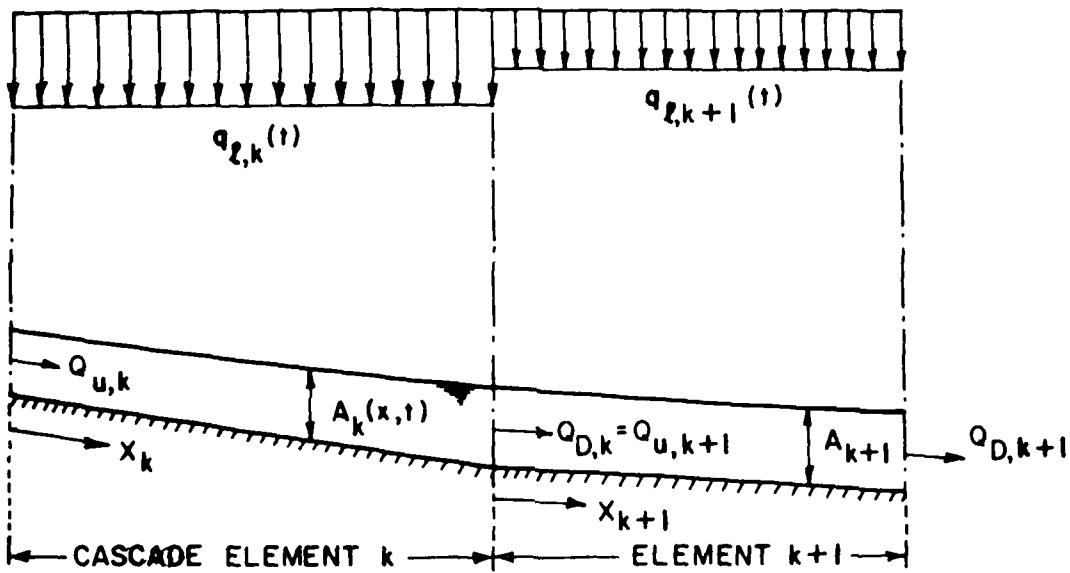
Fig. 4   Kinematic cascade with lateral inflow

2.3.2 Analytical Solution

Eqns. 25 and 26 can be solved using the method of characteristics (Eagleson, 1970). The basic steps of this method are given below for completeness. Assuming that α and n are constant on a given cascade element k and combining Eqns. 25 and 26 yields

$$\frac{\partial A}{\partial t} + \alpha n \, A^{n-1} \frac{\partial A}{\partial x} = q_\ell \quad . \tag{27}$$

The total differential of A yields

$$\frac{\partial A}{\partial t} \, dt + \frac{\partial A}{\partial x} \, dx = dA \quad . \tag{28}$$

Since the derivatives in Eqns. 25, 27, 28 do not exist along the characteristic paths, the determinant of the coefficient matrix corresponding to those equations must vanish at points on the characteristics. This requirement thus yields

$$\frac{dx}{dt} = \alpha n A^{n-1} = n\alpha^{\frac{1}{n}} Q^{(1 - \frac{1}{n})} \quad , \tag{29a}$$

or,

$$\frac{dt}{dx} = \frac{1}{\alpha n A^{n-1}} \quad . \tag{29b}$$

Obtaining the invariants of the solution gives

$$\frac{dA}{dt} = q_\ell \quad , \tag{30a}$$

or,

$$\frac{dA}{dx} = \frac{q_\ell}{\alpha n A^{n-1}} \quad . \tag{30b}$$

The sets of Eqns. 29A, 30A or 29b, 30b represent the characteristic form of the solution to the kinematic-wave approximation. They show that kinematic waves possess only one system of characteristics. Accordingly, kinematic-wave routing cannot be used in situations where there are downstream flow controls. Integrating Eqns. 30a and 30b with the initial and boundary conditions

$$A_I = A(x, t_0), \quad t_0 = 0, \tag{31}$$

$$A_U = A(x_0, t), \quad x_0 = 0, \tag{32}$$

results in the following respective expressions for the flow conditions along any characteristic $t = t(x)$ (Harley et al., 1970):

$$A(x,t) = A_0 + \int_{t_0}^{t} q_\ell[x, \xi(x)] \, d\xi \quad , \tag{33a}$$

and

$$A(x,t) = \{A_0^n + \frac{1}{\alpha} \int_{x_0}^{x} q_\ell[\eta, t(\eta)] \, d\eta\}^{\frac{1}{n}} , \tag{33b}$$

or

$$Q(x,t) = \alpha A_0^n + \int_{x_0}^{x} q_\ell[\eta, t(\eta)] \, d\eta. \tag{33c}$$

Substituting Eqns. 33a and 33b into Eqns. 29a and 29b, respectively, and on integration yield

$$x - x_0 = \alpha n \int_{t_0}^{t} \{\int_{t_0}^{t'} q_\ell[x, \xi(x)] \, d\xi + A_0\}^{n-1} \, dt', \tag{34a}$$

and

$$t - t_0 = \frac{1}{\alpha n} \int_{x_0}^{x} \{\frac{1}{\alpha} \int_{x_0}^{x'} q_\ell[\eta, t(\eta)] \, d\eta + A_0^n\}^{\frac{1-n}{n}} \, dx' \quad . \tag{34b}$$

In these equations, A_0 represents the initial flow area, A_I, along the characteristic C_0 (shown in Fig. 5), and the upstream inflow area, $A_U = [Q_U(t)/\alpha]^{1/n}$, along characteristics like C_1, C_2, and C_3. The above integrals are functionally integrable and yield simple expressions when $q_\ell(x,t)$ is either an explicit function of x and independent of time, or vice versa. In most applications, only discrete distributions of lateral inflows are available. For instance, rainfall intensities and/or infiltration rates are usually regarded as lateral inflows in hydrologic models. In these cases, it has been a common practice to use lateral
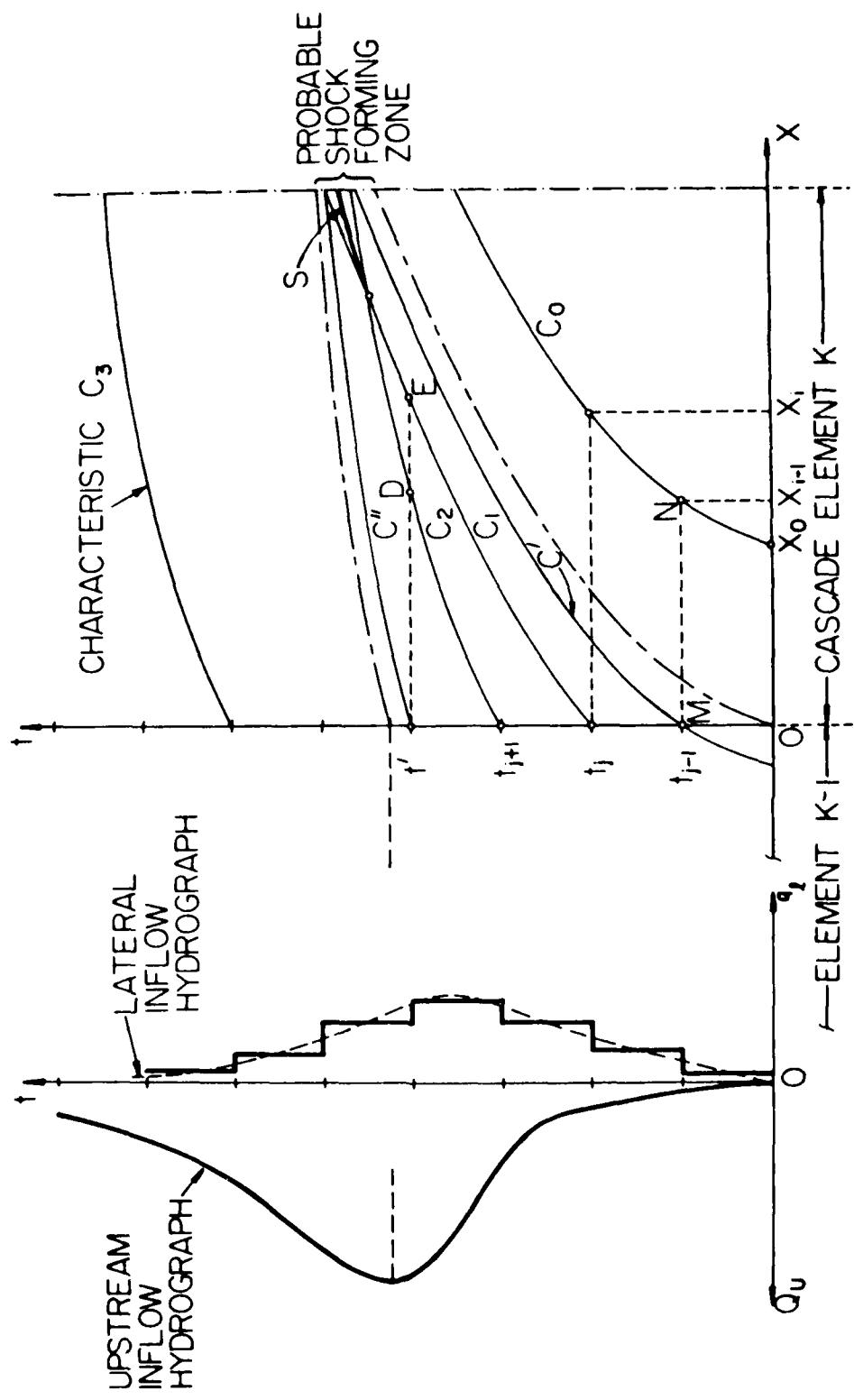
Fig. 5 Solution domain for a cascade element

inflows having a piece-wise uniform distribution in space (Fig. 4) and a piece-wise constant variation in time (Fig. 5). This form of lateral inflow distribution is also adopted in this paper. Thus, assuming $q_\ell(x,t)$ remains constant within small space and time increments the above expressions may be explicitly integrated. Discretizing Eqns. 33 and 34 between two points (x_{i-1}, t_{j-1}) and (x_i, t_j) on a characteristic path (Fig. 5) yields

$$A_{i,j} = A_{i-1,j-1} + q_{\ell,j}\, \Delta t_j \quad , \qquad (33'a)$$

$$A_{i,j} = (A_{i-1,j-1}^n + \frac{q_{\ell,j}}{\alpha}\, \Delta x_i)^{\frac{1}{n}} \quad , \qquad (33'b)$$

$$Q_{i,j} = Q_{i-1,j-1} + q_{\ell,j}\, \Delta x_i \quad , \qquad (33'c)$$

$$\Delta x_i = \frac{\alpha}{q_{\ell,j}} \left[(q_{\ell,j}\, \Delta t_j + A_{i-1,j-1})^n - A_{i-1,j-1}^n \right] \quad , \qquad (34'a)$$

and

$$\Delta t_j = \frac{1}{q_{\ell,j}} \left[(\frac{q_{\ell,j}}{\alpha}\, \Delta x_i + A_{i-1,j-1}^n)^{\frac{1}{n}} - A_{i-1,j-1} \right] \quad , \qquad (34'b)$$

where $\Delta x_i = x_i - x_{i-1}$, $\Delta t_j = t_j - t_{j-1}$, and $q_{\ell,j}$ is the rate of lateral inflow assumed constant over the time step Δt_j and the space increment Δx_i. The last two equations are not defined when $q_{\ell,j} = 0$; in this case Eqns. 29a and 29b yield

$$\Delta x_i = \alpha n\, A_{i-1,j-1}^{n-1}\, \Delta t_j \qquad (34'c)$$

and

$$\Delta t_j = \frac{1}{\alpha n}\, A_{i-1,j-1}^{1-n}\, \Delta x_i \quad . \qquad (34'd)$$

Eqns. 34' are used to trace the characteristic path by considering either Δx_i or Δt_j as a dependent variable and choosing a suitable value for the other. This increment must be chosen so that the lateral inflow can be assumed constant within the intervals Δt_j and Δx_i. Eqns. 33' are used in turn to compute the flow conditions on the same characteristic. Eqns. 33' and 34' are explicit and independent of each other, and therefore, they may be used in several different combinations. In this paper, the following scheme is used for computational efficiency. Since the lateral inflow is uniform along a cascade element and piece-wise constant with time, the best choice is to take the time increment Δt_j as the independent variable. This

I.28

time-increment is used in Eq. 33'a to compute $A_{i,j}$, and Eq. 26 is used to obtain $Q_{i,j}$. Then Eq. 33'c is solved for Δx_i. These steps constitute the scheme used to trace a characteristic across the cascade element and to compute the flow conditions along its path.

In general, a characteristic does not intersect the downstream boundary exactly at the beginning or end of a time step. A modification of the proposed scheme is used to determine the time of intersection. The last space increment $\Delta x_N = x_{N-1}$, where x_N is the length of the cascade element, is substituted in Eq. 33'c to compute Q_D and then Eq. 26 is solved for A_D. This value is then introduced into Eq. 33'a to solve for the time increment, Δt_N, and the time of intersection $t_D = t_{N-1} + \Delta t_N$. The discharges existing on all the characteristic paths at the time of their arrival to the downstream boundary define a discrete outflow distribution. This discrete distribution is smooted out by interpolation to obtain a continuous outflow hydrograph. The problem of hydrograph computation for any given cascade element is, thus, completely specified once the initial flow areas along the element at time zero (Eq. 31) and the inflow hydrograph, coming from the upstream element (Eq. 32), are known.

2.3.3   Formation of Shock Waves

The foregoing analytical solution remains valid as long as the characteristic paths do not intersect each other. When this occurs, the preceding theory does not give a unique solution since there is more than one characteristic passing through the intersection point, causing flow discontinuity. These discontinuities have properties analogous to those of shocks that arise in gas dynamics theory and, by analogy, are generally known as kinematic shock waves. Eq. 29a shows that the celerity of a wave moving along a characteristic path is a function of the flow area A. This dependence on A produces a nonlinear distortion of the wave as it propagates. Waves with higher values of A travel faster and finally overtake lower ones leading to the breaking of the wave profile as illustrated in Fig. 6. In this figure the lateral inflow has been ignored for simplicity and, thus, the flow areas do not change along the characteristic paths (Eq. 30). The wave profile at any instant $t = t_1 > 0$ is obtained by projecting the corresponding values of A on the verticals passing through the intersections of the characteristic paths and the line $t = t_1$. The wave breaking begins at the time $t = t_B$ when the free surface profile first develops an infinite slope. In the x-t plane this breaking

I.29
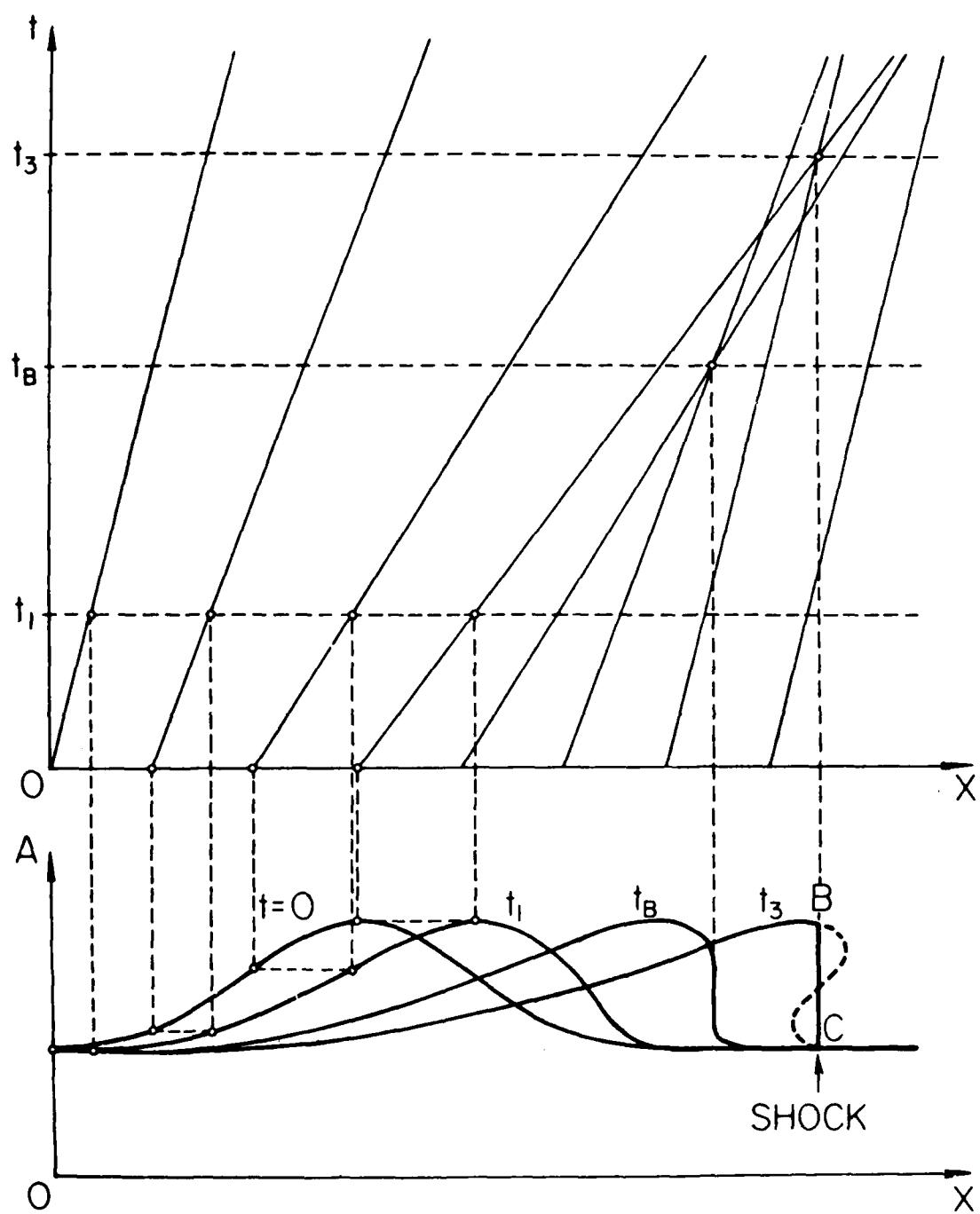
Fig. 6 Formation of shock waves (adapted from Whitham, 1974)

coincides with the intersection of two characteristics, where a single-valued flow area no longer exists. This sudden change in flow area is interpreted as the initiation of a shock. After its formation, the shock proceeds downstream with its own velocity, as discussed in the next section.

However, a shock will be formed only if, given any two consecutive characteristics, the first one is less steep than the following one. For example, Fig. 5 shows the characteristics C_1 and C_2 passing through the points E and D at the same time t'. Then, the necessary condition for shock formation is that

$$[\frac{dx}{dt}]_E^{(1)} < [\frac{dx}{dt}]_D^{(2)} \tag{35}$$

where the superscripts refer to the consecutive characteristics C_1 and C_2. Using Eqns. 26, 29a and 33a, Eq. 35 can be expressed as

$$[Q_{U,k}^{(2)}]^{\frac{1}{n_k}} - [Q_{U,k}^{(1)}]^{\frac{1}{n_k}} > (\alpha_k)^{\frac{1}{n_k}} q_{\ell,k} \Delta t_{j+1} \tag{36}$$

in which the subscript k indicates flow variables associated with the kth cascade element and $\Delta t_{j+1} = t_{j+1} - t_j$. This inequality indicates that characteristics emanating from the line t = 0 cannot intersect for either dry or uniform initial conditions. It is also clear from Eq. 36 that characteristics originating during steady upstream inflow or along the falling limb of the upstream hydrograph (i.e., characteristics C_3 in Fig. 5) will not intersect, unless the flow law changes from turbulent to laminar. These two zones are then free from shock formation. This does not mean that shocks originating upstream may not propagate into these zones. On the other hand, the characteristics originating along the rising limb of the upstream hydrograph may intersect depending upon the relative magnitude of the variables appearing in Eq. 36. For this reason, the domain bounded by the characteristics emanating from both ends of the rising limb can be regarded as the probable shock-forming zone. The solution in the shock-forming zone is influenced by the upstream boundary

conditions of the kth-element which, in turn, depend on the initial conditions on the element k-1. For example, applying Eq. 36 to the characteristics passing through the points M and N indicated in Fig. 5, and using Eqns. 29a and 33c, one obtains

$$(\frac{\alpha_{k-1}}{\alpha_k})^{\frac{1}{n_k}} (q_{\ell,k-1}\Delta t_{j-1})^{\frac{n_{k-1}}{n_k}} > q_{\ell,k}\Delta t_{j-1} . \tag{37}$$

This inequality shows that for uniform topography ($\alpha_{k-1} = \alpha_k$, $n_{k-1} = n_k$) a shock will be formed in element k whenever $q_{\ell,k-1} > q_{\ell,k}$; whereas, under conditions of uniformly distributed lateral inflow ($q_{\ell,k-1} = q_{\ell,k}$), a shock will occur wherever $\alpha_{k-1} > \alpha_k$ for $n_{k-1} = n_k$ and $n_{k-1} > n_k$ for $\alpha_{k-1} = \alpha_k$.

Harley et al. (1970), Kibler and Woolhiser (1970), and Li et al. (1976a,b) also studied the foregoing necessary conditions. The latter also discussed the sufficient conditions for two given characteristics to intersect within the boundaries of the cascade element. They suggested taking two consecutive characteristics far apart enough so as to avoid their intersection within the element (i.e., characteristics C' and C" in Fig. 5). However, once the necessary condition is met, the shock wave S may form within the cascade element and travel all the way to the downstream end (this is discussed in the next section). Therefore, not considering the solution domain between C' and C" serves only to ignore the possible existence of the shock but does not really avoid it. Given that the shock is an intrinsic part of the solution to the kinematic-wave approximation, a better routing procedure is one that considers the presence of the shock and its effect cn the outflow hydrograph. Such an approach is discussed in the next section.

2.3.4   Approximate Solution With Shock Fitting

After breaking occurs the kinematic wave theory ceases to be a strictly valid description of the physical process, because the flow area is inherently single-valued. However, the foregoing formulation can still be utilized by allowing discontinuities in the solution. Lighthill and Whitham (1955) proposed replacing the shock, as a first approximation, by a discontinuous wave ($\overline{BC}$, Fig. 6) that produces the appropriate variations in discharge and flow area as it moves downstream. These authors derived the velocity of the shock by considering the continuity of flow and the rate of

discharge crossing the shock front. Applying their result to an arbitrary points (x,t) on the shock path resulted in

$$U(x,t) = \frac{dx}{dt} = \frac{Q^b(x,t) - Q^a(x,t)}{A^b(x,t) - A^a(x,t)} \tag{38}$$

where the superscripts b and a indicate flow conditions behind and ahead of the shock, respectively. While the shock is moving downstream, infinitesimal waves traveling along characteristic paths will join the shock from ahead and behind continuously modifying the shock strength and velocity. Therefore, the locus of all the points, where those characteristics intersect each other, defines the path of the associates shock.

The important steps involved in routing a shock include finding the position where it originates and then tracing the shock downstream. An analytical method for finding the position where the shock originates was discussed by Whitham (1974). Because of its computational intricateness, his approach was not used in the present study, but, instead, the following simpler technique was developed. It is clear from Eq. 36 that once it is satisfied, the characteristics tend to converge. Thus, a shock may originate within the same element or in one of the following cascade elements, depending upon the magnitudes of α_k, n_k, and $q_{\ell,k}$ as they appear in Eq. 36. In this paper, the problem of finding the exact location of the shock origin is avoided by discretizing the upstream inflow hydrograph. By doing this, small artificial shocks are introduced all along the rising limb of the hydrograph, but they are routed across the characteristic plane only in those zones where Eq. 36 is satisfied. The remainder of the inflow hydrograph is routed according to the continuous solution from the characteristics. Thus, the shock fitting approximations introduced in this paper influence only those zones where shocks form, whereas the accuracy of the analytical solution is preserved in the other zones. The procedure is illustrated in Fig. 7, where individual characteristics are traced one at a time, starting at the upstream boundary of the characteristic plane. They are assumed to emanate from the half-time levels $t_{\frac{1}{2}}$, $t_{1+\frac{1}{2}}$, $t_{2+\frac{1}{2}}$, etc., where the continuous and discretized upstream-hydrographs coincide. The shock-forming condition, Eq. 36, is tested at each new time step. The

I.33
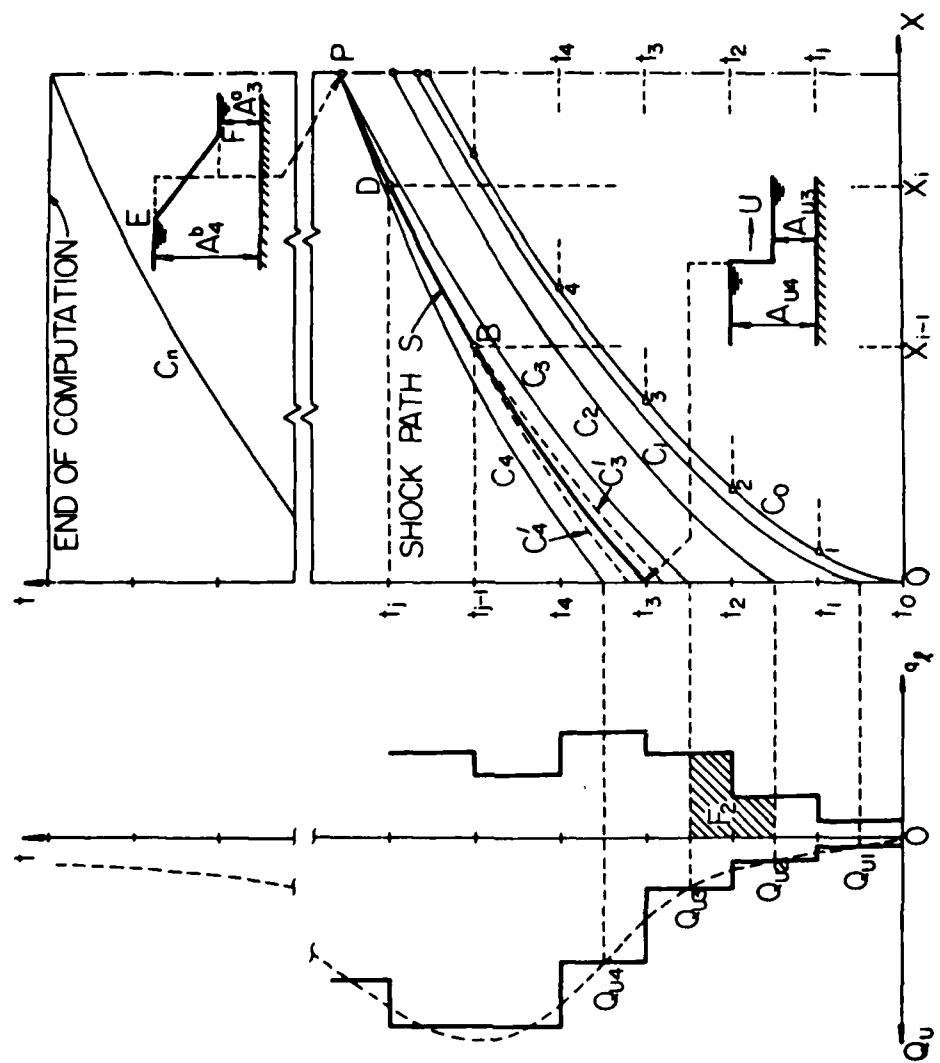
Fig. 7 Routing of characteristic and shock waves

discharges $Q_{U,k}^{(2)}$ and $Q_{U,k}^{(1)}$ appearing in this relationship are replaced by the discretized inflow rates at the new and previous time steps, respectively. In addition, the product $q_{\ell,k}\Delta t_{j+1}$ is replaced by the integral of the lateral inflow hydrograph over the interval $t_{j-\frac{1}{2}} \leq t \leq t_{j+\frac{1}{2}}$, to account for the fact that the characteristic paths arise from $t_{j+\frac{1}{2}}$ instead of t_{j+1}. Hence, if $j = 2$, for instance, Eq. 36 is given by

$$(Q_{U3})^{\frac{1}{n_k}} - (Q_{U2})^{\frac{1}{n_k}} > (\alpha_k)^{\frac{1}{n_k}} F_2,$$

where F_2, Q_{U2}, and Q_{U3} are defined in Fig. 7. When Eq. 36 is not satisfied, the corresponding characteristics are routed one at a time using Eqns. 33 and 34, as illustrated by C_0, C_1, and C_2 in Fig. 7. On the other hand, if Eq. 36 is met, an artificial shock is introduced at the time level t_j and then routed using the scheme presented below.

The problem of tracing the shocks in the characteristic plane has been discussed in detail by Whitham (1974). It consists essentially of determining the characteristics intersecting each other on the shock path, and the location of the point of intersection. The solution to this so called three-point problem, requires the simultaneous solution of the characteristic Eqns. 34 and the expression for the shock velocity, Eq. 38. This method was used by Kibler and Woolhiser (1970), who developed an iterative scheme to route shocks generated on a three-plane cascade under constant lateral inflow. In principle, this approach can be extended to include more complex geometries with varying lateral inflow. However, the computational details become excessively complicated, particularly when shock interactions occur. Therefore, an alternate approach is developed in this paper by restricting the above artificial shocks to small amplitudes (weak shocks). Consider the characteristic pair C_3, C_4 intersecting at the point P on the shock path (Fig. 7), and a similar pair C_3', C_4' joining the shock at an arbitrary point B. If the shock is weak, the flow areas carried by C_3' and C_3 (ahead of the shock) will not differ significantly from each other. Similarly, C_4' and C_4 will have approximately equal flow areas behind the shock. Since B is arbitrary, C_4' and C_3' may represent any of the infinite pairs of characteristics joining the shock (behind and ahead of it) along its trajectory. It is thus reasonable to postulate that the intersecting characteristics defining the shock path do not deviate

I.35

significantly from it. Then, as a further expedience, we assume that the shock path is defined by two sufficiently close (overlapping) characteristics, one representing the characteristics ahead of the shock and the other representing the characteristics behind the shock. These two characteristics will carry flow areas (depths) ahead and behind the shock as given by Eq. 33a or 33b. The common path of these characteristics, as well as the shock, is obtained by substituting Eqns. 33a and 26 or Eqns. 33b and 33c into Eq. 38; after integration they yield

$$x-x_0 = \frac{\alpha}{A_0^b-A_0^a} \int_{t_0}^{t} \{[A_0^b + \int_{t_0}^{t'} q_\ell(x,\xi(x))\ d\xi]^n - [A_0^a +$$

$$\int_{t_0}^{t'} q_\ell(x,\xi(x))\ d\xi]^n\}\ dt'\ , \tag{39a}$$

and

$$t-t_0 = \frac{1}{Q_0^b-Q_0^a} \int_{x_0}^{x} \{[(A_0^b)^n + \frac{1}{\alpha} \int_{x_0}^{x'} q_\ell(\eta,t(\eta))\ d\eta]^{\frac{1}{n}} - [(A_0^a)^n +$$

$$\frac{1}{\alpha} \cdot \int_{x_0}^{x'} q_\ell(\eta,t(\eta))\ d\eta]^{\frac{1}{n}}\}\ dx'\ , \tag{39b}$$

where (A_0^a, Q_0^a) and (A_0^b, Q_0^b) are the known flow conditions ahead and behind the shock, respectively, at a given point (x_0,t_0) on the shock trajectory.

Consider now any two consecutive points $B(x_{i-1},t_{j-1})$ and $D(x_i,t_j)$ on a shock trajectory S (Fig. 7). Applying Eqns. 39 between these two points and discretizing the results, gives

$$\Delta x_i = \frac{\alpha}{(n+1)q_\ell\ (A_{i-1,j-1}^b-A_{i-1,j-1}^a)} \{[q_\ell\Delta t_j + A_{i-1,j-1}^b]^{n+1} -$$

$$[q_\ell\Delta t_j + A_{i-1,j-1}^a]^{n+1} - (A_{i-1,j-1}^b)^{n+1} + (A_{i-1,j-1}^a)^{n+1}\}, \tag{40a}$$

and

$$\Delta t_j = \frac{\alpha n}{(n+1)q_\ell\ (Q_{i-1,j-1}^b-Q_{i-1,j-1}^a)} \{[\frac{q_\ell}{\alpha} \Delta x_i + (A_{i-1,j-1}^b)^n]^{\frac{n+1}{n}} -$$

$$[\frac{q_\ell}{\alpha} \Delta x_i + (A_{i-1,j-1}^a)^n]^{\frac{n+1}{n}} - (A_{i-1,j-1}^b)^{n+1} +$$

$$(A_{i-1,j-1}^a)^{n+1}\}, \tag{40b}$$

in which the lateral inflow is taken as constant over the finite increments Δx_i and Δt_j. Eqns. 40 are not valid when $q_\ell = 0$. In this case, a discrete approximation of Eq. 38 is used. Similar to the characteristic wave routing, Δt_j is taken as the independent variable. Eq. 33'a is used to compute $A^a_{i,j}$ and $A^b_{i,j}$ and using these two in Eq. 26 $Q^a_{i,j}$ and $Q^b_{i,j}$ are determined. Then Eq. 40a is used to compute Δx_i. These steps constitute an explicit scheme that is used to route the shock like a characteristic wave. Similar to the characteristic wave, the scheme is modified near the downstream boundary. Here, Eqns. 33'c and 26 are used to compute the flow conditions ahead and behind the shock, and Eq. 40b is used to find the exact arrival time of the shock. Although this scheme is based on an approximation that deviates from the uniqueness of the solution, its use does not significantly affect the accuracy of the computations. In the foregoing discussion the shock fronts have been considered mathematically as flow discontinuities fitted into regions where multiple values of the solution exist. Physically they will not be discontinuities; instead, the fronts will have finite lengths induced by diffusive effects as well as by breaking of the waves. In many instances, the front will take the smooth shape of a monoclinal flood wave (Whitham, 1974). Because of these smoothing tendencies, and for the sake of computational expedience, the shock front can be approximated by a linear profile as shown in Fig. 7 (segment EF). Thus, the flow condition at the shock itself can be computed as

$$A(x,t) = \frac{1}{2} \left[A^a(x,t) + A^b(x,t) \right]. \tag{41}$$

This could be viewed as a method to make an approximately continuous solution from one which was made discontinuous by discretizing the inflow hydrograph. The preceding routing approach, called herein a propagating shock-fitting (PSF) scheme, permits the use of essentially the same numerical procedure to route both characteristic and shock waves. This scheme is particularly efficient when the initial flow conditions are either dry or uniform, and only the outflow hydrograph is of interest. In these cases the calculations are performed only in the x-t subdomain bounded by the lines C_0 and C_n (Fig. 7), where C_n is the characteristic reaching the downstream boundary at the end of the routing interval. All

the characteristics emanating from the line $t = 0$ are parallel to C_0. Hence, the outflow conditions at times t_1, t_2, t_3,... are equal to those computed at the points 1, 2, 3,... on C_0. Within the above subdomain the step-by-step integrations along the wave trajectories use simple algebraic relationships. Moreover, values computed at interior points do not have to be stored since only outflow conditions are needed.

In the same manner that shocks arise from the intersection of characteristic waves, they can also meet with other shocks to form new shocks. In addition, shocks introduced in the shock-forming zone of a given cascade element will propagate into the downstream elements of the cascade interacting with each other and creating new shocks. These shock interactions cannot be treated by the above PSF scheme, because it tracks only one wave at a time. For this reason, a further simplification is introduced which consists of restricting the shock interactions to the junctions of the kinematic cascade. The shocks emanating from the discretized inflow hydrograph are tracked across the shock forming zone using the explicit scheme, Eqns. 40. When all the shocks have been projected to the downstream boundary, their fronts are smoothed out using Eq. 41. A smooth outflow hydrograph, incorporating the overall effect of the shocks formed upstream is thus obtained. The interaction of shocks carried by converging outflow hydrographs is then simulated by simple superposition of these hydrographs. The resulting outflow hydrograph, which satisfies flow continuity, is in turn used as upstream boundary condition to the next element and the procedure is repeated. This method will be called an approximate shock fitting (ASF) scheme. This scheme computes the outflow hydrograph at any junction of the cascade reflecting the overall effects of the shocks formed in the upstream elements.

2.4   SEDIMENT ROUTING

Sediment yield from agricultural catchments is controlled by physical principles governing the detachment and transport of sediment particles. The source of sediment erosion, or sediment supply, is the detachment by raindrop impact and by runoff. If the sediment load from upstream areas is less than the potential transport capacity of the flow, the supply is depleted and erosion occurs. If the sediment load is greater, deposition occurs. These processes are all interrelated and must satisfy, locally, the conservation principle of sediment mass. Therefore, in addition to the

equations of continuity and momentum for water, additional equations are required for sediment routing. These are the sediment continuity equation, and relations describing sediment supply and transport. These equations are presented below, and they are equally applied to overland and channel flow.

2.4.1   Sediment Continuity Equation

The continuity equation for the size classes $k = 1, 2, \ldots, n$, forming the sediment load can be written as

$$\frac{\partial G_{sk}}{\partial x} + \frac{\partial C_k A}{\partial t} + (1-\lambda) \frac{\partial Pz_k}{\partial t} = g_{\ell k} \tag{42}$$

where G_{sk} is the sediment transport rate by volume per unit time, λ is the soil porosity, P is the wetted perimeter, z_k is the land surface elevation, $g_{\ell k}$ is the lateral inflow, and

$$C_k = G_{sk}/Q \tag{43}$$

is the fraction concentration by volume (Fig. 8a). The concentration and bed elevation for the total load are

$$C = \sum_{k=1}^{n} C_k \; , \tag{44}$$

and

$$z_k = \sum_{k=1}^{n} z_k \; . \tag{45}$$

the third term in Eq. 42 will be denoted by

$$(1-\lambda) \frac{\partial Pz_k}{\partial t} = -g_{dk} \; . \tag{46}$$

This term can be envisioned as a sediment supply term for exchange between the flow and the detached bed material during erosion or deposition. Assuming that the sediment moves essentially at the same average velocity of flow, V, Eq. 42 can be expressed as

$$\frac{\partial}{\partial x} (C_k VA) \; \frac{\partial}{\partial t} (C_k A) = g_{\ell k} + g_{dk} \; . \tag{47}$$
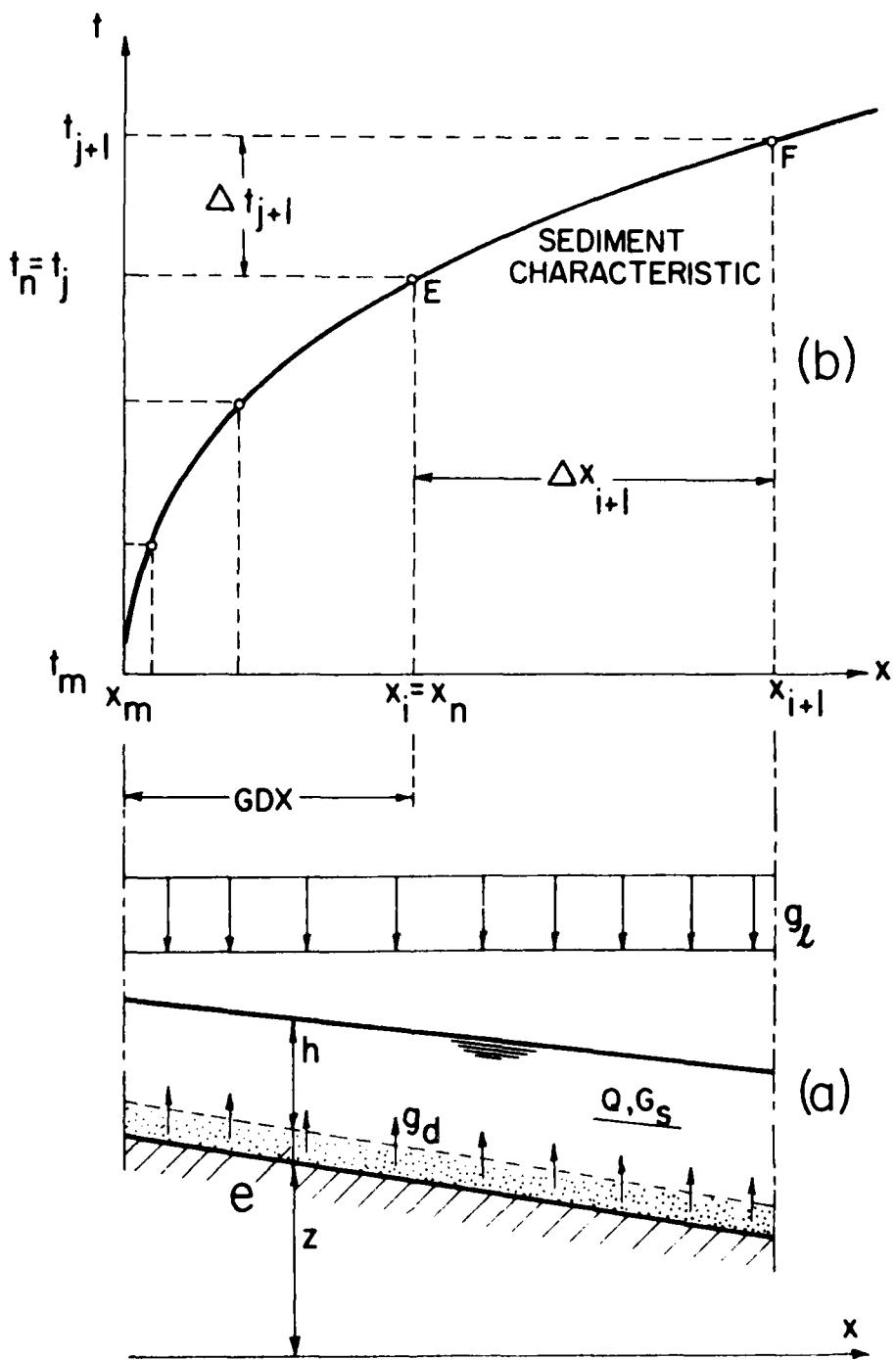
Fig. 8 Sediment processes simulated in a cascade element

Taking V as approximately constant over small space and time intervals, yields

$$\frac{\partial A_{sk}}{\partial t} + V \frac{\partial A_{sk}}{\partial x} = g_{\ell k} + g_{dk}$$

(48)

in which $A_{sk} = C_k A = G_{sk}/V$ is the volume of sediment fraction present in the flow per unit length. Eq. 48 is used to track the aggradation or degradation of the bed as explained in section 2.4.4.

The present model uses a power function to relate the wetted perimeter to the flow area. That is

$$P = aA^b$$

where a and b are coefficients depending on the cross-sectional shape of the flow reach. In particular $a = 1.0$ and $b = 0.0$ for overland segments.

2.4.2   Sediment Transport Formulas

These formulas are used to determine the sediment transport capacity for a specific set of flow and sediment characteristics. The formulas used in the present model were selected after a recent study by Alonso et al. (1981). They compared the predictions of nine transport formulas with flume and field data. The comparison was based on 40 field measurements, 523 flume experiments, and 176 tests on concave slopes, with sediments ranging from coarse sands to very fine soil particles. As expected, no formula satisfactorily represented the entire spectrum of sediment and flow characteristics. Nevertheless, three of the tested formulas gave satisfactory estimates of transport capacity over different subsets of the data range.

The total load formula of Yang (1973) best estimated streamflow carrying capacity in the range of fine to coarse sands. The total load formula of Laursen (1958) predicted reasonably well small streamflows carrying very fine sands and silts. It should be used with some reservations, however, for computing transport of lighter materials such as soil aggregates. The bed load formula of Yalin (1963) can be used to compute sediment transport capacities for overland flows. These conclusions are graphically summarized in Fig. 9. Each of these formulas

I.41

is presented below as the originator intended, but rewritten in terms of dimensionless parameters, (Alonso et al., 1981). Where the formulations required graphical solutions (i.e., determination of threshold conditions from Shield's curve), analytical equivalents (not shown here) have been worked out to facilitate their use in digital computation.

(i) Total load formula of Yang (1973): Yang based his formula on the premise that total load is dominated by the rate of potential energy expenditure per unit weight of water. He used this concept and dimensional analysis to derive his formula, the coefficients of which were determined from a large set of laboratory data. This formula is:

$$\Phi_k = \theta_k^{\frac{1}{2}} \, Z_k \, (V/u_*)[10^{\phi-6}/S], \qquad (49)$$

where

$$\phi = 5.435 - 0.286 \log (w_k d_k/v) - 0.457 \log (u_*/w_k) +$$

$$[1.799 - 0.409 \log (w_k d_k/v) - 0.314 \log (u_*/w_k)]$$

$$\log (V S_0/w_k - V_c S_0/w_k), \qquad (50)$$

$$V_c/w = 2.5/[\log(u_* d_k/v) - 0.06] + 0.06, \quad 0<u_* d_k/v<70, \qquad (51a)$$

$$V_c/w = 2.05, \quad u_* d_k/v \geqq 70. \qquad (51b)$$

(ii) Total Load Formula of Laursen (1958): based mostly on heuristic considerations, Laursen developed a formula relating the load concentration to the relative roughness and excess tractive force. This relationship is corrected by an empirical function of (u_*/w) which accounts for the effectiveness of turbulence in suspending the bed material. The contributions of each size fraction are added up to yield the total load. The formula is:

$$\Phi_k = 0.01 \sum_{k=1}^{n} P_k \, \theta_{50}^{\frac{1}{2}} \, (V/u_*) \, (Z_{50}/Z_k^{7/6}) \, [(\theta_k/\theta_{ck}) \, (V/u_*)^2$$

$$(1/58 \, Z_{50}^{1/3})-1] \, f(u_*/w_k), \qquad (52)$$

SANDS AND SILTS

LIGHT-WEIGHT MATERALS

YALIN	YANG
YALIN	LAURSEN

YALIN	YALIN
LAURSEN	YALIN

SEDIMENT SIZE (mm)

2.0

0.10

0.01

SHALLOW FLOWS STREAMFLOWS STREAMFLOWS SHALLOW FLOWS

SHALLOW FLOWS STREAMFLOWS STREAMFLOWS SHALLOW FLOWS
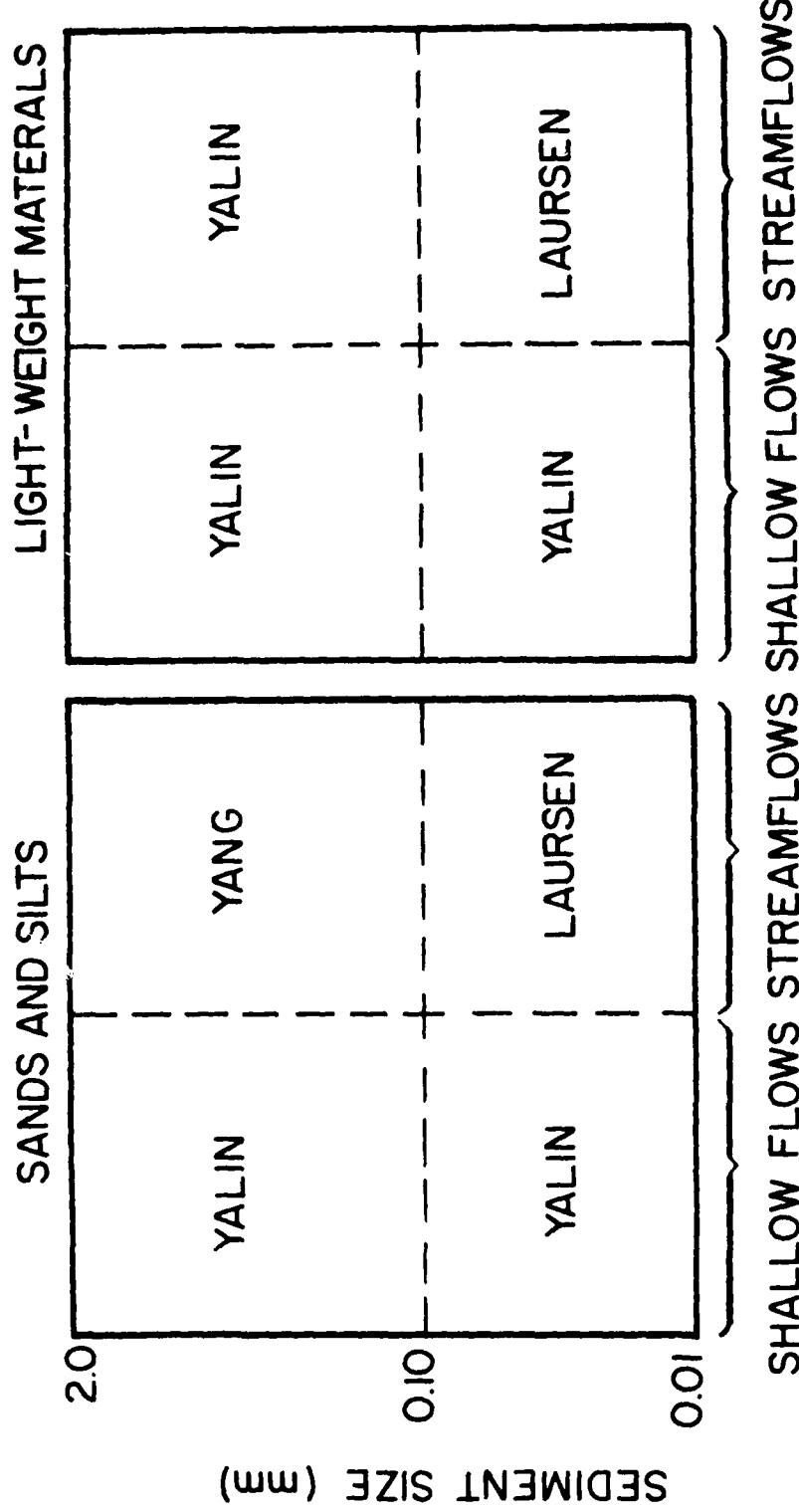
Fig. 9 Range of applicability of sediment transport formulas

I.43

where $f(u_*/w_k)$ is the empirical function obtained by Laursen from flume experiments.

(iii) Bed Load Function of Yalin (1963): this formula is based on a theoretical analysis of saltating particles, in which it is proposed that the bed load rate is related to the range of the particles' saltation rather than to the number of particles participating in the motion. The resulting formula is of the excess-shear type, and was calibrated on a limited set of laboratory data. This formula has the form

$$\Phi_k = 0.635 \; \theta_k^{3/2} \; [1 - (\theta_{ck}/\theta_k)] \; [(1/\theta_{ck})$$

$$- (1/a\sigma \; \theta_{ck}) \; \ln(1 + a\sigma], \tag{53}$$

in which

$$a = 2.45 \; S^{-2/5} \; \theta_{ck}^{\frac{1}{2}} \; , \tag{54}$$

$$\sigma = (\theta_{50}/\theta_{ck}) - 1 = [u_*^2/\theta_{ck}(S-1) \; gd_k] - 1. \tag{55}$$

In Eqns. 49 through 55 Φ_k is the dimensionless volume transport rate, θ_k and Z_k are the mobility number and relative roughness based on the d_k fraction size, w_k is the settling velocity of sediment, and the subscript c denotes threshold conditions. These parameters are defined as

$$\Phi_k = (G_{sk}/\gamma PS)/[(S-1)gd_k^3]^{\frac{1}{2}}, \tag{56}$$

$$\theta_k = u_*^2/[(S-1)gd_k], \tag{57}$$

and

$$Z_k = y/d_k, \tag{58}$$

where S is the specific gravity of the sediment fraction, u_* is the bed shear velocity, and γ and ν are the specific weight and kinematic viscosity of water, respectively.

2.4.3   Equations of Sediment Supply

Soil eroded from land areas with distributed and concentrated flows is the source of most of the sediment transported in a catchment system. Soil erosion is a complex process of detaching soil particles and transportng them downslope through the action of raindrop impact and runoff. Erosion begins when raindrops strike the land surface and detach soil particles by splash. Whenever the soil surface is not protected by vegetation, or any other cover, raindrops can detach very large quantities of soil. Most of this eroded soil is moved downstream by surface runoff. When runoff reaches sufficient intensity, the rate of soil erosion becomes also dependent on the runoff characteristics and on the susceptibility of the soil to the forces of the flowing water. The following sections describe the approaches used in the present model to simulate these major sources of eroded sediment.

2.4.3.1   Soil Detachment by Raindrop Impact: Past research on the process of soil detachment by raindrop impact suggested that the rate of detachment is proportional to the square of the net rainfall intensity (Meyer and Wischmeier, 1969). However, bare soils differ in their susceptibility to detachment by raindrop impact due to a variety of properties such as primary particle size distribution, soil structure, organic matter content, etc. Therefore, an erodibility parameter, a_r, is introduced to describe the rate of erosion as

$$D_r = a_r \, I^2 . \tag{59}$$

This relationship has been recently confirmed by Meyer (1980) who reported extensive field studies showing that Eq. 59 is a valid approximation for a wide range of soils and cropping conditions. Eq. 59 is the basic equation for rainfall detachment. Parameters must be added to account for other factors that influence the rate of detachment. Meyer (1980) has shown that the I^2 law is not affected by the stage of canopy development, but the a_r coefficient is dependent on the erodibility of the soil and decreases as the vegetative cover changes from first growth to full canopy. To account for this effect a cover factor is added based on the cropping-management factor C used in the USLE (Wischmeier and Smith, 1978). The factor C is defined as the ratio of soil loss from land cropped under specified conditions to the corresponding loss from tilted, continuous fallow.

I.45

Wischmeier (1972) presented a method and the necessary graphs for determining C for situations were data are not readily available. In this method C is treated as the product of three subfactors depending on (i) canopy cover, (ii) mulch and ground cover, and (iii) residual effects of the land use, C_{III}, respectively. Approximating the first two subfactors as linear functions of the densities D_c and D_g introduced in section 2.1, the factor C can be expressed as

$$C = 0.2C_{III}[(1-D_c)(1-D_g) + H_cD_c(1-D_g)]$$

where H_c is a function of the average fall height of drops from the canopy cover. Introducing C in Eq. 59, neglecting the term depending on H_c for simplicity, and incorporating the coefficient $0.2C_{III}$ into a_r, yields

$$D_r = a_rI_n^2 (1-D_c)(1-D_g). \tag{60}$$

Ponded water deeper than a critical depth cushions the impact of raindrops and also diminishes the erosion caused by the dissipation of impact energy. Mutchler and Young (1975) suggested that a water depth of more than three times the median drop size essentially eliminated detachment by raindrop impact. Consequently, detachment can take place only if the raindrops can penetrate through the water depth, h, and the thickness of detached soil, e, accumulated from previous events. Laws and Parsons (1943) found that the median drop size, expressed in millimeters, is related to rainfall intensity as

$$D_{50} = 2.23 I^{0.182} \tag{61}$$

Using this formula, the effect of water pondage is described by modifying Eq. 60 as

$$D_r = a_r I_n^2 (1-D_c)(1-D_g)[1-(h + e)/3D_{50}], \text{ if}$$

$$(h + e) \leq 3D_{50}, \tag{62}$$

and $D_r = 0$ otherwise. A similar expression has been proposed by Li (1979). The amount of soil detached by raindrop impact during a time step Δt, and to be added to the current storage of detached soil is, therefore,

$$\Delta e_{rk} = a_r I_n^2 (1-D_c)(1-D_g)(1-(h+e)/3D_{50}]p_k \Delta t, \quad (h+e) \leqq 3D_{50}, \quad (63a)$$

$$\Delta e_{rk} = 0, \quad (h+e) > 3D_{50}, \quad (63b)$$

where p_k is the percentage of sediment material in the kth-size fraction.

2.4.3.2 Soil Detachment by Flow: Erosion by overland flows usually occurs in many single rills. However, for modeling applications rill erosion is assumed to be uniformly distributed overland, and erosion by concentrated flows is restricted to channels. Erosion by flow potentially occurs if the sediment load carried by the incoming flow is less than the transport capacity of the flow. If the sediment load is greater, deposition occurs. Erosion by flow is assumed to occur at capacity rate if no sediment is present in the flow. But if the transport capacity of the flow is partially filled a corresponding depletion of the detached soil available for transport is computed. If the transport capacity is less than the available detached soil, transport is the limiting factor and no erosion by flow takes place. If the available detached soil is less than the transport capacity, additional soil is detached by the flow to compensate for the insufficient supply. These concepts are implemented as follows. The amount of sediment that the flow can potentially carry downstream during the time increment Δt is transformed into an equivalent thickness Δe^P, as explained in the following section. If this thickness is less than the layer of available detached soil, e (Fig. 8a), no detachment by flow occurs. If $\Delta e^P > e$, the available detached soil is not enough for transport and the flow can potentially detach the additional amount e - Δe^P. However, the resistance of the soil to the erosive forces of the flow depends on the soil properties and structure, as well as on the condition of the land surface (Olson and Wischmeier, 1963; Kemper, 1966; Wischmeier and Mannering, 1969; Grissinger, 1980). Consequently, the potential thickness of detachment by flow is modified by a flow detachment coefficient, a_f, yielding the following amount of soil detached by flow:

$$\Delta e_{fk} = -a_f \ (\Delta e^P - e) \ p_k,$$ (64)

where a_f ranges from zero to 1.0 depending on the soil erodibility. The detachment coefficients in Eqs. 63 and 64 are optimization parameters that are calibrated by fitting the sediment discharge rates to observed data.

2.4.4 Numerical Procedure for Sediment Routing

The equations of sediment supply and sediment mass conservation are coupled to the water routing scheme using the procedure described below to track the evolution of the sediment load, and to compute the aggradation and degradation of the land surface and stream channels.

Eq. 48 is a linear hyperbolic equation that may be solved by the method of characteristics. The steps given below follow those presented in section 2.3.2. The total differential of $A_{sk}(x,t)$,

$$\frac{\partial A_{sk}}{\partial x} \ dx + \frac{\partial A_{sk}}{\partial t} \ dt = dA_{sk},$$ (65)

and Eq. 48 form a system of two equations in the two unknown partial derivatives of A_{sk}, that is

$$\begin{bmatrix} 1 & V \\ dt & dx \end{bmatrix} \begin{bmatrix} \partial A_{sk}/\partial t \\ \partial A_{sk}/\partial x \end{bmatrix} = \begin{bmatrix} g_{\ell k} + g_{dk} \\ dA_{sk} \end{bmatrix} .$$ (66)

Since these derivatives do not exist along the characteristic paths, the determinant of the coefficient matrix vanishes at points on the characteristics. This condition yields the characteristic equation

$$\frac{dx}{dt} = V = Q/A$$ (67)

in agreement with the assumption that the sediment moves with the same velocity of the flow. One of the invariants of this solution also gives

$$\frac{dA_{sk}}{dt} = g_{\ell k} + g_{dk} ,$$ (68)

or, by integrating Eq. 68

$$A_{sk}(x,t) = A_{sk}(x_o,t_o) + \int_{t_o}^{t} (g_{\ell k} + g_{dk})d\xi, \qquad (69)$$

where $A_{sk}(x_o,t_o)$ is an initial value of A_{sk}. Applying this equation to two points $E(x_{i-1},t_{j-1})$ and $F(x_i,t_j)$ on a characteristic path (Fig. 9) and expressing the result in discrete form, gives

$$(A_{sk})_{i,j} = (A_{sk})_{i-1,j-1} + [(g_{\ell k})_{i,j} + (g_{dk})_{i,j}]\Delta t_j , \qquad (70)$$

in which $g_{\ell k}$ and g_{dk} are assumed uniformly distribured in the interval $x_{i-1} \leqq x \leqq x_i$. The potential transport capacity of the flow, C_k^P, is obtained from the formulas in section 2.4.2 using the average of the flow characteristics computed at E and F, and the sediment properties at point E. Substituting $(C_k^P \bar{A})$ for the right-hand-side of Eq. 70 and solving for $(g_{dk})_{i,j}$ yields

$$(g_{dk}^P)_{i,j} = \frac{1}{\Delta t_j} [C_k^P \bar{A} - (A_{sk})_{i-1,j-1}] - (g_{\ell k})_{i,j} , \qquad (71)$$

where the overbar denotes the average flow area, and g_{dk}^P is the potential change in detached soil storage caused by either erosion or deposition. <u>Deposition</u>: If $g_{dk}^P < 0$, the potential carrying capacity of the flow is less than the sediment present in the flow. Consequently, the sediment load transport rate is

$$Q (C_k)_{i,j} = \bar{Q} C_k^P , \qquad (72)$$

and the excess load, $- g_{dk}^P$, is deposited on the bed. However, whether this amount will reach the bed during the time step Δt depends on this being not less than the average time for the sediment particles to settle to the channel bed. Data by Jobson and Sayre (1970) and by Lean (1971) indicate that this settling time may be computed using the particle fall velocities in the quiescent fluid. Therefore, the actual deposition of a size fraction during the interval Δt is calculated from

$$(D_k)_{i,j} = -(g^P_{dk})_{i,j} \text{ , if } \beta \geq 1, \tag{73a}$$

or

$$(D_k)_{i,j} = -\beta(g^P_{dk})_{i,j} \text{ , if } \beta < 1, \tag{73b}$$

where $\beta = w_k \, \Delta t / \bar{h}$. The new bed elevation is

$$Z_{i,j} = Z_{i,j-1} + \frac{1}{\bar{P}} \sum_{k=1}^{n} \frac{(D_k)_{i,j}}{1-\lambda} . \tag{74}$$

Erosion: If $g^P_{dk} > 0$ the potential carrying capacity exceeds the amount of material in transport and, therefore, the flow will entrain additional material. In this case, one of two possible events may occur depending on whether g^P_{dk} is equal to or greater than the thickness, $(e_k)_{i,j-1}$, of the available detached soil. Let

$$(e_k)_{i,j} = (e_k)_{i,j-1} + (\Delta e_{rk})_{i,j-1} - (\Delta e^P_k)_{i,j} \tag{75}$$

denote the depth of detached soil in storage at the end of the time step Δt_j, in which

$$(\Delta e^P_k)_{i,j} = (g^P_{dk})_{i,j} \, \Delta t_j / \bar{P} . \tag{76}$$

is the depth of potential erosion by flow.

(i) If $(e_k)_{i,j} \geq 0$ the available detached soil is enough to supply the sediment entrained by the flow. In this case no erosion (of undetached soil) occurs, the transport rate at the end of the time step Δt_j is equal to the carrying capacity (Eq. 72), and $(Z_k)_{i,j} = (Z_k)_{i,j-1}$.

(ii) If $(e_k)_{i,j} < 0$ the availability of detached soil is less than the potential entrainment, and additional soil is detached by the flow. The depth of erosion by flow is

$$(\Delta e_{fk})_{i,j} = -a_f(e_k)_{i,j} , \tag{77}$$

from which

$$(g_{dk})_{i,j} = \bar{P}[(e_k)_{i,j-1} + (\Delta e_{rk})_{i,j} + (\Delta e_{fk})_{i,j}]/\Delta t_j. \qquad (78)$$

From Eqns. 70 and 78, the concentration of the updated load is

$$(C_k)_{i,j} = \frac{(A_{sk})_{i-1,j-1}}{\bar{A}} + \frac{\Delta t_j}{\bar{A}} (g_{\ell k})_{i,j}$$

$$+ \frac{\bar{P}}{\bar{A}} [(e_k)_{i,j-1} + (\Delta e_{rk})_{i,j} + (\Delta e_{fk})_{i,j}]. \qquad (79)$$

Finally, the new elevation of the eroded bed is

$$Z_{i,j} = Z_{i,j-1} + \sum_{k=1}^{n} \frac{(\Delta e_{fk})_{i,j}}{1-\lambda}. \qquad (80)$$

Substituting Eq. 72 or 79 into Eq. 44 gives the concentration of the total sediment load. The total concentrations existing on all the characteristics paths reaching a certain location define the outflow sedimentgraph at that location.

In some instances, the time step size selected for water routing may yield a cluster of small space increments (Fig. 8b). Repeating the sediment calculations for each of these increments may not be necessary when the sediment routing parameters are only required at points spaced farther apart. In these cases it is more efficient to combine a number of space and time steps used for water routing, into larger steps for sediment routing. To this end, the program contains an option to compute the sediment routing parameters only at points satisfying the conditions

$$x_n = x_m + \sum_{i=m}^{n} \Delta x_i \text{ , such that } \sum_{i=m}^{n} \Delta x_i \leq GDX, \qquad (81a)$$

$$t_n = t_m + \sum_{j=m}^{n} \Delta t_j \text{ ,} \qquad (81b)$$

where GDX is a user supplied parameter (Fig. 8b).

To illustrate the relative accuracy of the present model, it is applied to several examples reported in the literature. These are the hypothetical three-plane cascade discussed by Kibler and Woolhiser (1970); the experiments performed by Iwagaki (1955) involving unsteady, open-channel flow with lateral inflow; the runoff studies carried out by Schaake (1970) in a small urban catchment; and two agricultural catchments reported by Burford and Clark (1973). The PSF and ASF schemes are compared on the three plane cascade example. The results from the ASF shock-fitting scheme are also compared with those obtained with the implicit finite-difference (FD) scheme presented by Li et al. (1975a).

The computational parameters used in each example are given in Table 1. The kinematic wave parameter n, Eq. 26, is kept fixed at 1.50 (Kibler and Woolhiser, 1970; Singh, 1975). With n fixed, the calculations only required characterization of the parameter α. The values of α, estimated by Kibler and Woolhiser (1970), are used in the three-plane cascade computations. In all the other examples, this parameter is computed, using the relationship proposed by Singh (1975)

$$\alpha = C_1 + C_2 \, (S_0)^{\frac{1}{2}} \, , \tag{82}$$

where C_1 and C_2 are constants to be optimized in each case. This relationship was chosen only for its simplicity. However, any other expression could have been used, since the computational efficiency of the schemes is not contingent on the manner α is estimated.

3.1   HYPOTHETICAL KINEMATIC CASCADE

Kibler and Woolhiser (1970) used a three-plane kinematic cascade to illustrate the formation of kinematic shock waves. The planes are 400 ft. long with slopes 0.04, 0.01, and 0.0025, respectively. The lateral inflow is a rainfall pulse with an intensity of 0.75 inch/hr and a duration of 30 min. The necessary condition (Eq. 37) is satisfied at the unions of the three planes. Thus, shock-forming regions exist in the rising limbs of the upstream inflows to the second and third planes.

The characteristics and shock paths crossing the x-t domain of the cascade are presented in Fig. 10. The shock paths were computed using the PSF scheme. Because there is no upstream inflow to the first plane, the
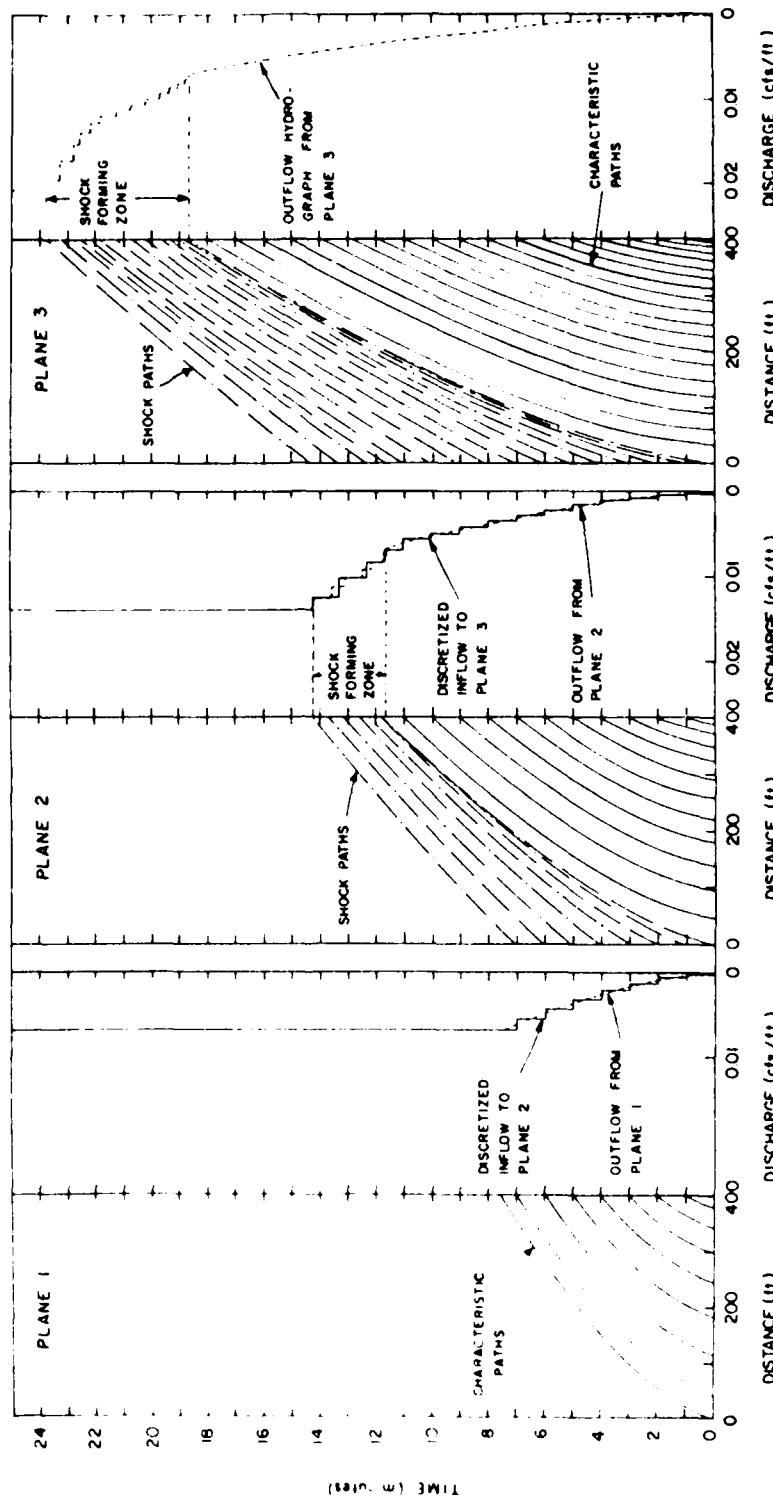
Fig. 10 Propagation of shocks across the three plane cascade

outflow from this plane is a smooth hydrograph generated by the characteristic waves emanating from dry ground conditions. This hydrograph is used as inflow to the second plane. The rising limb satisfies the shock forming conditions (Eq. 36), and so, small shocks are introduced by discretizing this portion of the hydrograph. These shocks are projected to the downstream boundary along with the characteristics emanating from the initial dry ground condition. There they define an outflow hydrograph containing a smooth rising limb formed by the characteristic waves, followed by a piecewise continuous part formed by the shock waves. To reduce the number of shocks to be traced in this example, shocks arriving within the same time step are assumed to merge and proceed as a single shock to the next plane. The same procedure is applied in routing over the third plane. The hydrograph at the cascade outlet contains all the shocks crossing the last two planes. The shocks slow down as they enter the third plane, reflecting the decrease in the value of α. The complete outflow hydrograph is compared in Fig. 11 to the analytical solution of Kibler and Woolhiser (1970). Their solution displays the two shocks emanating from the unions of the planes. The two hydrographs are quite close, which shows that the approximation introduced in formulating the PSF solution does not detract from its accuracy.

The same hydrograph calculation was carried out using the ASF and FD schemes. The ASF solution is plotted in Fig. 11. It exhibits a smooth rising limb showing the overall effect of the shock waves, and is in good agreement with the two other solutions. Moreover, it is twice as fast as the PSF scheme (Table 1). It is thus evident that the ASF scheme, in addition to being easier to work with, gives results as accurate as the analytical solution. For these reasons the PSF technique was abandoned in favor of the more efficient ASF solution.

The hydrograph computed, using the FD scheme with the same values of α, is compared in Fig. 12 with the ASF solution. Although the hydrographs agree in their predicted yields, the FD solution exhibits a pronounced delay and reduction of the peak. In an attempt to improve this solution, the FD calculation was repeated using a new optimized value of the kinematic parameter. The result shows improvement in the peak estimate but an overall deterioration of the hydrograph shape (Fig. 12). This inability of the FD scheme to reproduce the analytical solution is further discussed in the context of the next example.
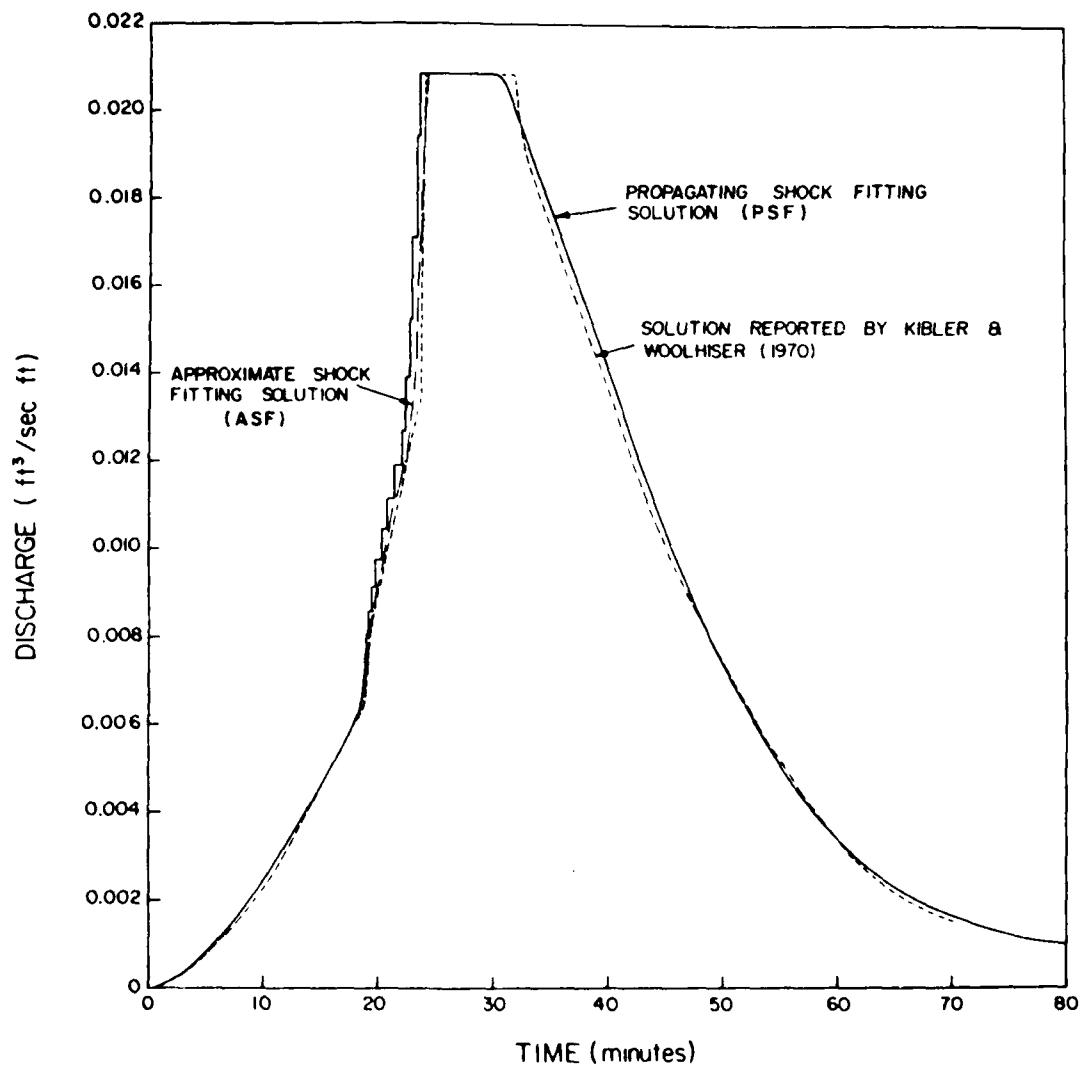
Fig. 11 Outflow hydrograph for three-plane cascade showing effect of shocks

1.55
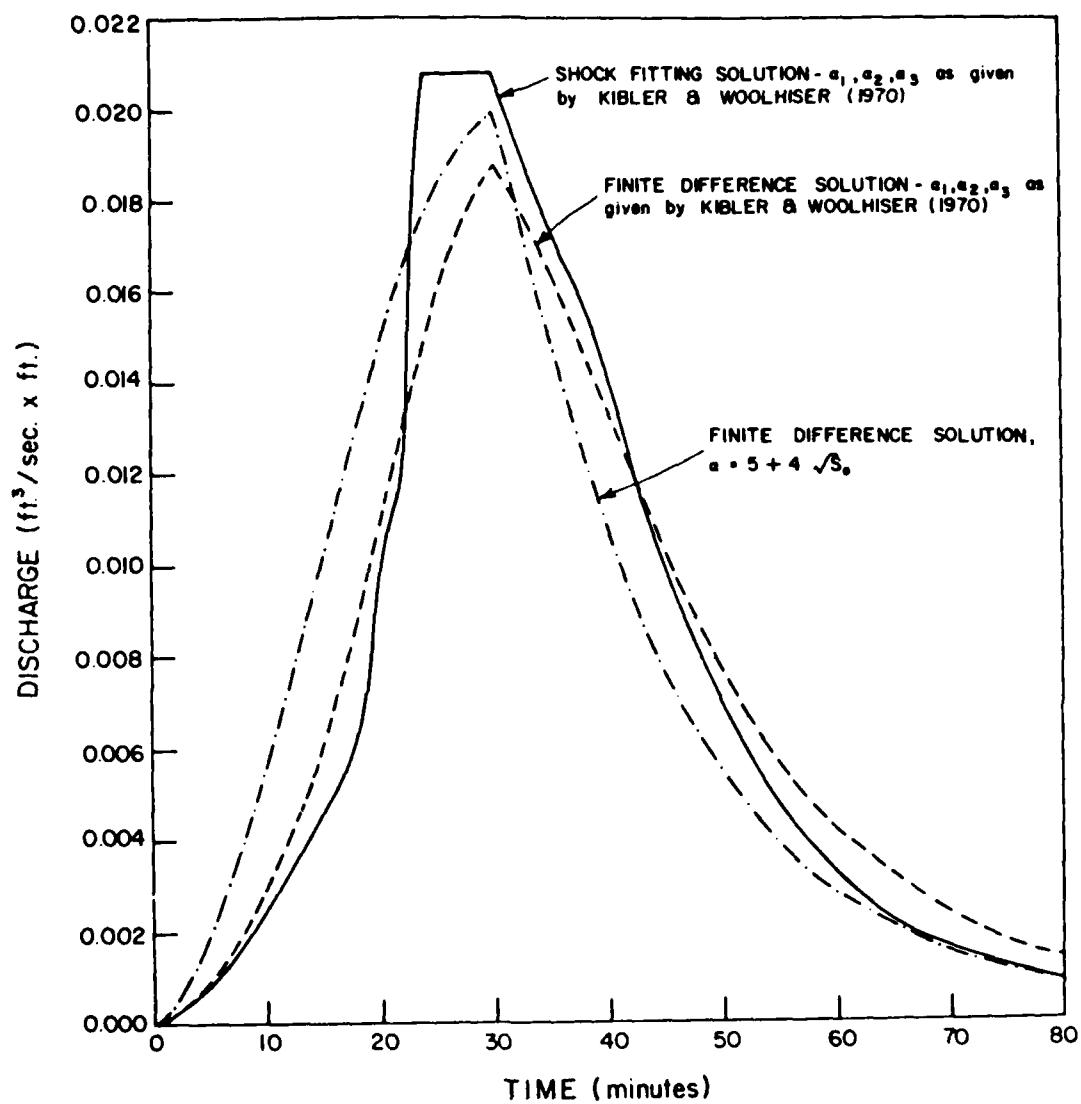
Fig. 12 Comparison of finite-difference results with approximate
shock-fitting solution

3.2 UNSTEADY CHANNEL FLOW

Iwagaki (1955) reported a set of laboratory experiments of unsteady flow with lateral inflow in a smooth open channel 7.3 ft long. The channel was divided into three sections of equal lengths and different slopes. From the upstream end, the slopes were 0.020, 0.015, and 0.010. The lateral inflow was adjusted so that each section would receive a constant rate of inflow, with the upper, middle, and lower receiving 0.0425, 0.0251, and 0.0315 inch/sec. The durations of lateral inflow used in the experiments were 10, 20, and 30 sec. Under these flow conditions, Eq. 37 predicts a shock forming zone at the union of the upper and middle sections.

Figs. 13, 14, and 15 show that the hydrographs computed with the ASF scheme are in good agreements with the partial-equilibrium hydrographs, measured by Iwagaki. The kinematic parameter α was adjusted by fitting the data plotted in Fig. 13. Because the slopes, geometries, and hydraulic roughness were the same in all three experiments, the same value of α was used in the calculation of the other two hydrographs. These solutions correctly simulated the shock formation and its arrival time at the outlet. This is clearly depicted in Fig. 15, where the hydrograph peaks immediately after the lateral inflow terminates and falls continuously, until a sudden rise occurs when the shock arrives. Fig. 14 shows the shock arriving shortly after the first peak, whereas in Fig. 13 the shock arrives well ahead of the peak.

Two different hydrographs computed with the FD scheme are given in the same figures. The hydrographs computed with the values of α used in the ASF solution do not agree very well with the measurements and, in addition, they do not reproduce the aforementioned shock effect. A second solution was obtained by recalibrating the kinematic parameter but the new hydrographs do not exhibit any better agreement. In the present example, the shock formation is an intrinsic part of the solution to the kinematic wave approximation. However, because of its smoothing effect, the FD scheme is unable to reproduce this important aspect of the analytical solution. In addition, this scheme required between 50 and 100 percent more computing time that the ASF solution (Table 1).
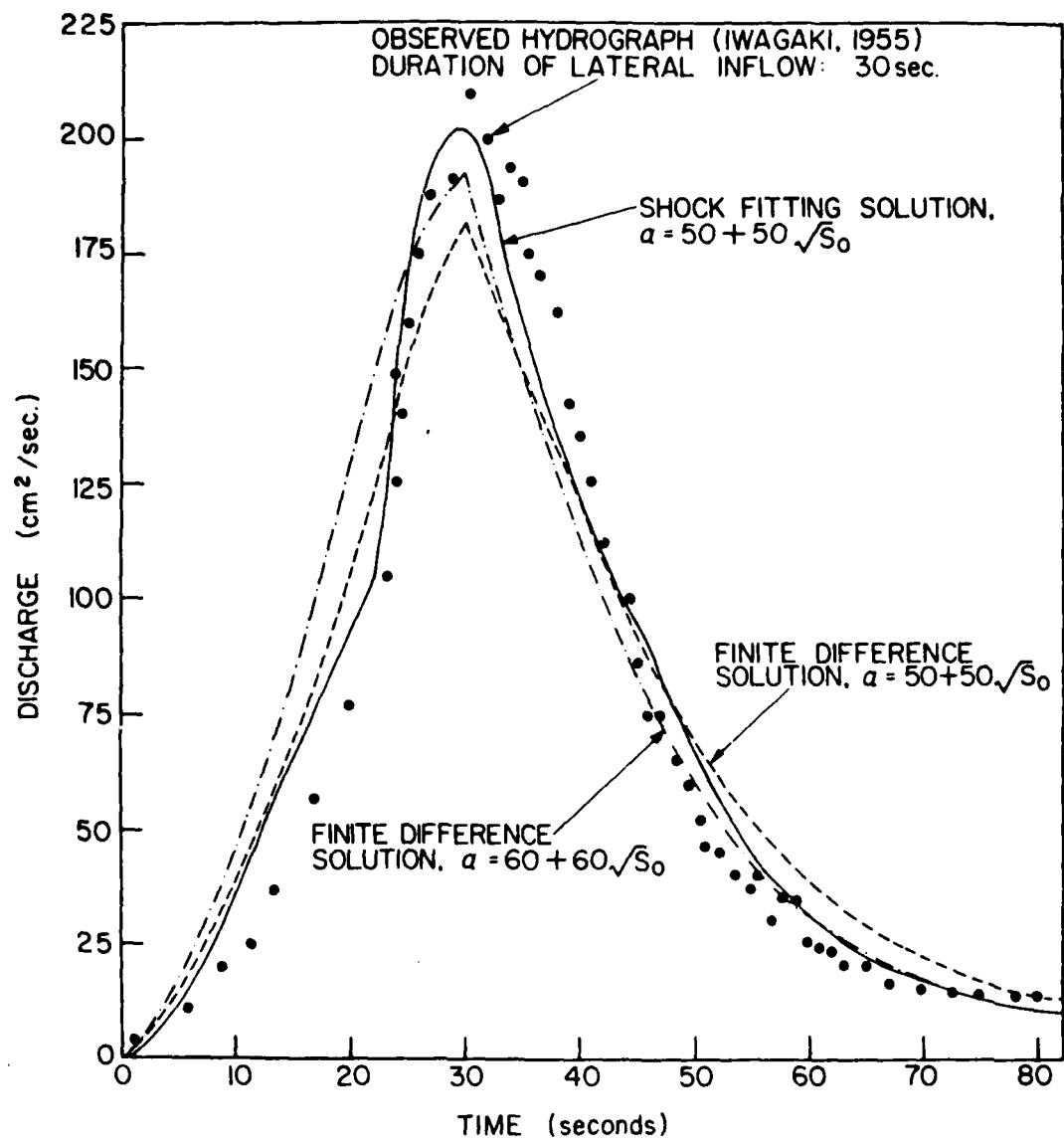
Fig. 13 Simulation of Iwagaki's partial-equilibrium hydrograph for lateral inflow duration of 30 sec

I.58
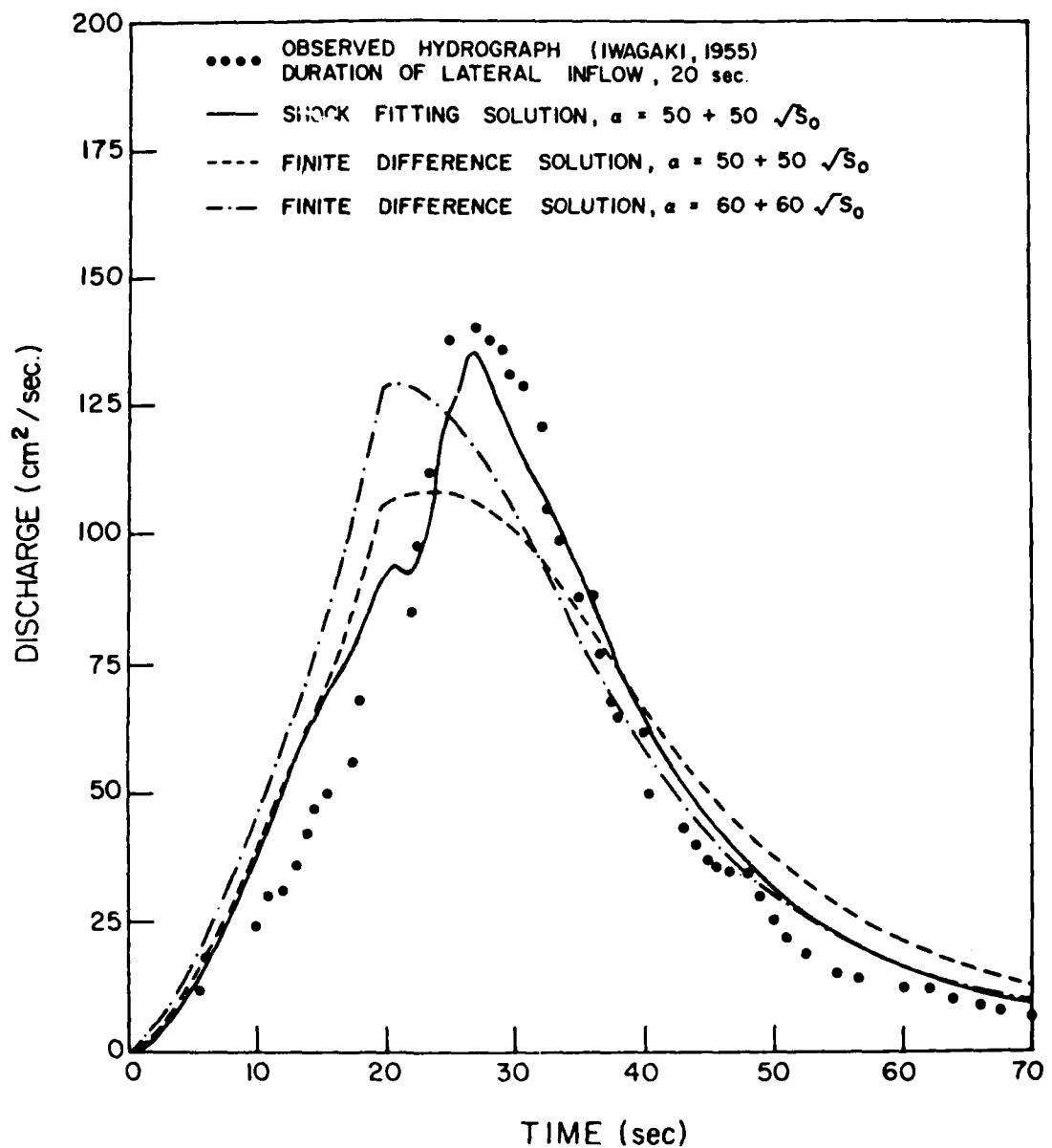
Fig. 14 Simulation of Iwagaki's partial-equilibrium hydrograph for lateral
inflow duration of 20 sec

I.59
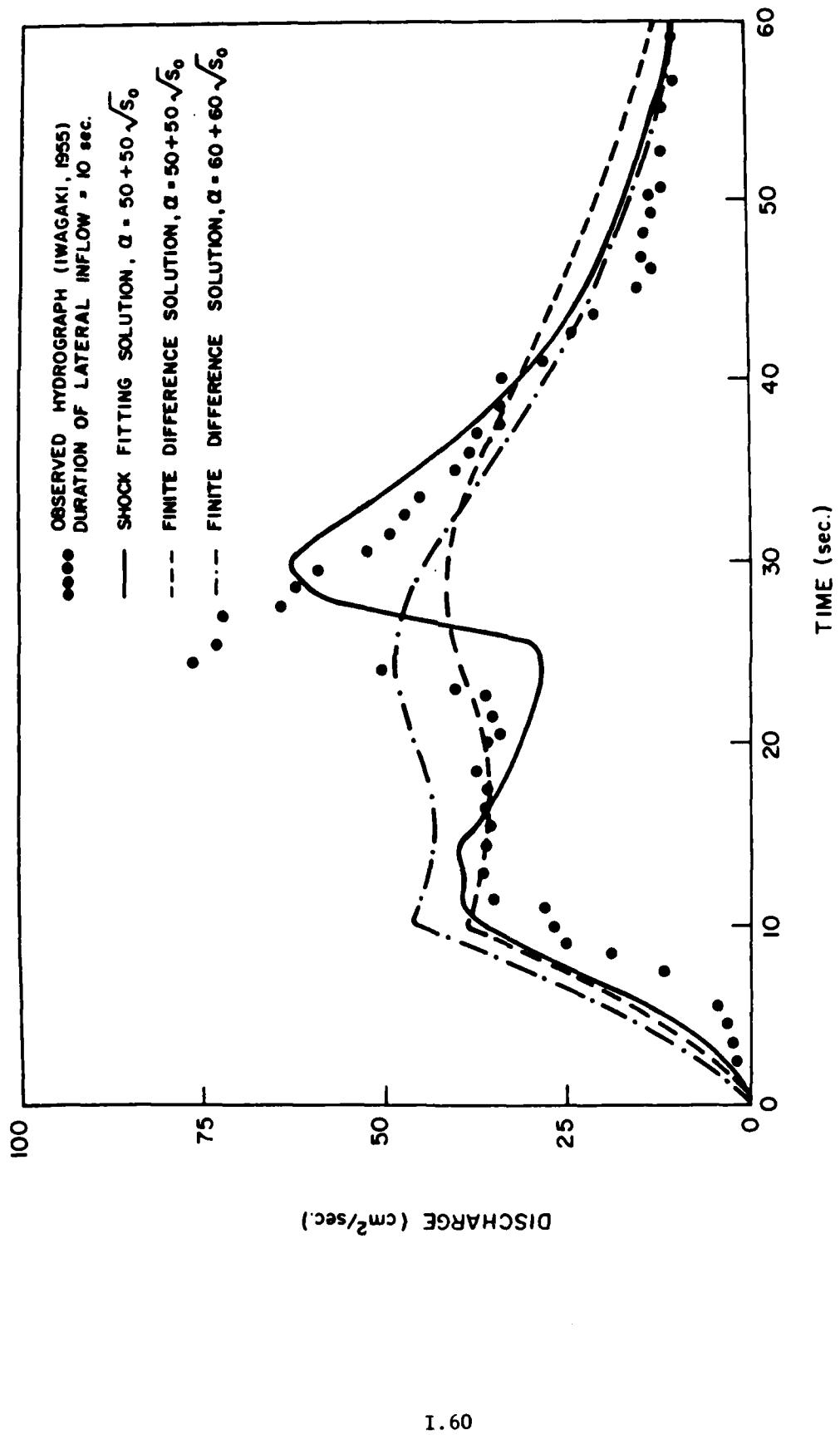
Fig. 15 Simulation of Iwagaki's partial-equilibrium hydrograph for lateral inflow duration of 10 sec
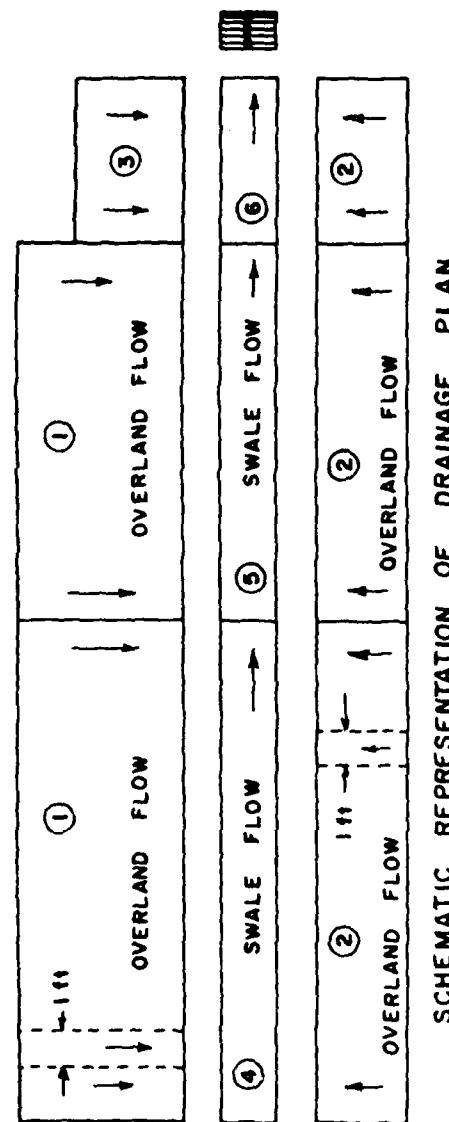
3.3   URBAN CATCHMENT

This example is used to illustrate that the shock-fitting technique presented in this report is applicable to a combination of interconnected overland and channel segments. The case considered herein is the small urban catchment, reported by Schaake (1970). In this publication Schaake describes an event labeled 3 SPL1 on a 0.39 acre impervious parking lot labeled SPL1. He represented the catchment by a number of interconnected overland segments and V shaped channels (Fig. 16). The overland segments vary from 20 to 36 ft in length, and their slopes range from 0.0167 to 0.019. The V-shaped channels have lengths varying from 50 to 165 ft, and slopes ranging from 0.0148 to 0.0213. The channel-side slopes were all 1:113. The same geometric representation is used in the simulations reported herein.

The runoff hydrographs measured at the outlet of the catchment and the hydrographs computed with the ASF and FD schemes are shown in Fig. 17. The value of α was obtained by fitting the measured data. The result obtained with the ASF scheme overpredicts the first peak but agrees very well with the rest of the data. The FD calculation obtained with the same α does not predict the second peak well. In an attempt to improve the second peak, a second calculation using the FD scheme was made by recalibrating α. This improved the second peak but did not help the rest of the hydrograph (Fig. 17). In general, the hydrographs predicted by the FD scheme do not exhibit the significant deviations shown in the previous calculations. This is because, in this example the lateral inflow rate changes rather smoothly, thus reducing the magnitudes and effects of shocks. Also, the slopes in the previous two examples exaggerate the development of shocks, whereas in this example the slopes are nearly the same, thus leading to much smaller shocks. Nevertheless, these solutions take twice as much computing time as the ASF calculation (Table 1).

3.4   AGRICULTURAL CATCHMENTS

The data used in these tests were obtained from the USDA experimental catchments W-5 southwest of Holly Springs, MS, and R-5 near Chickasha, OK (Burford and Clark, 1973). Catchment W-5 drains a 1.76 mile^2 area (Fig. 18), with a good mixture of cultivated land, timber, pasture, and idle land. Catchment R-5 has an area of 23.7 acres, and is range land with an excellent native grass cover (Fig. 19). These catchments were chosen

I.61

SCHEMATIC REPRESENTATION OF DRAINAGE PLAN

SEGMENT	LENGTH (ft)	WIDTH OR DIA. (ft)	SLOPE (ft/ft)	SIDE SLOPE	INFLOW TO SEGMENT	
					LATERAL INFLOW	UPSTREAM INFLOW
①	36	1	.019	—	RAINFALL	
②	20	1	.0167	—	RAINFALL	
③	25	1	.019	—	RAINFALL	
④	165	—	.0148	113:1	RAINFALL	① AND ②
⑤	100	—	.0213	113:1	① AND ②	④
⑥	50	—	.0213	113:1	② AND ③	⑤

PHYSICAL CHARACTERISTICS OF COMPONENTS IN THE SCHEMATIC REPRESENTATION

Fig. 16 Characteristics of small urban catchment (after Schaake, 1970)

I.62
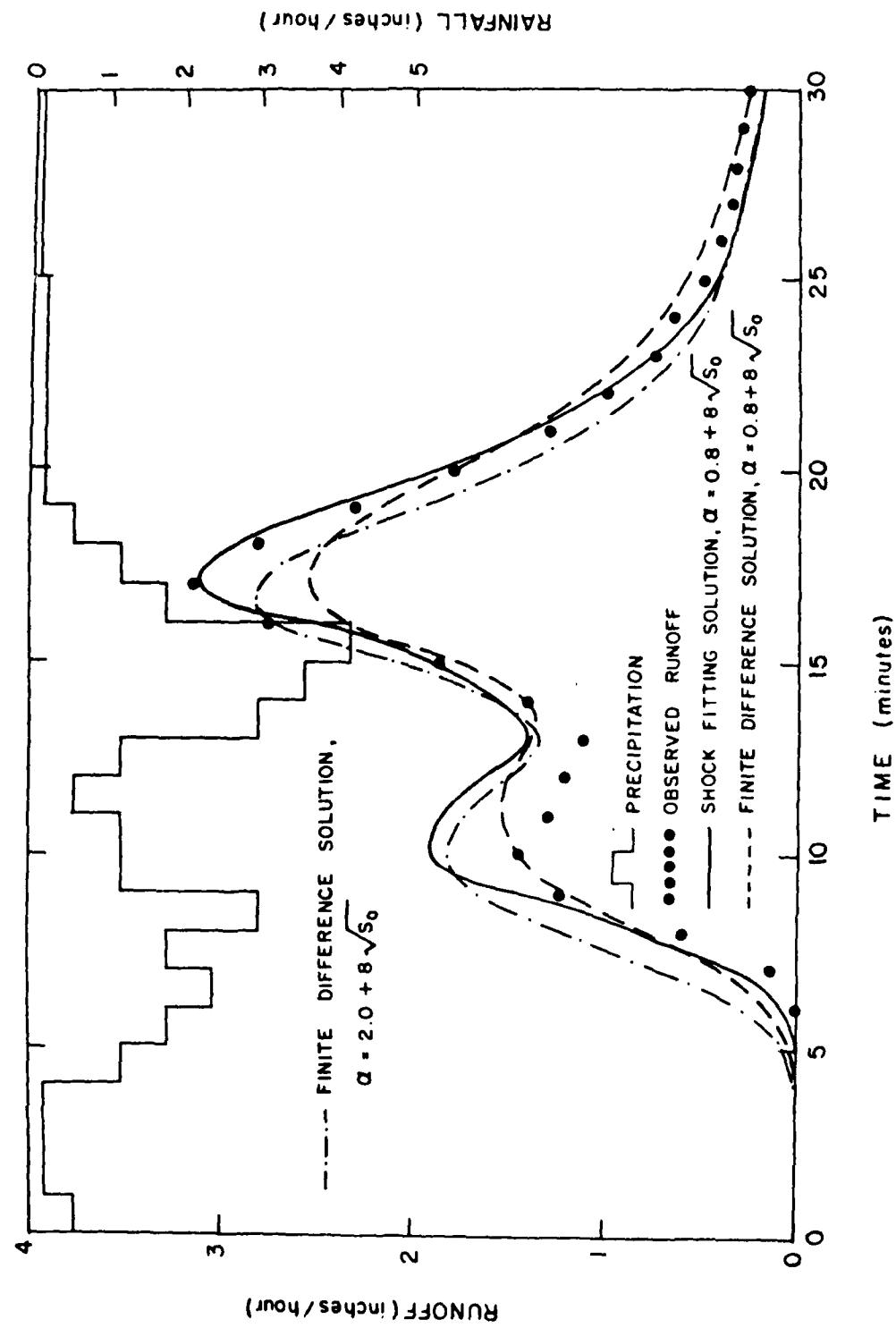
Fig. 17 Simulation of runoff from small urban catchment

because of diversity and availability of most of the required data. Sediment records were available for catchment R-5, but the sediment yield was so small that no comparisons were made between measured and computed sediment discharges.

The model was calibrated using the event of February 21, 1971, on catchment W-5, and the event of May 6, 1969, on catchment R-5. Infiltration parameters for catchment W-5 were estimated from information reported by Smith and Parlange (1978) for Colby swelling type soils, because very little infiltration data were available. The infiltration parameters for catchment R-5 were obtained from an average infiltration curve obtained from a large number of infiltrometer runs conducted in the fall of 1977. The calibrations were carried out by adjusting first the flow resistance parameters (Eq. 82) to match the hydrographs, and then the sediment-model parameters (Eqns. 63 and 64) were adjusted to fit the sedimentgraphs. These same parameters were used in simulating all the remaining events. The results of these tests were reported in an earlier paper by Alonso et al. (1978).

Examples of the comparison between the simulated and the measured hydrographs and sedimentgraphs are shown in Figs. 20, 21, and 22. A total of nine events on catchment W-5 and two on catchment R-5 were simulated. The agreement between the shapes of measured and simulated events is satisfactory. Comparisons between measured and computed water yield, peak runoff rates, sediment yield, and peak sediment discharge are given in Figs. 23 and 24. These plots show that the model estimates both yields and peaks within a range of about ±40 percent of measured values. The limited number of events used in this study precluded an estimation of the confidence level of the range of variability. The results presented in Figs. 20 through 24 indicate that simulations of different size events using only one set of parameters for each catchment, were satisfactory. This suggests that the model could be used to predict the response of a catchment to different management practices, if the model parameters associated with each practice could be accurately estimated. Also, the above results indicate that the model could be readily transferred to ungaged catchments, if the model parameters were properly regionalized.
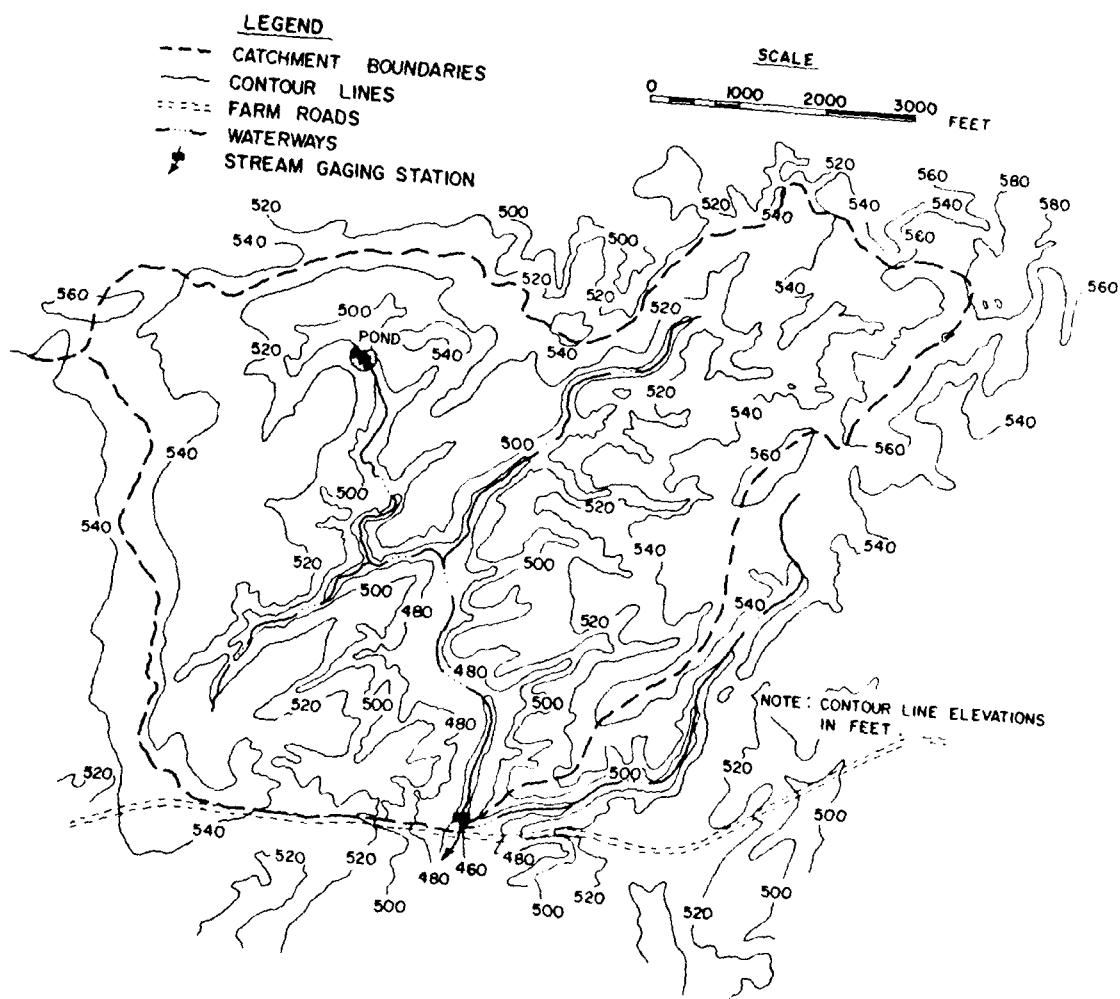
Fig. 18 Topographic map of catchment W-5 near Holly Springs, Mississippi

I.65
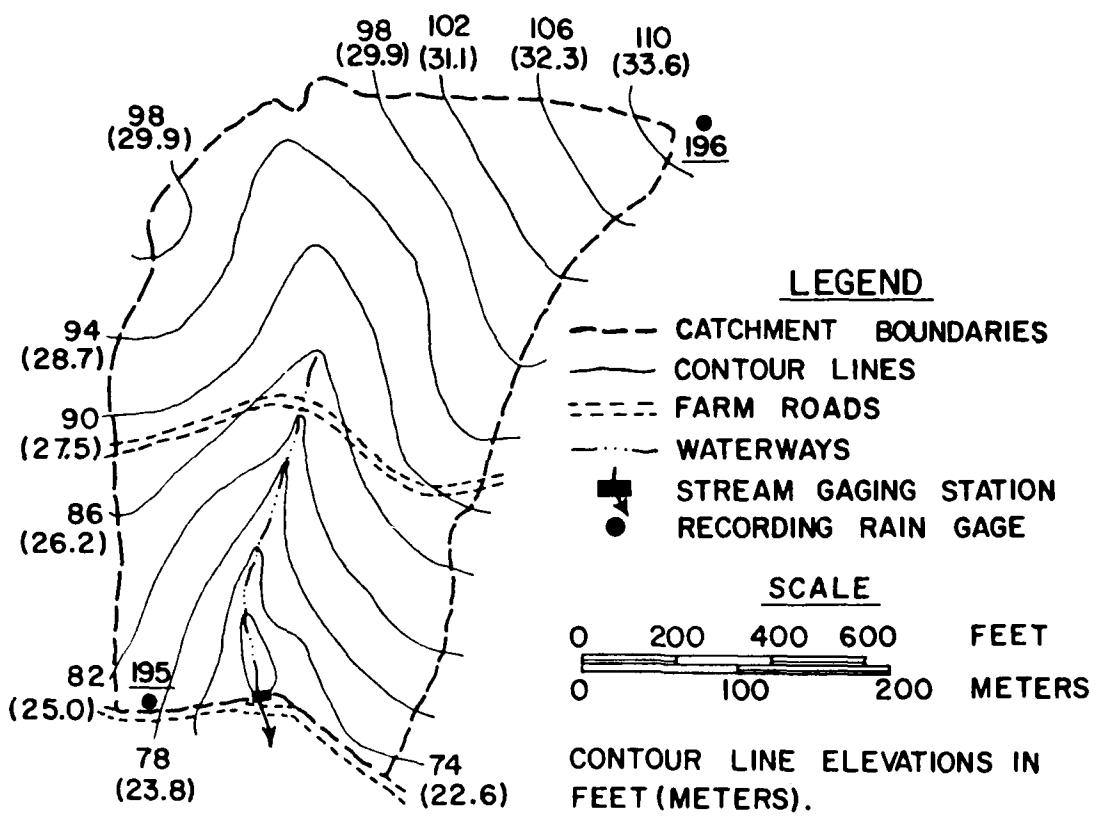
Fig. 19 Topographic map of catchment R-5 near Chickasha, Oklahoma

1.66
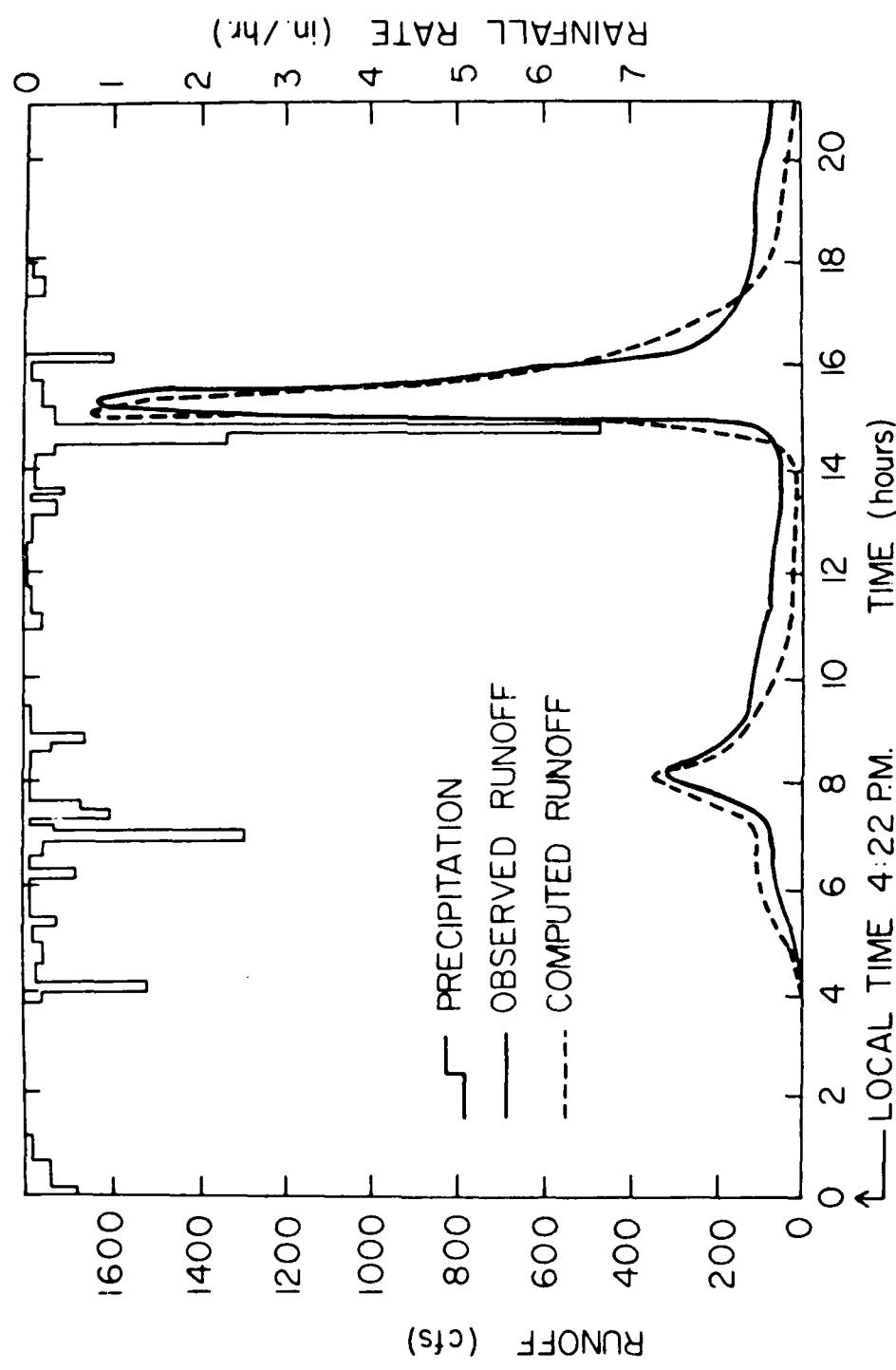
Fig. 20 Runoff hydrograph from catchment W-5 for the February 21, 1971 event
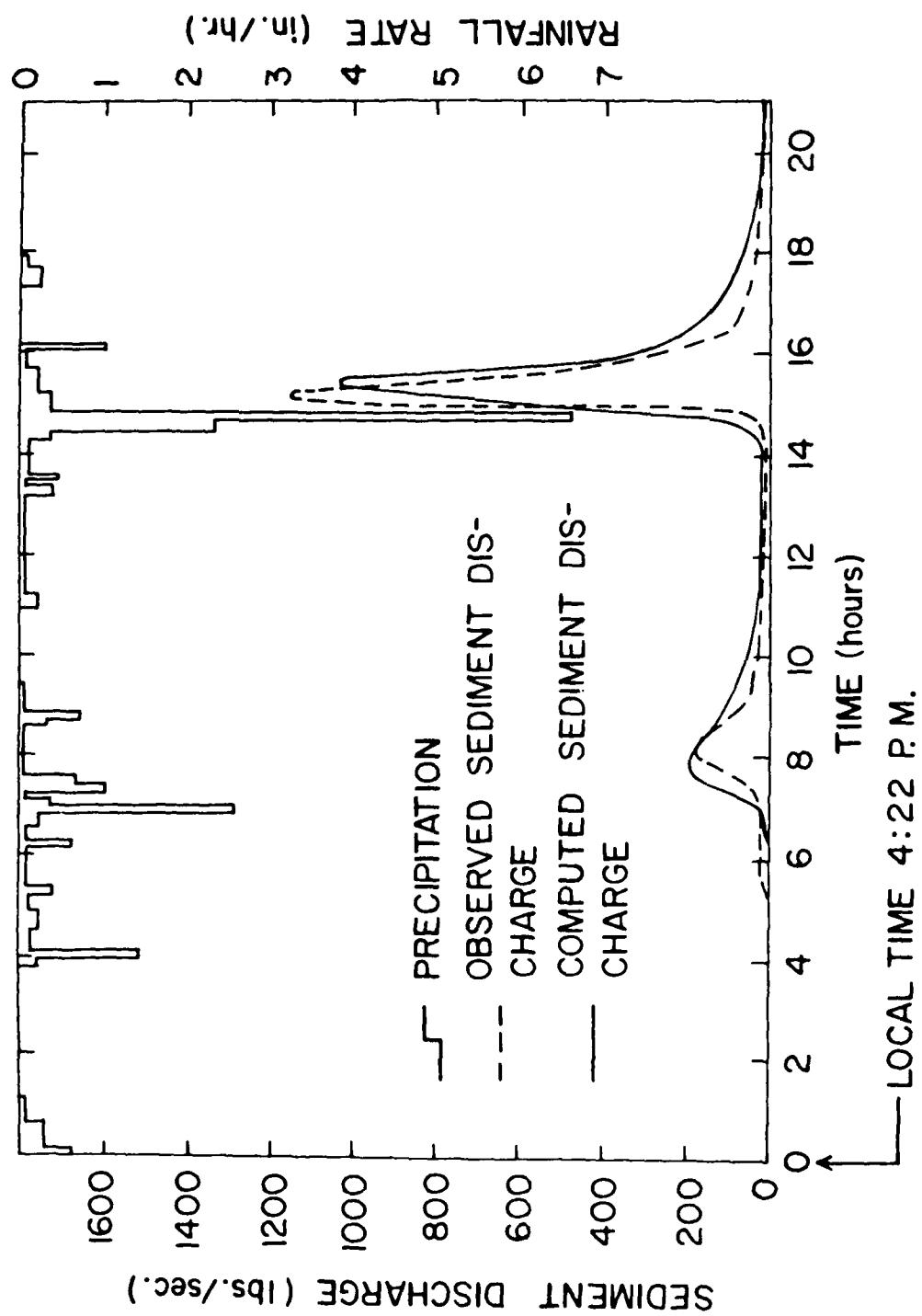
Fig. 21 Sedimentgraph from catchment W-5 for the February 21, 1971 event
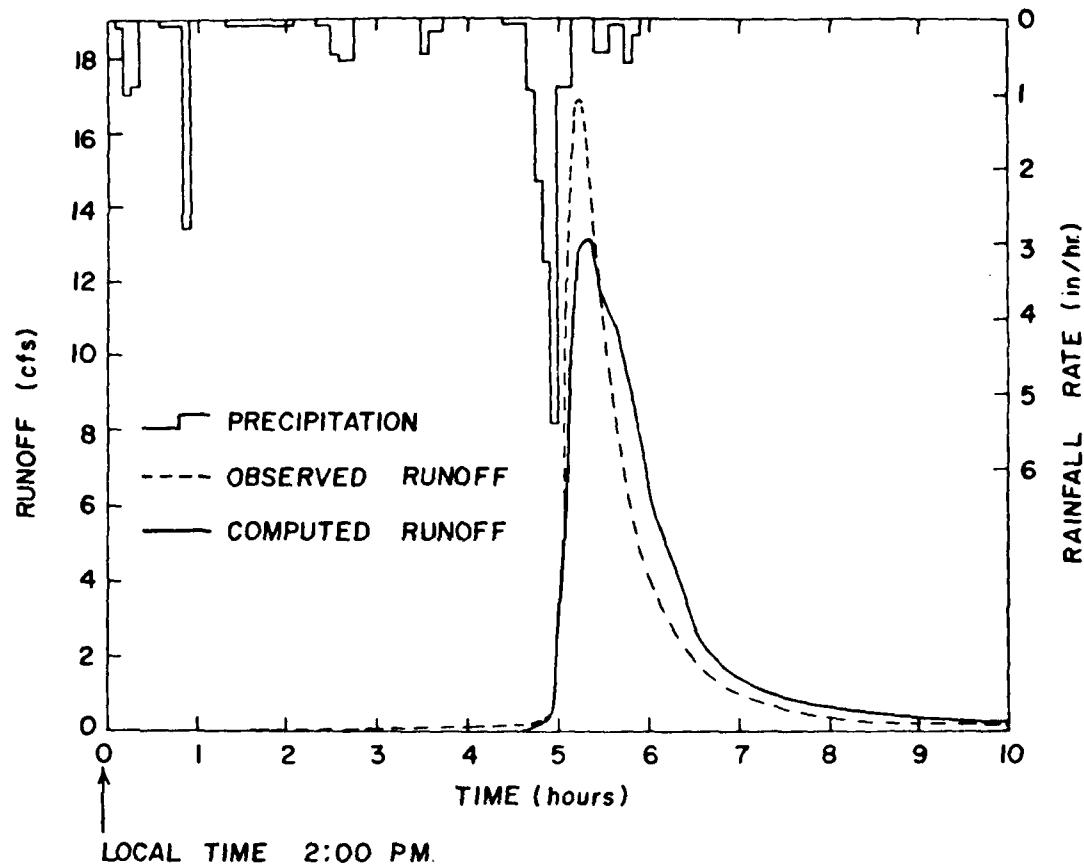
Fig. 22 Runoff hydrograph from catchment R-5 for the May 6, 1969 event
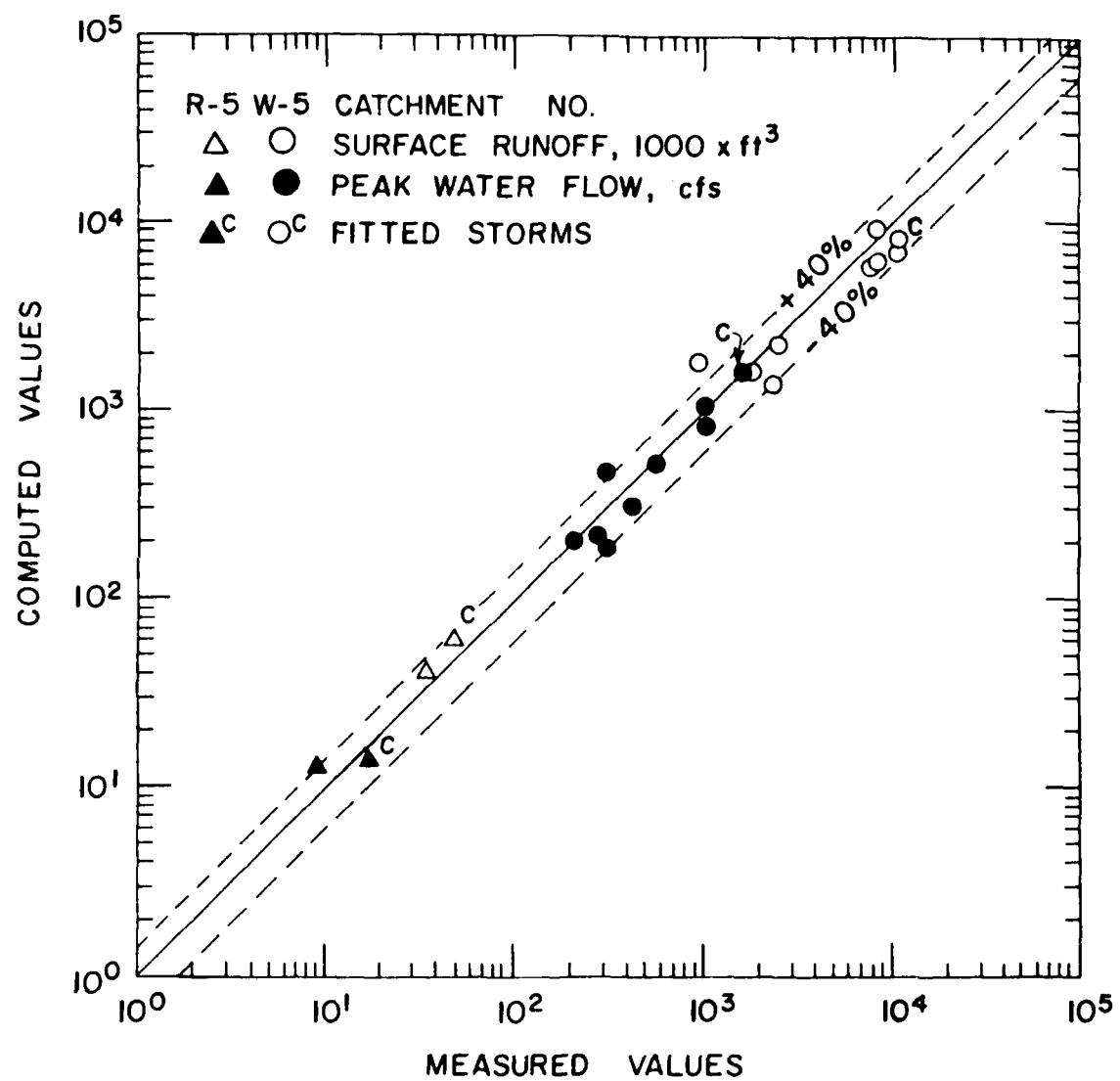
Fig. 23 Comparison of measured and computed water yields and peaks

I.70
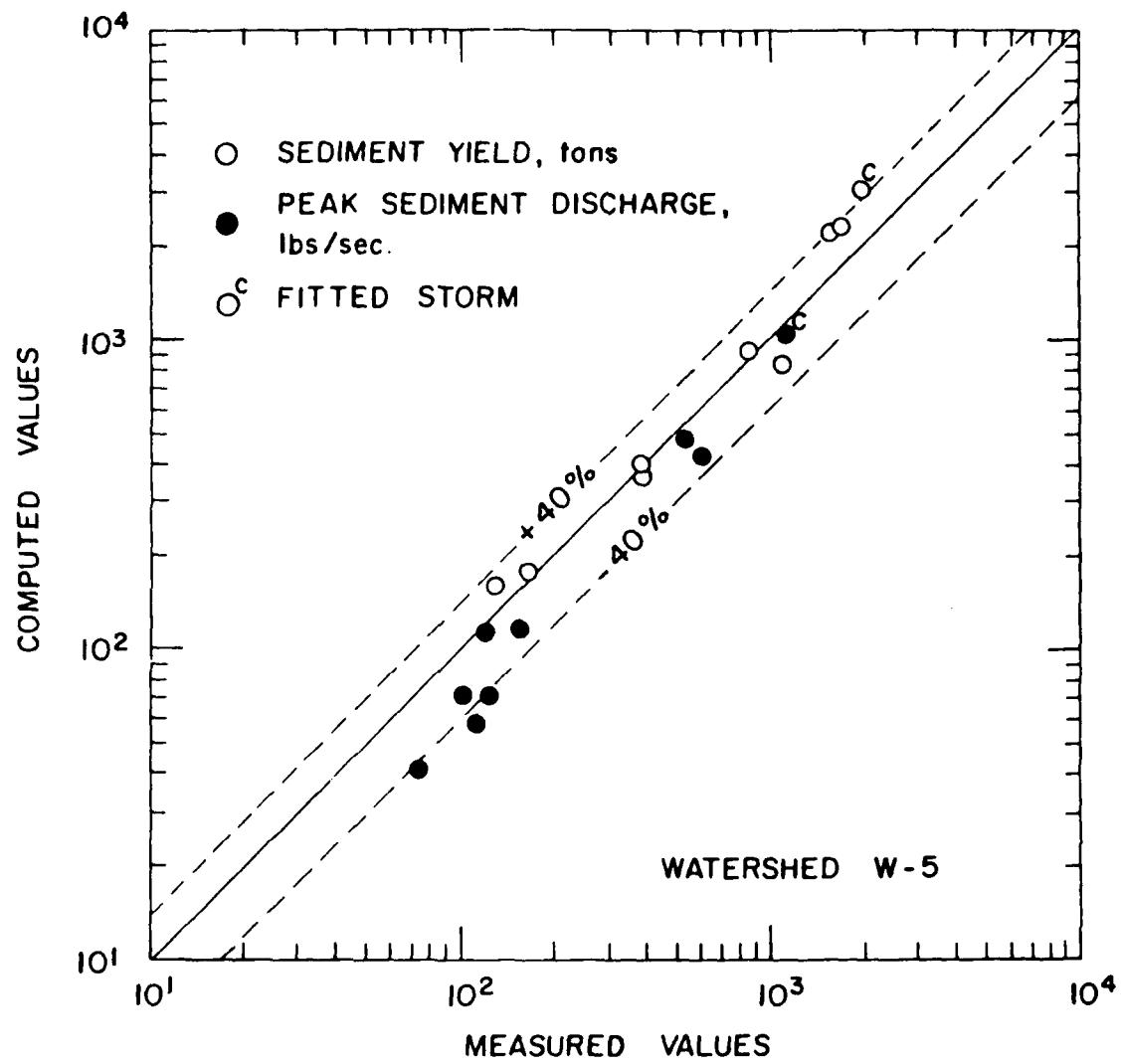
Fig. 24 Comparison of measured and computed sediment yields and peaks

Table 1. Flow routing parameters and computing times

Example		Δt	n	α	C_1	C_2	Δx Approx. Shock Fitting	Δx Finite Difference	CPU Time[c] Approx. Shock Fitting	CPU Time[c] Finite Difference	Results shown in Figure No.
Three-Plane Kinematic Cascade		60 sec	1.50	α_1=10.0 α_2= 5.0 α_3= 2.5	--	--	variable	24.4 m[d]	2.27[e] sec	2.47 sec	11,12
Unsteady Channel Flow with Lateral Inflow		60 sec	1.50	--	5	4	--	24.4 m	--	2.37 sec	12
	30[a] sec	1 sec	1.50	--	50	50	variable	1 m	1.97 sec	3.02 sec	13
		1 sec	1.50	--	60	60	--	1 m	--	2.74 sec	13
	20[a] sec	1 sec	1.50	--	50	50	variable	1 m	1.90 sec	3.42 sec	14
		1 sec	1.50	--	60	60	--	1 m	--	2.58 sec	14
	10[a] sec	1 sec	1.50	--	50	50	variable	1 m	1.95 sec	3.05 sec	15
		1 sec	1.50	--	60	60	--	1 m	--	2.78 sec	15
Small Urban Catchment		60 sec	1.50	--	0.80	8	variable	(1)[b]-2.19 m (2)-2.03 m (3)-2.54 m (4)-10.07 m (5)-6.10 m (6)-5.08 m	0.83 sec	1.73 sec	17
		60 sec	1.50	--	2	8	variable	(1)[b]-2.19 m (2)-2.03 m (3)-2.54 m (4)-10.07 m (5)-6.10 m (6)-5.08 m	--	1.68 sec	17
Agricultural catchment		5 min	1.50	--	0.35	2.5	variable	variable	42.3 sec	74.9 sec	20

a - lateral inflow duration.
b - Kinematic-cascade component (Figure 16).
c - Calculations were performed in a DEC 10 high-speed digital computer.
d - 0.3048 m = 1 ft
e - CPU time for PSF solution: 5.58 sec (Figure 11).

I.72

4   CONCLUSIONS AND RECOMMENDATIONS

4.1   CONCLUSIONS

1. A numerical model for routing water and sediment on small catchments has been developed. The model accepts any single rainfall hyetograph and produces runoff and sediment hydrographs for the modeled catchment.

2. The model is developed on a general basis so that it may be applied to any agricultural catchment by changing only the input data. The approximate range of basins over which the model is applicable is from a few acres to about 5 square miles.

3. The model is based on the physical processes governing the mechanics of water and sediment movement and requires the calibration of four parameters.

4. The model can be used to simulate the effect of different land uses on the water and sediment yields from the modeled catchment.

5. The model predicts the surface component only. It does not presently predict subsurface and groundwater movement.

6. The applicability of the model is restricted to streams where the channel geometry does not change significantly during a storm event, and in which the kinematic-wave approximation for flow routing is valid.

7. The present model simulates single storm events; the user must estimate the initial conditions for the storm. The model can still be applied to a sequence of rainfall events if the user can make satisfactory estimates of the initial soil moisture conditions. In this case the model can be used to predict a sequence of surface runoff and sediment transport events.

8. The model has been validated with several data sets including data from the natural catchments W-5 in northern Mississippi, and R-5 near Chickasha, Oklahoma. The shape of water and sediment hydrograph and total water and sediment yields of a number of events were satisfactorily simulated.

4.2   RECOMMENDATIONS

1. It is recommended that the model be put to work on real systems. The evaluation and continuous updating of the model are essential to its credibility and effectiveness.

2. It is recommended that the model be further developed, or modified, to permit continuous simulation over long time spans (20 to 50 years). This is essential in evaluating the long term response of a catchment, or stream network, which is dependent not only on the history of management practices, but also on the sequence of storm events.

3. It is recommended that the model be further developed to track the channel geometry of streams that become unstable due to bank erosion and deposition.

4. It is recommended that data gathering efforts be continued to provide an adequate base for further model development and validation.

REFERENCES

Agricultural Research Service, "Present and Prospective Technology for Predicting Sediment Yields and Sources," Proceedings, Sediment-Yield Workshop, Oxford, MS, 1972 (USDA Publication ARS-S-40, 285 p., 1975).

Alonso, C. V., DeCoursey, D. G., Prasad, S. N., and Bowie, A. J., "Field Test of a Distributed Sediment Yield Model," Proceedings, 26th Annual Hydraulics Division Specialty Conference, ASCE, pp. 671-678, 1978.

Alonso, C. V., Neibling, W. H., and Foster, G. R., "Estimating Sediment Transport Capacity in Watershed Modeling," paper accepted for publication in the Transactions of the American Society of Agricultural Engineers, 1981.

Amerman, C. R., Klute, A., Skaggs, R. W., and Smith, R. E., "Soil Water," Reviews of Geophysics and Space Physics, Vol. 13, No. 3, pp. 451-454, 1975.

Borah, D. K., The Dynamic Simulation of Water and Sediment Movement in Watersheds, Ph.D. Dissertation, School of Engineering, The University of Mississippi, University, Mississippi, 184 p., 1979.

Borah, D. K., Prasad, S. N., and Alonso, C. V., "Kinematic Wave Routing Incorporating Shock Fitting," Water Resources Research, Vol. 16, No. 3, pp 529-541, 1980.

Brakensiek, D. L., "A Simulated Watershed Flow System for Hydrograph Prediction: A Kinematic Application," Proceedings, Int. Hydrology Symposium, Paper No. 3, Fort Collins, Colorado, 1967.

Burford, J. B., and Clark, J. M., Compilers, "Hydrologic Data for Experimental Agricultural Watersheds in the United States," USDA Miscellaneous Publication No. 1262, 634 p., July, 1973.

Chow, V. T., Runoff, Section 14, Handbook of Applied Hydrology, McGraw-Hill, New York, 1964.

Crawford, N. H., and Linsley, R. K., "Digital Simulation in Hydrology: Stanford Watershed Model IV," Technical Report, No. 39, Dept. of Civil Engr., Stanford University, Stanford, California, July, 1966.

Dawdy, D. R., Litchy, R. W., and Bermann, J. M., "A Rainfall-Runoff Simulation Model for Estimation of Flood Peaks for Small Drainage Basin," USGS professional paper 506-B, 1972.

Donigian, A. S., and Crawofrd, N. H., "Modeling Pesticides and Nutrients on Agricultural Lands," Report EPA-600/2-76-043, Environmental Protection Agency, 332 p., 1976.

Eagleson, P. S., Dynamic Hydrology, McGraw-Hill, New York, 1970.

Gottschalk, L. C., and Brune, G. M., "Sediment Design Criteria for the Missouri Basin Loess Hills," Technical Publication No. 97, USDA-SCS, 1950.

Graf, W. H., Hydraulics of Sediment Transport, McGraw-Hill Co., New York, 1971.

Grissinger, E. H., "Bank Erosion of Cohesive Materials," Proceedings, International Workshop on Engineering Problems in the Management of Gravel-Bed Rivers, Greggnog Hall, Newton, Powys, United Kingdom, June 1980.

Hagan, R. M., Haise, H. R., and Edminster, T. W., Editors, "Irrigation of Agricultural Lands," Monograph 11, American Society of Agronomy, Madison, Wisconsin, 1967.

Harley, B. M., Perkins, F. E., and Eagleson, P. S., "A Modular Distributed Model of Catchment Dynamics," Hydrodynamics Laboratory Report No. 133, MIT, Department of Civil Engineering, 1970.

Heinemann, H. G., and Piest, R. F., "Soil Erosion-Sediment Yield, Research in Progress," Transactions, AGU, Vol. 56, No. 3, pp. 149-159, 1975.

Holtan, H. N., and Lopez, N. C., "USDAHL-70, Model of Watershed Hydrology," Technical Bulletin No. 1435, USDA-ARS, 84 p., 1971.

Horton, R. E., "Rainfall Interception," Mon. Weather Rev., Vol. 47, pp. 603-23, 1919.

Huggins, L. F., and Monke, E. J., "A Mathematical Simulation of Hydrologic Events on Ungaged Watershed," Technical Report 14, Water Resources Research Center, Purdue University, 46 p., 1970.

Iwagaki. Y., "Fundamental Studies on Runoff Analysis   (ᴧ cteristics," Bulletin No. 10, Disaster Prevention Resea⋅   Inst⌐ᴧate, Kyoto University, Kyoto, Japan, p. 25, 1955.

Jobson, H. E., and Sayre, W. W., "Vertical Transfer in Open Channel Flow," Journal of the Hydraulics Division, ASCE, Vol. 96, No. HY3, pp. 703-724, 1970.

Johnson, A. I., and Meyer, G., "Groundwater," Reviews of Geophysics and Space Physics, Vol. 13, No. 3, pp. 455-458, 1975.

Kemper, W. D., "Aggregate Stability of Soils from Western United States and Canada," ARS Technical Bulletin No. 1355, U.S. Dept. Agri., 52 p., 1966.

Kibler, D. F., and Woolhiser, D. A., "The Kinematic Cascade as a Hydrologic Model," Hydrology Paper No. 39, Colorado State University, Fort Collins, Colorado, p. 27, 1970.

Laursen, E., "The Total Sediment Load of Streams," Journal of the Hydraulics Div., ASCE, Vol. 84, No. HY1, Paper 1530, 1958.

Laws, J. O., and Parsons, D. A., "The Relation of Rain Drop Size to Intensity," Transactions, AGU, Vol. 24, pp. 452-459, 1943.

Lean, G. H., "The Settling Velocity of Particles in Channel Flow," in International Symposium on Stochastic Hydraulics, Edited by C. L. Chiu, University of Pittsburgh, pp. 339-351, 1971.

Li, R. M., Simons, D. B., and Stevens, M. A., "Nonlinear Kinematic Wave Approximation for Water Routing," Water Resour. Research, Vol. 11, No. 2, pp. 245-252, 1975a.

Li, R. M., Simons, D. B., and Stevens, M. A., "On Overland Flow Water Routing," Proceedings, Nat. Symp. Urban Hydro. and Sediment Control, Lexington, Kentucky, pp. 237-244. July, 1975b.

Li, R. M., Simons, D. B., Shiao, L. S., and Chen, Y. H., Kinematic Wave Approximation for Flood Routing, Proceedings, Third Annual Symposium of the Waterways, Harbors and Coastal Engineering Division, ASCE, Vol. I, 377-398, Fort Collins, Colorado, 1976a.

Li, R. M., "Water and Sediment Routing from Watersheds," Chapter 9, Modeling of Rivers, Edited by H. W. Shen, John Wiley and Sons, New York, 1979.

Lighthill, M. J., and Whitham, C. B., "On Kinematic Waves. I. Flood Movement in Long Rivers," Proceedings, Royal Soc. London, Vol. 229, Series A, pp. 281-316, 1955.

Linsley, R. K., Jr., Kohler, M. A., and Paulhus, J. L. H., Hydrology for Engineers, McGraw-Hill, New York, 1958.

Luthin, J. N., Editor, "Drainage of Agricultural Lands," Monograph VII, American Society of Agronomy, Madison, Wisconsin, 1957.

Meyer, L. D., and Wischmeier, W. H., "Mathematical Simulation of the Process of Soil Erosion by Water," Transactions, ASAE, Vol. 12, No. 6, 1969.

Meyer, L. D., "Soil Erosion by Water on Upland Areas," River Mechanics, Vol. 2, Chapter 27, Edited and Published by H. W. Shen, Fort Collins, Co, 1971.

Meyer, L. D., "How Rain Intensity Affects Interrill Erosion," Paper No. 80-2503, ASAE Winter Meeting, Chicago, Ill., 1980.

Musgrave, C. W., "Quantitative Evaluation of Factors in Water Erosion, A First Approximation," Journal Soil and Water Conservation, Vol. 2, No. 3, pp. 133-138, 1947.

Mutchler, C. K., and Young, R. A., "Soil Detachment by Raindrops," Proceedings, Sediment-Yield Workshop, Oxford, MS, 1972 (USDA Publication ARS-S-40, pp. 113-117, 1975).

Negev, M., "A Sediment Model on a Digital Computer," Technical Report No. 76, Dept. Civil Engineering, Stanford University, 1967.

Nielsen, D. R., Jackson, R. D., Cary, J. W., and Evans, D. D., Editors, " Soil-Water," American Society of Agronomy, Madison, Wisconsin, 1972.

Nordin, C. F., "Erosion and Sedimentation," Reviews of Geophysics and Space Physics, Vol. 13, No. 3, 1975, pp. 458-460.

Olson, T. C., and Wischmeier, W. H., "Soil-Erodibility Evaluations for Soils on the Runoff and Erosion Stations," Soil Science Society of America, Proceedings, Vol. 27, No. 5, pp. 590-592, 1963.

Onstad, C. A., and Foster, G. R., "Erosion Modeling on a Watershed," Transactions, ASAE, Vol. 18, No. 2, pp. 288-292, 1975.

Pierre, W. H., et al., Editors, " Plant Environment and Efficient Water Use," American Society of Agronomy, Madison, Wisconsin, 1966.

Schaake, J. C., "Deterministic Urban Runoff Model," Proceedings, Institute on Urban Water Systems, Fort Collins, Colorado, pp. 357-383, 1970.

Schaake, J. C., "Surface Waters," Reviews of Geophysics and Space Physics, Vol. 13, No. 3, pp. 445-451, 1975.

Simons, D. B., Li, R. M., and Stevens, M. A., "Development of Models for Predicting Water and Sediment Routing and Yield from Storms on Small Watersheds," Report CER 74-75DBS-RML-MAS-24, Colorado State University, Fort Collins, CO, 130 p., 1975.

Smith, R. E., and Woolhiser, D. A., "Overland Flow on an Infiltrating Surface," Water Resources Research, Vol. 7, No. 4, pp. 899-913, 1971.

Singh, V. P., "A Distributed Approach to Kinematic Wave Modeling of Watershed Surface Runoff," Proceedings, Nat. Symp. Urban Hydro. and Sediment Control, Lexington, Kentucky, pp. 227-263, July, 1975.

Smith, R. E., "Simulating Erosion Dynamics with a Deterministic Distributed Watershed Model," Proceedings, Third Federal Inter-Agency Sediment Conference, Denver, Colorado, pp. 163-173, 1976.

Smith, R. E., and Parlange, J. Y., "A Parameter-Efficient Hydrologic Infiltration Model," Water Resources Research, Vol. 14, No. 3, pp. 533-538, 1978.

Tennessee Valley Authority, "Upper Bear Creek Experimental Project, A Continuous Daily Streamflow Model," Research Paper No. 8, TVA, 1972.

Van Shilfgaarde, J., Editor, "Drainage for Agriculture," Monograph 17, American Society of Agronomy, Madison, Wisconsin, 1974.

Whitham, C. B., Linear and Nonlinear Waves, John Wiley, New York, 1974.

Williams, J. R., "Sediment Yield Prediction with Universal Equation Using Runoff Energy Factor," Proceedings, Sediment-Yield Workshop, Oxford, MS, 1972 (USDA-ARS Publication ARS-S-40, pp. 244-252, 1975).

Wischmeier, W. H., "Estimating the Soil Loss Equation's Cover and Management Factor for Undisturbed Areas," Proceedings, Sediment-Yield Workshop, Oxford, MS, 1972 (USDA-ARS Publication ARS-S-40, 1975).

Wischmeier, W. H., and Mannering, J. V., "Relation of Soil Properties to its Erodibility," Soil Science Society of America, Proceedings, Vol. 33, No. 1, pp. 131-137, 1969.

Wischmeier, W. H., and Smith, D. D., "Predicting Rainfall-Erosion Losses from Cropland East of the Rocky Mountains," Handbook No. 282, USDA-ARS, 1965.

Wischmeier, W. H., and Smith, D. D., "Predicting Rainfall Erosion Losses - A Guide to Conservation Planning," USDA, Agriculture Handbook No. 537, 1978.

Wooding, R. A., "A Hydraulic Model for the Catchment-Stream Problem, 1, Kinematic-Wave Theory," Journal of Hydrology, Vol. 3, pp. 254-267, 1965.

Woolhiser, D. A., "Overland Flow on a Converging Surface," Transactions, ASAE, Vol. 12, No. 4, pp. 460-462, 1969.

Woolhiser, D. A., and Liggett, J. A., "Unsteady, One-Dimensional Flow Over a Plane-The Rising Hydrograph," Water Resources Research, Vol. 3, No. 3, pp. 753-771, 1967.

Yalin, M. S., "An Expression for Bed-Load Transportation," J. Hydraulics Division, ASCE, Vol. 89, HY3, pp. 221-250, 1963.

Yang, C. T., "Incipient Motion and Sediment Transport," J. Hydraulics Division, ASCE, Vol. 99, No. HY10, pp. 1679-1704, 1973.

Zinke, P. J., "Forest Interception Studies in the United States," International Symposium on Forest Hydrology, edited by W. E. Sopper and H. W. Lull, pp. 137-161, September 1965.

ADDENDUM 1. DESCRIPTION OF DATA INPUT AND COMPUTER PROGRAM

The structure of the program SEDLAB, a software system developed for the simulation of water and sediment movements in agricultural catchments is described. The numerical schemes on which the program is based have been described in detail in Part 2. A description of the data input and important variables used in the program is given in the following sections of this addendum. The last section presents a complete list of the program.

The system SEDLAB consists of a main program and several subroutines. The sequence of operations performed by the main program is shown in Fig. 1.1. The main program inputs the required data to the system, calls the subroutines according to the computation scheme, and prints out the calculated results. Subroutine INTCPN computes the evaporation and interception losses, and determines the net rainfall rate. Subroutine INFLTN computes the ponding time, and the infiltration losses in a segment for one time step. Subroutine WROUT routes flow through a segment for one time step and it calls in turn subroutine SROUT. This subroutine performs sediment routing through a segment for one time step. Subroutines LAURSN, SETVEL, SHIELD, YALIN, and YANG are called by SROUT to compute potential carrying capacities and sediment transport parameters. The program has been designed to process the entire network of segments for one time step according to the computational sequence described in section 1.2 of this addendum. Once the entire network has been processed the simulation moves to the next time step. This sequence is repeated until the entire simulation period is computed.

The computer code requires 49,710 words on a Mod Comp Classic computer system. This is a 16-bit machine that uses two words for each single precision variable. The execution time for the event of February 21, 1971, on catchment 5 is 90 seconds.

A1 1   DATA INPUT

Data required to run program SEDLAB includes:

m.   data area, length, bed slope, bed elevation, and wetted
              relations.

                    and ground cover density, interception
                    ground covers, and ratio of evaporating
                    ground cover.
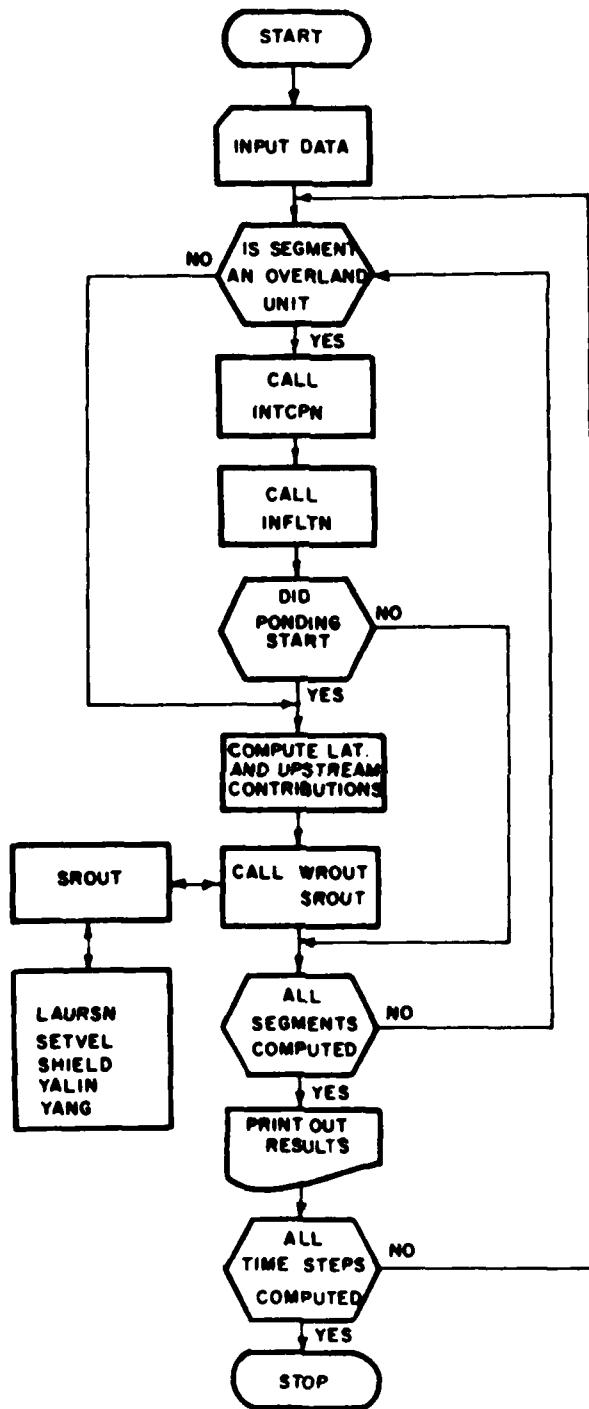
Fig. 1.1 Flow chart for the main program SEDLAB

I.82

Soil data: soil saturated hydraulic conductivity, soil sorptivity, specific gravity and size distribution of bed material.

Flow and sediment routing parameters: constants describing flow resistance, parameters describing soil detachment by raindrop impact and surface runoff, maximum penetration depth of raindrop impact, and computational sequence.

Storm characteristics: rainfall intensity, mean evaporation rate, and initial interception storage content.

A detailed description of the data input is given below:

Card No.	FORTRAN Variable	Description	Units	Format
1	TITLE	Alphanumerical identification of simulation run.	-	20A4
2	AREA	Drainage area of catchment	acres	F10.4
	NOV	Total number of overland segments	-	I4
	NCH	Total number of channel segments with negligible infiltration	-	I4
	NCI	Total number of channel segments with significant infiltration	-	I4
	NSTRM	Total number of storm events simulated in the run	-	I4
3	(This card must be repeated for each overland segment)			
	SEG	Number identifying overland segment Segments are numbered sequentially from 1 to NOV.	-	I4
	OVA	Area of overland segment	ft^2	F12.3
	SLEN	Slope length of overland segment. This length is computed by dividing OVA by the length of the receiving channel reach.	ft	F10.4
	SLOPE	Slope of overland segment.	ft/ft	F10.4
	CPER	Coefficient in the wetted perimeter versus flow area relation (the default value is one)	-	F10.4

I.83

EPER	Exponent in the wetted perimeter versus flow area relation (the default value is zero)	–	F10.4

4		(This card must be repeated for each channel segment)		
	SEG	Number identifying channel segments. These segments are numbered sequentially from (NOV+1) to (NOV+NCH) if there are no channel reaches with significant infiltration. Otherwise, the channel segments are numbered from (NOV+1) to (NOV+NCH+NCI).	–	I4
	SLEN	Length of channel segment	ft	F10.4
	SLOPE	Bed slope of channel segment	ft/ft	F10.4
	CPER	Coefficient in the wetter perimeter versus flow area relation.	–	F10.4
	EPER	Exponent in the wetted perimeter versus flow area relation.	–	F10.4

5	VOG	Interception storage capacity for a typical ground cover.	inches	F10.4
	SRG	Ratio of evaporating surface to the horizontal projected area of typical ground cover	ft^2/ft^2	F10.4
	VOR	Ratio of the interception storage capacity of a typical canopy cover to that of a typical ground cover.	–	F10.4
	HLR	Average height of ground cover in channels.	ft	F10.4

6	NSOIL	Number of representative sediment size fractions used in the simulation.	–	I4
	SPGR	Specific gravity of sediment	–	F10.4
	AIM	Coefficient of soil detachment by raindrop impact (a_r). User supplied optimization parameter.	–	F10.8
	ADF	Coefficient of soil erosion by surface flow (a_f). User supplied optimization parameter.	–	F10.8

I.84

	GMAX	Maximum penetration depth of raindrops (Eq. 61).	ft	F10.4
	GDX	Space increment adopted for sediment routing. User supplied parameter.	ft	F10.4
7	D50	Median size of sediment fractions. The program can accomodate up to five fractions.	mm	10F7.3
8	PC	Percentage of sediment fractions.	-	10F7.3
9		(This card must be repeated for each segment in the sequences used for cards 3 and 4)		
	CANO	Canopy cover density for the segment	ft^2/ft^2	F10.4
	GCOV	Ground cover density for the segment	ft^2/ft^2	F10.4
	HYCND	Saturated hydraulic conductivity for the segment	in/hr.	F10.4
10		(This card must be repeated for each segment)		
	ISEG	Index identifying the position of the segment in the computational sequence (see following section)	-	I4
	IARY	Array containing the storage locations of the inflows and outflows computed for the segment (see following section)	-	5I4
11	TEMP	Water temperature	Celsius	F10.4
	GAMA	Specific weight of water	lb/ft^3	F10.4
	SNU	Kinematic viscosity of water	ft^2/sec	F10.8
	EXP	Exponent in Eq. 26	-	F10.4
	C1	First coefficient describing kinematic-wave friction parameter (Eq. 82). User supplied optimization parameter	-	F10.4
	C2	Second coefficient in Eq. 82. User supplied optimization parameter	-	F10.4
12	NEED(I)	Vector representing the following output options:	-	6I4
		NEED (1) input data		

NEED (2) Bed elevation changes computed for
each segment at the end of the
simulation period

NEED (3) water budget and sediment yield

NEED (4) Computed infiltration rates. Measured
and computed hydrographs and sedimentgraphs

NEED (5) Plots of hyetograph and hydrograph

NEED (6) Plots of hyetograph and sedimentgraph

When NEED(I) > 0, the program prints selected output;
when NEED(I) = 0 the program does not print selected
output.

13	(Cards 13 through 17 must be repeated for each storm event)			
	STORM	Alphanumerical identification of the storm event	-	5A4
	DTM	Size of time step	min	F10.4
	ITMAX	Number of time steps in rainfall duration	-	I4
	ITCOM	Number of time steps in simulation period	-	I4
	EVP	Mean evaporation rate	in/hr	F10.4
	VIN	Initial interception storage, defined as the ratio of the initial storage to the interception storage capacity	in/in	F10.4
14	(This card must be repeated every eight segments until all the segments are included)			
	SORPTY	Sorptivity parameter for each of the eight consecutive segments ($S^2/2$, Fig. 3)	in²/hr	8F7.7
15	(This card must be repeated every twelve time steps until all the rainfall intensities are read in)			
	DR	Rainfall intensity for each of the twelve consecutive time steps	in/hr	12F6.3
16	(This card must be repeated every twelve time steps until all ITCOM steps are included)			
	QMES	Water discharge measured at the catchment outlet for each of the twelve consecutive time steps	ft³/sec	12F6.2

17	(This card must be repeated every twelve time steps until all ITCOM steps are included)		
	GMES	Total sediment discharge measured at the catchment outlet for each of the twelve consecutive time steps	lbs/sec	12F6.2

A1.2   PREPARATION OF INPUT ARRAYS ISEG AND IARY

The first step in preparing these data is to divide the catchment into interconnected overland and channel segments, each homogeneous within itself, and to assign an identification number to each segment. The principal direction of flow is determined for each overland segment from the contour line map of the catchment. The flow path through the cascade of segments is established by following the logics of gravity and flow continuity. The order in which the segment numbers appear in the flow path defines the computational sequence. This procedure is illustrated in Fig. 1.2 which presents the segmentation used in simulating the catchment W-5 described in section 3.4. The arrows shown in the figure denote the flow direction in each overland segment. It should be noticed that the segmentation is restricted to no more than two overland flow segments as input to a channel segment, and at most two inflow channel segments to a downstream channel segment.

After the segmentation of the catchment has been completed, two arrays must be set up by the user. The first, ISEG, tells the program the sequence for computing flow and sediment discharge for each segment. The other, IARY, tells the program for any segment where to find previously computed inflows and where to store the computed outflows. These inflows and outflows are stored in different columns of the matrices Q and GS described in the next section.

A table, AUX (Fig. 1.3), is used as an aid to set up the two arrays. AUX and the matrices Q and GS have the same number of columns. The table is constructed as follows. Starting with one of the most upstream channel segments, its inflow segments are selected. Then their numbers are placed in the first available columns of AUX and in separate rows. This will usually mean an overland flow segment number in row 1, column 1, and another in row 2, column 2. The channel segment number is then placed in the next available row and the first available column if no further inflows to the segment need to be computed. An available column is one that does

I.87
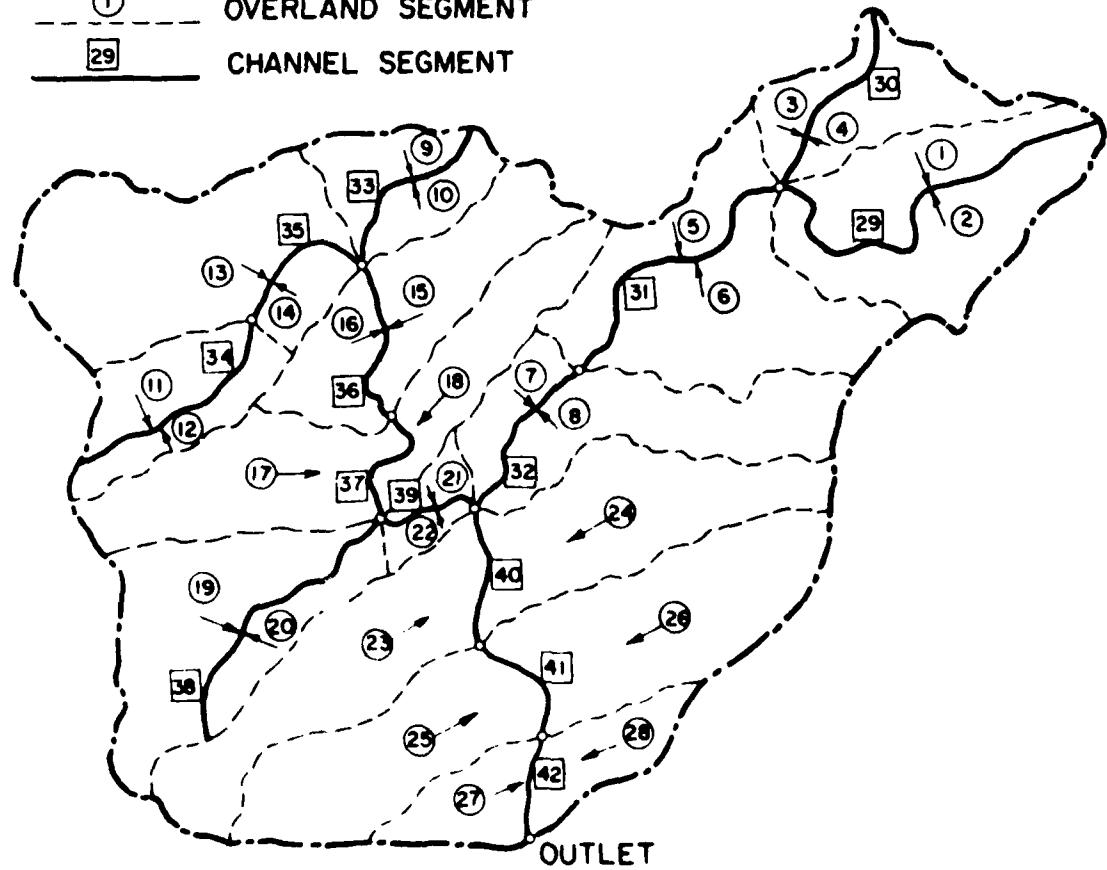
Fig. 1.2 Geometric segmentation and flow path for catchment W-5

not have the number of a segment waiting to be combined in some further downstream segment. This procedure is continued through the flow path, inserting segment numbers in the table until the outlet of the catchment is reached. If a junction with another channel segment is reached, then what has been computed must be retained while the area upstream of the junction *is computed*.

To illustrate consider Fig. 1.2. Channel segment 29 is chosen as the first most upstream channel segment. Other segments which could have been chosen as well to start are 30, 33, 34, 35, or 20. The overland flow segments for segment 29 are 1 and 2. These are placed respectively in row 1, column 1, and row 2, column 2. When the two overland flow segments are combined to give the channel outflow in 29, they are no longer needed. This allows the outflow from 29 to be entered in column 1 of the next row. Next, the outflow from channel segment 30 must be computed. This requires computing the overland flow segments 3 and 4. They are entered in columns 2 and 3 because 29 must be saved and is in the column 1. When 30 is computed it must be saved also until the inputs 5 and 6 to segment 31 have been computed. When 29, 30, 5, and 6 have all been computed, then 31 can be computed and placed in the first column of the next row. None of the segments previously computed need to be retained at this point. When segment 32 has been computed it must be retained until segment 39 has been computed which requires moving to upstream segments above 39. The channel segments 12, 33, and 38, and their corresponding lateral inflows, are the upstream starting points above 39.

In the given example, the segment numbers entered in AUX occupy five columns. However, a finer segmentation or a denser drainage network would have resulted in a larger number of columns. The number of rows of AUX is always equal to the total number of segments because each segment is computed only once in each time step.

When AUX is completed, ISEG and IARY are constructed from it and then AUX is discarded. To construct the column matrix ISEG, the number of the segment in each row of AUX is placed in the corresponding row of ISEG (Fig. 1.3). The order of segment numbers in ISEG gives the computational sequence used by the program to route water and sediment through the flow path.

Vector Matrix ISEG / **Table AUX**

ISEG	1	2	3	4	5
1	1				
2		2			
29	29				
3		3			
4			4		
30		30			
5			5		
6				6	
31	31				
7		7			
8			8		
32	32				
9		9			
10			10		
33		33			
11			11		
12				12	
34			34		
13				13	
14					14
35			35		
15				15	
16					16
36		36			
17			17		
18				18	
37		37			
19			19		
20				20	
38			38		
21				21	
22					22
39		39			
23			23		
24				24	
40	40				
25		25			
26			26		
41	41				
27		27			
28			28		
42	42				

Segment Number / **Matrix IARY**

Segment	1	2	3	4	5
1	0	0	0	0	1
2	0	0	0	0	2
3	0	0	0	0	2
4	0	0	0	0	3
5	0	0	0	0	3
6	0	0	0	0	4
7	0	0	0	0	2
8	0	0	0	0	3
9	0	0	0	0	2
10	0	0	0	0	3
11	0	0	0	0	3
12	0	0	0	0	4
13	0	0	0	0	4
14	0	0	0	0	5
15	0	0	0	0	4
16	0	0	0	0	5
17	0	0	0	0	3
18	0	0	0	0	4
19	0	0	0	0	3
20	0	0	0	0	4
21	0	0	0	0	4
22	0	0	0	0	5
23	0	0	0	0	3
24	0	0	0	0	4
25	0	0	0	0	2
26	0	0	0	0	3
27	0	0	0	0	2
28	0	0	0	0	3
29	1	2	0	0	1
30	2	3	0	0	2
31	3	4	1	2	1
32	2	3	1	0	1
33	2	3	0	0	2
34	3	4	0	0	3
35	4	5	3	0	3
36	4	5	2	3	2
37	3	4	2	0	2
38	3	4	0	0	3
39	4	5	2	3	2
40	3	4	1	2	1
41	2	3	1	0	1
42	2	3	1	0	1

Fig. 1.3 Assemblage of input arrays ISEG and IARY for catchment W-5

I.90

To construct IARY, each segment in the catchment is considered. The information for segment number n is placed in the nth-row of IARY. Columns 1 and 2 of IARY contain information about any overland flow segments which are input to that segment. These columns will contain a zero if there are no overland flow segments, and will contain the column locations for the overland flow segments in AUX if there are (Fig. 1.3). For example, segment 16 is an overland segment receiving no overland contributions itself. Thus columns 1 and 2 of row 16 in IARY have zeros. The lateral inflows to segment 39 come from the overland segments 21 and 22 which are found in columns 4 and 5 of AUX. Thus columns 1 and 2 of row 39 in IARY have the numbers 4 and 5, respectively.

Columns 3 and 4 of IARY store information about the channel inflows for downstream channel segments. If the nth-segment is a channel segment receiving channel inflows, columns 4 and 5 of the nth-row in IARY will have the column location of these inflow segments in AUX. For example, segment 12 is an overland flow segment and has no channel inflows, thus columns 3 and 4 of IARY's row 12 are zeros. Similarly, segment 29 is a channel segment with no upstream channel inflows, thus columns 3 and 4 of row 29 in IARY are also zeros. Alternatively, segment 41 has one upstream channel inflow (segment 40) which is found in column 1 of AUX when computed. Therefore, column 3 of row 41 in IARY contains a 1 while column 4 is a zero. Segment 39 has two channel inflows (segments 37 and 38). When these upstream segments are computed they are entered respectively in columns 2 and 3 of AUX. Therefore, columns 3 and 4 of row 39 in IARY contain 2 and 3, respectively.

Column 5 of IARY contains the column location in AUX of the computed segment outflows. For example, the outflow from segment 16 when computed is entered in column 5 of AUX. Thus row 16, column 5, of IARY contains a 5. Similarly, the outflow of segment 28 is found in column 3 of AUX. Thus row 28, column 5, of IARY contains a 3.

The matrices ISEG and IARY are used sequentially to route water and sediment through the flow path for each time step. For each segment number listed in ISEG, the numbers in the corresponding row of IARY tell the program where the associated inflows are stored in Q and GS. When all the segments have been worked through, the entire procedure is repeated for the next time step.

I.91

A1.3   FORTRAN VARIABLES NOT INCLUDED IN THE INPUT DATA LIST

Name	Description	Units
ACCLN	Gravitational acceleration	ft/sec^2
ADP	Thickness of detached soil at the start of the current time step	ft
ALP	Kinematic-wave friction coefficient in Eq. 26	$ft^{\frac{1}{2}}/sec$
AP	Cross-sectional area of flow at the start of the current time step	ft^2
BEG	Distance of space increment used in sediment routing to the upstream boundary of the segment	ft
CND	Canopy cover density	ft^2/ft^2
CONC	Volume concentration of individual material fraction at carrying capacity	ft^3/ft^3
CP	Volume concentration of individual material fraction at the start of the current time step	ft^3/ft^3
DFT	Medium size of sediment fraction	ft
DX	Space increment used in sediment routing	ft
END	Distance travelled by sediment characteristic at the end of the current time step, and measured from upstream boundary of segment	ft
ERO	Volume rate of soil detachment by raindrop impact	ft^3/ft^2 sec
GCD	Ground cover density	ft^2/ft^2
GDLAT	Volume rate of lateral inflow of material fraction to segment during current time step	$ft^3/ft.$ sec
GDUP	Volume rate of upstream inflow of material fraction to segment	ft^3/sec
GS	Volume discharge of individual material fraction. This is a five-column matrix used to store the sediment inflow and outflow for a segment. This matrix has as many rows as time steps in the simulation period.	ft^3/sec
GTOT	Total sediment discharge at the catchment outlet	lbs/sec
HYR	Flow depth in overland segments, and hydraulic radius in channels	ft

ITPON	Number of time steps until time of ponding from the start of the simulation period	-
ITYPE	Index defining type of flow in segment. Set ITYPE equal to 1 for overland flow, 2 for channel flows with negligible infiltration, and 3 for channel flows with significant infiltration	-
KOUT	Column in matrix IARY containing storage location of segment outflow computed at the end of the current time step.	-
KS	Number of time steps until the time of formation of a characteristic, or shock, wave.	-
K1	Number of the current time step	-
K2	Index identifying a characteristic wave emanating from dry ground (K2=0), or from upstream boundary (K2>0)	-
NO	Number of current space increment when routing a sediment characteristic	-
NSEG	Total number of segments in the catchment	-
PERM	Saturated hydraulic conductivity	in/hr
POR	Porosity of bed material	ft^3/ft^3
Q	Water discharge. This is a five-column matrix used to store the water inflow and outflow computed for a segment. This matrix has as many rows as time steps in the simulation period.	ft^3/sec
QE	Water discharge at the end of the current sediment routing step.	ft^3/sec
QINF	Rate of infiltration during the current time step	in/hr
QLAT	Lateral inflow of water to segment during the current time step.	$ft^3/ft. sec$
QOUT	Water discharge at the catchment outlet	ft^3/sec
QUP	Upstream inflow of water to segment	ft^3/sec
RAIN	Rain precipitation	inches
RNET	Net rainfall intensity	in/hr
S	Specific gravity of sediment	-
TC	Critical bed tractive force	lbs/ft^2

UST	Bed shear velocity	ft/sec
VEL	Average velocity of flow	ft/sec
VINT	Total interception per unit area of land	inches
VS	Settling velocity in quiescent water for material fraction	ft/sec
X	Distance measured from upstream boundary of segment	ft
XS	Distance travelled by a characteristic or shock water wave during the current time step	ft
XSS	Space increment used for sediment routing (Eq. 81)	ft
ZD	Thickness of detached soil for any one material fraction	ft
ZL	Bed elevation	ft

END
DATE
FILMED
7 81
DTIC

```
      PROGRAM SEDLAB
C     **************
C
      DIMENSION TITLE(20),SEG(100),ISEG(100),QOUT(300),CTOT(300),
     $SLEN(100),SLOPE(100),CPER(100),EPER(100),IARY(100,5),QMES(300),
     $GMES(300),ZZ(3),C(71),OVA(100),NEED(6),CANO(100),GCOV(100),
     $HYCND(100),SORPTY(100),STORM(5)
      INTEGER SEG
      COMMON /GEN/ ITMAX,ITCOM,ITPON,DT,DTS
      COMMON /COV/ CND,GCD,HLR,HIR
      COMMON /RAI/ DR(300),RNET(300),QINF(300)
      COMMON /INT/ VOR,VOG,SRG,VIN,EVP,VINT,RAIN
      COMMON /INF/ PERM,SORP
      COMMON /FLO/ Q(300,5),ALP,EXP,K,ITYPE,SLN,SLP,CPR,EPR,
     $KOUT,QUP(300),QLAT(300)
      COMMON /SED/ GS(300,5,5),ZL(100),ZD(100,5),CDUP(300,5),
     $GDLAT(300,5),POR(5),CP(5),D50(5),PC(5),VS(5),ERO(300),
     $BEG(100),END(100),ADF,SNU,EMV,HCC,SGC,QE,AP,K1,BRE,APS,ITS,X,
     $XS,XSS,NO,BET,DX,SUBW,SPGR,ACCLN,GAMA,K2,KS,GMAX,NSOIL
      DATA ZZ/'I','M','C'/,DEC/'.'/,BLANK/' '/
C
C  DATA INPUT
C
      READ(5,501) TITLE
C  WATERSHED GEOMETRY
      READ(5,502) AREA,NOV,NCH,NCI,NSTRM
      NTO=NOV+NCH
      NSEG=NTO+NCI
      IC=NOV+1
      READ(5,503) (SEG(I),OVA(I),SLEN(I),SLOPE(I),CPER(I),EPER(I),
     $I=1,NOV)
      READ(5,504) (SEG(I),SLEN(I),SLOPE(I),CPER(I),EPER(I),I=IC,NSEG)
C  VEGETATIVE COVER AND SOIL CHARACTERISTICS
      READ(5,505) VOG,SRG,VOR,HLR
      READ(5,506) NSOIL,SPGR,AIM,ADF,GMAX,GDX
      READ(5,516) (D50(I),I=1,NSOIL)
      READ(5,517) (PC(I),I=1,NSOIL)
      READ(5,507) (CANO(I),GCOV(I),HYCND(I),
     $I=1,NSEG)
C  COMPUTATIONAL SEQUENCE
      READ(5,508) (ISEG(I),(IARY(I,J),J=1,5),I=1,NSEG)
C  WATER PROPERTIES AND FLOW ROUTING PARAMETERS
      READ(5,509) TEMP,GAMA,SNU,EXP,C1,C2
C  OUTPUT OPTIONS
      READ(5,510) (NEED(I),I=1,6)
C
C  LISTING OF INPUT DATA
C
      WRITE(6,601) TITLE
      IF(NEED(1).EQ.0) GO TO 95
      WRITE(6,603) AREA,NOV,NCH,NCI,NSEG,NSTRM
      WRITE(6,604) (SEG(I),OVA(I),SLEN(I),SLOPE(I),CPER(I),EPER(I),
     $CANO(I),GCOV(I),HYCND(I),I=1,NOV)
      WRITE(6,605) (SEG(I),SLEN(I),SLOPE(I),CPER(I),EPER(I),CANO(I),
     $GCOV(I),HYCND(I),I=IC,NSEG)
      WRITE(6,606) VOG,SRG,VOR,HLR,     NSOIL,SPGR,AIM,ADF,GMAX,GDX
      WRITE(6,616)
      WRITE(6,617) (I,D50(I),PC(I),I=1,NSOIL)
      WRITE(6,618)
      WRITE(6,607) (ISEG(I),SEG(I),(IARY(I,J),J=1,5),I=1,NSEG)
```

```
            WRITE(6,608) TEMP,GAMA,SNU,EXP,C1,C2
95      CONTINUE
C
C  INVARIANT INFORMATION
        ACCLN=32.2
        SUBW=(SPGR-1.0)*GAMA
C  POROSITY AND SETTLING VELOCITY
        DO 88 I=1,NSOIL
        POR(I)=1.-0.245-0.0864/(0.1*D50(I))**0.21
        DMM=D50(I)
        CALL SETVEL(DMM,TEMP,SPGR,W)
        VS(I)=W
        D50(I)=D50(I)/304.8
88      CONTINUE
C
        TRAIN=0.0
        TVINT=0.0
C
C  COMPUTATION FOR EACH STORM
        DO 100 N=1,NSTRM
C
C  STORM DATA INPUT
        READ(5,511) STORM,DTM,ITMAX,ITCOM,EVP,VIN
        READ(5,512) (SORPTY(I),I=1,NSEG)
        READ(5,513) (DR(I),I=1,ITMAX)
        READ(5,514) (QMES(I),I=1,ITCOM)
        READ(5,515) (GMES(I),I=1,ITCOM)
        DT=DTM/60.0
        DTS=DTM*60.0
C
C  LISTING OF STORM DATA
        IF(NEED(1).GT.0) WRITE(6,611) STORM,VIN,EVP,DTM,ITMAX,ITCOM
        IF(NEED(1).GT.0) WRITE(6,612) (SORPTY(I),I=1,NSEG)
C
C  POTENTIAL EROSION BY RAINDROP IMPACT
        DO 130 IT=1,ITCOM
        IF(IT.GT.ITMAX) DR(IT)=0.0
        ERO(IT)=AIM*(DR(IT)/43200.0)**2.0
130     CONTINUE
C
C  ROUTING SEGMENTS ACCORDING TO COMPUTATIONAL SEQUENCE
        WRITE(6,621)
        IF(NEED(2).GT.0) WRITE(6,648)
        DO 101 I=1,NSEG
C
        K=ISEG(I)
        IF(K.LE.NOV) ITYPE=1
        IF(K.GT.NOV.AND.K.LE.NTO) ITYPE=2
        IF(K.GT.NTO) ITYPE=3
        SLN=SLEN(K)
        SLP=SLOPE(K)
        CPR=CPER(k)
        EPR=EPER(K)
        CND=CANO(K)
        GCD=GCOV(K)
        PERM=HYCND(K)
        SORP=SORPTY(K)
        EMV=HLR*(1.0-GCD)
        IF(GCD.EQ.0.0) EMV=0.0
        HIR=0.0
```

```
                HGC=HIR*GCD
                SGC=GCD-HGC
                BRE=(1.0-CND)*(1.0-GCD)
                OVF=OVA(K)/(AREA*43560.0)
      C
      C   SELECT SPATIAL INCREMENT FOR SEDIMENT ROUTING
                RDX=SLN/GDX
                NDX=INT(RDX)
                IF((RDX-NDX).GT.0.0) NDX=NDX+1
                IF(NDX.LT.2) NDX=2
                DX=SLN/FLOAT(NDX)
      C   KINEMATIC FRICTION PARAMETERS
                ALP=C1+C2*SLP**0.5
      C
      C   INITIALIZE SURFACE ELEVATION AND DETACHED SOIL STORAGE
                DO 107 J=1,100
                ZL(J)=0.0
                DO 87 L=1,NSOIL
                ZD(J,L)=0.0
      87        CONTINUE
      107       CONTINUE
                IF(ITYPE.EQ.2) GO TO 108
      C
      C   COMPUTING NET RAINFALL RATE
                CALL INTCPN
                IF(ITYPE.EQ.1) TRAIN=TRAIN+RAIN*OVF
                IF(ITYPE.EQ.1) TVINT=TVINT+VINT*OVF
      C
      C   COMPUTING PONDING TIME AND POTENTIAL INFILTRATION
                CALL INFLTN
                IF(ITPON.EQ.0) GO TO 151
      108       CONTINUE
      C
      C   WATER AND SEDIMENT ROUTING
      C
      C   UPSTREAM INFLOW AND LATERAL INFLOW/OUTFLOW
                DO 102 IT=ITPON,ITCOM
                QUP(IT)=0.0
                QLAT(IT)=0.0
                DO 81 L=1,NSOIL
                GDUP(IT,L)=0.0
      81        GDLAT(IT,L)=0.0
                IF(IARY(K,3).EQ.0) GO TO 103
                DO 104 J=1,2
                IF(IARY(K,2+J).EQ.0) GO TO 103
                JJ=IARY(K,J+2)
                QUP(IT)=QUP(IT)+Q(IT,JJ)
                DO 82 L=1,NSOIL
      82        GDUP(IT,L)=GDUP(IT,L)+GS(IT,JJ,L)
      104       CONTINUE
      103       IF(ITYPE.GT.1) GO TO 105
                QLAT(IT)=QLAT(IT)+(RNET(IT)-QINF(IT))/43200.0
      105       IF(IARY(K,1).EQ.0) GO TO 102
                DO 106 J=1,2
                IF(IARY(K,J).EQ.0) GO TO 102
                JJ=IARY(K,J)
                QLAT(IT)=QLAT(IT)+Q(IT,JJ)
                DO 83 L=1,NSOIL
      83        GDLAT(IT,L)=GDLAT(IT,L)+GS(IT,JJ,L)
      106       CONTINUE
```

```
102    CONTINUE
       KOUT=IARY(K,5)
C
       CALL WROUT
C
C  LISTING THE FINAL SURFACE LEVEL OF THE SEGMENT
       IF(NEED(2).GT.0) WRITE(6,649) K
       IF(NEED(2).GT.0) WRITE(6,650) (BEG(J),END(J),ZL(J),J=1,NO)
C
101    CONTINUE
C
C  RUNOFF AND SEDIMENT DISCHARGE AT THE CATCHMENT OUTLET
       DO 121 IT=1,ITCOM
       IF(IT.GE.ITPON) GO TO 122
       QOUT(IT)=0.0
       GTOT(IT)=0.0
       GO TO 121
122    QOUT(IT)=Q(IT,1)
       GTOT(IT)=0.0
       DO 84 L=1,NSOIL
84     GTOT(IT)=GTOT(IT)+CS(IT,1,L)*GAMA
121    CONTINUE
       WRITE(6,622)
C
C  COMPUTED YIELDS, PEAKS AND TIME TO PEAKS OF WATER AND SEDIMENT
       TQOUT=0.0
       QCPK=0.0
       TGOUT=0.0
       GCPK=0.0
       DO 123 IT=ITPON,ITCOM
       IF(QOUT(IT).LT.QCPK) GO TO 124
       QCPK=QOUT(IT)
       IQC=IT
124    TQOUT=TQOUT+QOUT(IT)*DTS
       IF(GTOT(IT).LT.GCPK) GO TO 125
       GCPK=GTOT(IT)
       IGC=IT
125    TGOUT=TGOUT+GTOT(IT)*DTS
123    CONTINUE
       TQPSF=TQOUT/(AREA*43560.0)*12.0
       GO TO 126
151    CONTINUE
C
C  SMALL EVENT GENERATING NO RUNOFF
       TQOUT=0.0
       TQPSF=0.0
       QCPK=0.0
       IQC=0
       TGOUT=0.0
       GCPK=0.0
       IGC=0
126    CONTINUE
       IF(NEED(3).EQ.0) GO TO 96
C
C  WATER BUDGET
       TINF=TRAIN-(TVINT+TQPSF)
C
C  MEASURED YIELDS, PEAKS AND TIME TO PEAKS OF WATER AND SEDIMENT
       TQMES=0.0
       QMPK=0.0
```

```
            TGMES=0.0
            GMPK=0.0
            DO 127 IT=1,ITCOM
            IF(QMES(IT).LT.QMPK) GO TO 128
            QMPK=QMES(IT)
            IQM=IT
128         TQMES=TQMES+QMES(IT)*DTS
            IF(GMES(IT).LT.GMPK) GO TO 129
            GMPK=GMES(IT)
            IGM=IT
129         TGMES=TGMES+GMES(IT)*DTS
127         CONTINUE
C
C   PERCENTAGE DIFFERENCE OF COMPUTED VALUES TO MEASURED VALUES
            PCWY=(TQMES-TQOUT)/TQMES*100.0
            PCWP=(QMPK-QCPK)/QMPK*100.0
            PCWT=FLOAT(IQM-IQC)/FLOAT(IQM)*100.0
            PCSY=(TGMES-TGOUT)/TGMES*100.0
            PCSP=(GMPK-GCPK)/GMPK*100.0
            PCST=FLOAT(IGM-IGC)/FLOAT(IGM)*100.0
C
C   OUTPUT OF WATER BUDGET
            WRITE(6,651) TRAIN,TVINT,TINF,TQPSF
C
C   OUTPUT OF YIELDS, PEAKS AND TIME TO PEAKS OF WATER AND SEDIMENT
            WRITE(6,652) TQMES,TQOUT,PCWY,QMPK,QCPK,PCWP,IQM,IQC,PCWT,TGMES,
           $TGOUT,PCSY,GMPK,GCPK,PCSP,IGM,IGC,PCST
96          CONTINUE
            IF(NEED(4).EQ.0) GO TO 115
C
C   OUTPUT OF RAINFALL INTENSITIES, AND MEASURED AND COMPUTED HYDROGRAPHS
            WRITE(6,656)
            IP=ITPON-1
            WRITE(6,657) (J,DR(J),RNET(J),QMES(J),QOUT(J),GMES(J),GTOT(J),
           $J=1,IP)
            WRITE(6,658) (J,DR(J),RNET(J),QINF(J),QMES(J),QOUT(J),GMES(J),
           $GTOT(J),J=ITPON,ITCOM)
115         CONTINUE
C
C   OUTPUT OF HEITOGRAPH, MEASURED AND COMPUTED HYDROGRAPH
            IF(NEED(5).EQ.0) GO TO 97
            WRITE(6,660)
            QMAX=QMPK
            IF(QCPK.GT.QMPK) QMAX=QCPK
            DO 141 J=1,71
141         G(J)=BLANK
            DO 142 J=1,ITCOM,2
            G(1)=DEC
            IR=DR(J)*7.0
            IRR=71 -IR
            DO 143 J1=IRR,71
143         G(J1)=ZZ(1)
            IM=QMES(J)/QMAX*70.0
            G(IM)=ZZ(2)
            IC=QOUT(J)/QMAX*70.0
            G(IC)=ZZ(3)
            WRITE(6,661)J,G
            DO 144 J1=1,71
144         G(J1)=BLANK
142         CONTINUE
```

```
97      CONTINUE
C
C  OUTPUT OF HEITOGRAPH, MEASURED AND COMPUTED SEDIMENTGRAPH
        IF(NEED(6).EQ.0) GO TO 98
        WRITE(6,662)
        GMAX=GMPK
        IF(GCPK.GT.GMPK) GMAX=GCPK
        DO 161 J=1,71
161     G(J)=BLANK
        DO 162 J=1,ITCOM,2
        G(1)=DEC
        IR=DR(J)*7.0
        IRR= 71-IR
        DO 163 J1=IRR,71
163     G(J1)=ZZ(1)
        IM=GMES(J)/GMAX*70.0
        G(IM)=ZZ(2)
        IC=GTOT(J)/GMAX*70.0
        G(IC)=ZZ(3)
        WRITE(6,663)J,G
        DO 164 J1=1,71
164     G(J1)=BLANK
162     CONTINUE
98      CONTINUE
        WRITE(6,659)
100     CONTINUE
C
501     FORMAT(20A4)
502     FORMAT'F10.4,4I4)
503     FORMAT(I4,F12.3,4F10.4)
504     FORMAT(I4,4F10.4)
505     FORMAT(5F10.4)
506     FORMAT(I4,F10.4,2F10.8,2F10.4)
516     FORMAT(10F7.3)
517     FORMAT(10F7.3)
507     FORMAT(3F10.4)
508     FORMAT(6I4)
509     FORMAT(2F10.4,F10.8,3F10.4)
510     FORMAT(6I4)
511     FORMAT(5A4,F10.4,2I4,2F10.4)
512     FORMAT(8F7.4)
513     FORMAT(12F6.3)
514     FORMAT(12F6.2)
515     FORMAT(12F6.2)
601     FORMAT(1H1///X,20A4///)
603     FORMAT(30X,'CATCHMENT GEOMETRY'//41X,' DRAINAGE AREA = ',
       $F7.1,' ACRES '/38X,'OVERLAND SEGMENTS = ',I5/10X,'CHANNEL ',
       $'SEGMENTS WITH NEGLIGIBLE INFILTRATION = ',I5/8X,'CHANNEL ',
       $'SEGMENTS WITH CONSIDERABLE INFILTRATION = ',I5/41X,'TOTAL ',
       $'SEGMENTS = ',I5//30X,'NUMBER OF COMPUTED STORMS = ',I5////
       $24X,'PHYSICAL CHARACTERISTICS OF SEGMENTS'// X,'----------------
       $----------------------------------------'
       $/36X,'RELATION BETWEEN  CANOPY  GROUND  SATURATED'/X,'SEGMENT  OVE
       $RLAND   LENGTH    SLOPE   WETTED PERIMETER COVER   COVER   HYDRAULIC
       $'/X,'NUMBER     AREA',21X,'AND FLOW AREA    DENS.   DENSITY  CONDU
       $CT.'/X,'& TYPE   (SQ  FT)    (FT) (FT/FT) COEFF.   EXP.',20X,
       $'(INCH/HR)'/X,'----------------------------------------------',
       $,'------------------------------'//)
604     FORMAT(X,I3,' OV',X,F10.1,X,F7.1, 2X,F7.5,2X,F5.1,3X,F5.3,4X,F5.3,
       $3X,F5.3,4X,F5.3)
```

```
605    FORMAT(X,I3,' CH',13X,F7.1,X,F7.5,2X,F5.1,3X,F5.3,4X,F5.3,3X,
      $F5.3,4X,F5.3)
606    FORMAT(////27X,'GROUND COVER CHARACTERISTICS'//6X,
      $'INTERCEPTION STORAGE CAPACITY FOR GROUND COVER = ',
      $F9.3,' INCHES',/6X,'RATIO OF EVAPORATING SURFACE',
      $' TO PROJECTED AREA = ',F9.3/7X,'RATIO BETWEEN INTERCEPTION'.
      $' STORAGE CAPACITIES'/19X, 'OF CANOPY COVER  AND GROUND COVER',
      $' = ',F9.3/10X,'AVERAGE HEIGHT OF GROUND COVER IN CHANNELS',
      $' = ',F9.3,' FEET'
      $    ////18X,'SOIL CHARACTERISTICS AND DETACHMENT PARAMETERS'//
      $27X,'NUMBER OF SEDIMENT SIZE FRACTIONS = ',I5/
      $32X,'SPECIFIC GRAVITY OF SEDIMENT = ',F8.2/11X,
      $'COEFFICIENT OF SOIL DETACHMENT BY RAINDROP IMPACT =    ',
      $E10.3/17X,'COEFFICIENT OF SOIL EROSION BY SURFACE FLOW =   ',
      $E10.3/22X,'MAXIMUN PENETRATION DEPTH OF RAINDROPS = ',F9.3,
      $' FEET'/20X,'SPACE INCREMENT USED IN SEDIMENT ROUTING',
      $' = ',F8.2,'FEET'//)
616    FORMAT(15X,'------------------------------------------------'
      $/16X,'SERIAL NO. OF     MEDIUM SIZE OF        PERCENTAGE'/16X,
      $'SED. FRACTION    SEDIMENT FRACTION    OF SEDIMENT'/37X,
      $'(MM)',13X,'FRACTION'/15X,'--------------   ',
      $'--------------    -----------------'//)
617    FORMAT(19X,I4,13X,F7.3,12X,F5.1)
618    FORMAT(////5X,'--------------   ------------------------------'
      $,'---------------------'/9X,'ISEG',30X, 'IARY'/27X,'THIS ARRAY ',
      $'CONTAINS THE STORAGE LOCATIONS'/5X,'COMPUTATIONAL',9X,'OF ',
      $'COMPUTED INFLOWS AND OUTFLOWS IN THE'/8X,'SEQUENCE',11X,'WATER',
      $'(Q) AND SEDIMENT(GS) DISCHARGE MATRICES'/
      $22X,'--------------------------------------------'/
      $11X,'#',10X,'SEGMENT #  LATERAL INFLOWS  UPSTREAM INFLOWS  ',
      $'OUTFLOW'/5X,'--------------   ----------   ---------------   ',
      $'----------------   --------'//)
607    FORMAT(10X,I3,11X,I3,9X,I1,6X,I1,9X,I1,8X,I1,8X,I1)
608    FORMAT(////18X,'WATER PROPERTIES AND KINEMATIC FRICTION ',
      $'PARAMETERS'//31X,'WATER TEMPERATURE ='
      $,F8.2,' DEG. CENT.'/24X,'SPECIFIC WEIGHT OF WATER ='
      $,F8.2,' LBS/CU.FT.'/20X,'KINEMATIC VISCOSITY OF WATER = ',
      $2X,E10.3,' SQ.FT./SEC.'/13X,
      $'EXPONENT IN KINEMATIC WAVE EQUATION = ',F7.2/19X,
      $'KINEMATIC FRICTION PARAMETERS :   C1=',F6.2,',   C2 =',F6.2//)
611    FORMAT(//36X,'STORM DATA'//37X,'STORM DATE = ',5A4/16X,
      $'ANTECEDENT INTERCEPTION STORAGE = ',F10.4,' INCHES'/26X,
      $'MEAN EVAPORATION RATE = ',F10.4,' INCHES PER HOUR'//
      $25X,'TIME STEP DURING STORM =',F8.1,'    MINUTES'/
      $8X,'NUMBER OF TIME STEPS IN RAINFALL PERIOD = ',
      $I5/6X,'NUMBER OF TIME STEPS IN SIMULATION PERIOD = ',
      $I5///21X,'SORPTIVITY FOR EACH CATCHMENT SEGMENT',
      $/28X,'(SQUARE INCHES PER HOUR)'//)
612    FORMAT(X,10F8.4)
621    FORMAT(////20X,'*********************************************'//
      $20X,'*   START OF WATER AND SEDIMENT ROUTING   *'
      $         /20X,'*********************************************')
648    FORMAT(////9X,'----------------------------',
      $'-----------------------------------------'/9X,'DISTANCE',
      $' FROM U/S END  DISTANCE FROM U/S END  CHANGE OF BED ELEV.'/
      $8X,'OF SEGMENT TO START OF  OF SEGMENT TO END OF    ',
      $'FOR THE SPACE'/10X,'SPACE INCREMENT (FT)',2X,'SPACE ',
      $'INCREMENT (FT)',5X,'INCREMENT(FT)' /9X,'--------------------  ',
      $'--------------------'//)
649    FORMAT(36X,'FOR SEGMENT ',I4)
```

I.101

```
650    FORMAT(15X,F7.1,17X,F7.1,15X,F6.3)
622    FORMAT(////15X,'*****************************************',
      $'*******'/15X,'*        END OF WATER AND SEDIMENT ROUTING',
      $'         *'/15X,'*****************************************',
      $'*******************'//)
651    FORMAT(//35X,'WATER BUDGET'//32X,'PRECIPITATION = ',F8.2,
      $' INCHES'/13X,'LOSS DUE TO INTERCEPTION STORAGE = ',F8.2,
      $' INCHES'/21X,'LOSS DUE TO INFILTRATION = ',F8.2,' INCHES'/
      $34X,'WATER YIELD = ',F8.2,' INCHES'///)
652    FORMAT(//33X,'SUMMARY OF RESULTS'/X,'----------------',
      $'-----------------------------------------------------',
      $'----'/8X,'ITEM ',15X,'MEASURED',7X,'COMPUTED',9X,'UNITS',8X,
      $'PER CENT'/73X,'DIFFER.'/X,'-----------------------',2X,'------',
      $'--------',2X,'--------------  ----------------  ----------'//
      $6X,'WATER YIELD',7X,F12.1,3X,F12.1,6X,'CUBIC FEET',6X,F6.1,/X,
      $'WATER DISCHARGE PEAK' ,7X,F8.1,7X,F8.1,4X,'CUBIC FEET/SEC',
      $4X,F6.1/2X,'TIME TO WATER PEAK',9X,I5,10X,I5,9X,'TIME STEPS',
      $5X,F6.1/4X,'SEDIMENT YIELD',6X,F12.1,3X,F12.1,8X,'POUNDS',8X,
      $F6.1/2X,'SEDIM. DISCHARGE PEAK',5X,F8.1,7X,F8.1,5X,'POUNDS ',
      $'PER SEC',       F9.1/X,'TIME TO SEDIMENT PEAK',7X,I5,10X,I5,
      $9X,'TIME STEPS',5X,F6.1//)
656    FORMAT(///X,'-----------------------------------------',
      $'-----------------------------------'/X,'TIME',3X,'PRECIP'
      $,5X,'NET',6X,'POTENTIAL',9X,'RUNOFF',8X,'SEDIMENT DISCHARGE'/X,
      $ 'STEP',11X,'RAINFALL  INFILTRATION',2X,'------------------'
      $,2X,'-------------------'/40X,'MEASURED  COMPUTED  MEASURED  ',
      $'COMPUTED'/3X,'#',5X,'IN/HR',3X,'IN./HR.',5X,'IN./HR.',7X,
      $'CFS',7X,'CFS',5X,'LBS/SEC',3X,'LBS/SEC'/X,'-----  ------  ',
      $'--------  ------------  --------  --------  --------  --------'
      $/)
657    FORMAT(X,I4,3X,F6.3,3X,F6.3,8X,'-',8X,F7.1,3X,F7.1,
      $3X,F7.1,3X,F7.1)
658    FORMAT(X,I4,3X,F6.3,3X,F6.3,6X,F6.3,5X,F7.1,3X,F7.1,
      $3X,F7.1,3X,F7.1)
659    FORMAT(//8('**********'))
660    FORMAT(///4X,7('**********'),'*'/4X,'*    PLOTS OF HYETOGRAPH(I);',
      $' COMPUTED(C) AND MEASURED(M) HYDROGRAPHS    *'   /4X,
      $7('**********'),'*'//14X,'(Q/QMAX)*100 --->',19X,'<--- PRECIP',
      $'(INCHES/HOUR)'/2X,'TIME'/2X,'STEP',37X,'5      4      3      2',
      $'         1        0'/3X,'#',4X,'0     10     20     30     40     50',
      $'    60     70     80     90    100'/2X,'---- I',10('------I'))
661    FORMAT(2X,I4,2X,71A1)
662    FORMAT(///4X,7('**********'),'*'/4X,'*    PLOTS OF HYETOGRAPH(I);',
      $' COMPUTED(C) AND MEASURED(M)  SEDIGRAPHS   *'   /4X,
      $7('**********'),'*'//14X,'(G/GMAX)*100 --->',19X,'<--- PRECIP',
      $'(INCHES/HOUR)'/2X,'TIME'/2X,'STEP',37X,'5      4      3      2',
      $'         1        0'/3X,'#',4X,'0     10     20     30     40     50',
      $'    60     70     80     90    100'/2X,'---- I',10('------I'))
663    FORMAT(2X,I4,2X,71A1)
       END FILE 6
       STOP
       END
       SUBROUTINE INTCPN
C   THIS SUBROUTINE COMPUTES INTERCEPTION LOSSES AND NET RAINFALL
C   INTENSITY
       COMMON /GEN/ ITMAX,ITCOM,ITPON,DT,DTS
       COMMON /COV/ CND,GCD,HLR,HIR
       COMMON /RAI/ DR(300),RNET(300),QINF(300)
       COMMON /INT/ VOR,VOG,SRG,VIN,EVP,VINT,RAIN
C
```

```
C   INITIALIZING.CUMMULATIVE VALUES AND STORAGE CAPACITIES
      TR1=0.0
      TR2=0.0
      TR3=0.0
      TR4=0.0
      TRC=0.0
      TRG=0.0
      VOC=VOR*VOG
      SRC=VOR*SRG
      CCAP=(1.0-VIN)*VOC
      GCAP=(1.0-VIN)*VOG
C
C   COMPUTING NET RAINFALL FOR EACH TIME INTERVAL
      DO 201 IT=1,ITCOM
C   RATE OF INTERCEPTION ON CANOPY AND THROUGHFALL FROM CANOPY
      TR1=TR1+DR(IT)*DT
      IF(TR1.LE.CCAP) DRC=DR(IT)
      IF(TR1.GT.CCAP) DRC=EVP*SRC
      IF(TR1.GT.CCAP.AND.TRC.LT.CCAP) DRC=(CCAP-TRC)/DT
      TRC=TRC+DRC*DT
      RTHO=DR(IT)-CND*DRC
C   RATE OF INTERCEPTION ON GROUND COVER AND NET RAINFALL RATE
      TR2=TR2+RTHO*DT
      IF(TR2.LE.GCAP) DRG=RTHO
      IF(TR2.GT.GCAP) DRG=EVP*SRG
      IF(TR2.GT.GCAP.AND.TRG.LT.GCAP) DRG=(GCAP-TRG)/DT
      TRG=TRG+DRG*DT
      RNET(IT)=RTHO-GCD*DRG
      TR3=TR3+RNET(IT)*DT
201   CONTINUE
C   TOTAL RAINFALL AND TOTAL INTERCEPTION STORAGE
      RAIN=TR1
      VINT=TR1-TR3
      RETURN
      END
C
      SUBROUTINE INFLTN
C
C   THIS SUBROUTINE COMPUTES THE PONDING TIME AND THE DECAY OF
C   POTENTIAL INFILTRATION FROM THE TIME OF PONDING
C
      COMMON /GEN/ ITMAX,ITCOM,ITPON,DT,DTS
      COMMON /RAI/ DR(300),RNET(300),QINF(300)
      COMMON /INF/ PERM,SORP
C
C   PONDING TIME
      SL=0.0
      ITPON=0
      DO 251 IT=1,ITCOM
      IF(ITPON.GT.0) GO TO 252
      SL=SL+RNET(IT)*DT
      IF(RNET(IT).LE.PERM) GO TO 251
      SR=SORP/(RNET(IT)-PERM)
      IF(SL.LT.SR) GO TO 251
      ITPON=IT
      RP=RNET(IT)
      FP=SL
      AIN=RP
      C=RP-PERM
      C1=C/PERM
```

```
          C2=C/RP
          GO TO 253
C
C  POTENTIAL INFILTRATION, THE DECAY EQUATION IS SOLVED BY NEWTON'S
C    METHOD
252       SATI=PERM*FLOAT(IT-ITPON)*DT
          ITR=0
254       IF(AIN.LE.PERM) GO TO 253
          C3=C2*AIN/(AIN-PERM)
          FF=SATI-FP*((RP-AIN)/(AIN-PERM)-C1*ALOG(C3))
          DFF=FP*C*(1.0-(AIN-PERM)/AIN)/(AIN-PERM)**2.0
          AINN=AIN-FF/DFF
          TOL=ABS((AINN-AIN)/AINN)
          AIN=AINN
          ITR=ITR+1
          IF(ITR.GT.100) GO TO 255
          IF(TOL.GT.0.01) GO TO 254
253       IF(AIN.LE.PERM) AIN=PERM
          QINF(IT)=AIN
251       CONTINUE
          GO TO 256
255       WRITE(6,261)
          STOP
256       RETURN
261       FORMAT(20X,'********** ITERATION EXCEEDS 100 ; INFILTRATION',
         $' EQUATION **********')
          END
C
          SUBROUTINE WROUT
C
C  THIS SUBROUTINE ROUTES WATER FROM OVERLAND AND CHANNEL UNITS.
C  THE ROUTING PROCEDURE IS BASED ON THE CHARACTERISTIC SOLUTION
C  OF THE KINEMATIC WAVE APPROXIMATION
          COMMON /GEN/ ITMAX,ITCOM,ITPON,DT,DTS
          COMMON /COV/ CND,GCD,HLR,HIR
          COMMON /RAI/ DR(300),RNET(300),QINF(300)
          COMMON /FLO/ Q(300,5),ALP,EXP,K,ITYPE,SLN,SLP,CPR,EPR,
         $KOUT,QUP(300),QLAT(300)
          COMMON /SED/ GS(300,5,5),ZL(100),ZD(100,5),GDUP(300,5),
         $GDLAT(300,5),POR(5),CP(5),D50(5),PC(5),VS(5),ERO(300),
         $BEG(100),END(100),ADF,SNU,EMV,HGC,SGC,QE,AP,K1,BRE,APS,ITS,X,
         $XS,XSS,NO,BET,DX,SUBW,SPGR,ACCLN,GAMA,K2,KS,GMAX,NSOIL
C
          EXP1=EXP+1.0
          BET=1.0/EXP
          EXM1=EXP-1.0
          TERM=EXP*ALP*DTS
C
          K1=ITPON
          K2=0
301       IF(K1.GT.ITCOM) GO TO 391
          KS=K1
          ITS=K1
          NO=0
          QB=QUP(K1)
          AB=(QB/ALP)**BET
          QP=QB
          AP=AB
          APS=AP
          DO 381 L=1,NSOIL
```

```
              CP(L)=0.0
381       IF(QP.GT.0.0) CP(L)=GDUP(K1,L)/QP
          QL=QLAT(K1)
          IF(ITYPE.NE.3) GO TO 302
          APF=AP+QL*DTS
          IF(APF.GT.0.0) PERIM=CPR*APF**EPR
          IF(APF.LE.0.0) PERIM=0.0
          QL=QL-PERIM*QINF(K1)/43200.0
302       IF(QL.LE.0.0.AND.QB.EQ.0.0) GO TO 303
          X=0.0
          XSS=0.0
          IF(K2.GT.0) GO TO 304
          AP=0.0
          QP=0.0
          DO 382 L=1,NSOIL
382       CP(L)=0.0
          GO TO 305
304       IF(QB.EQ.0.0) GO TO 305
C  TESTING FOR SHOCK FORMATION
          QA=0.0
          IF(K1.GT.1) QA=QUP(K1-1)
          AA=(QA/ALP)**BET
          IF(AA.GE.AB) GO TO 305
          SHOCK=AB-AA
          ADD=QL*DTS*0.5
          IF(K1.GT.1) ADD=ADD+QLAT(K1-1)*DTS*0.5
          IF(SHOCK.LE.ADD) GO TO 305
C
C  SOLUTION WITH SHOCK
311       IF(K1.GT.ITCOM) GO TO 312
          QL=QLAT(K1)
          IF(ITYPE.NE.3) GO TO 313
          APF=AP+QL*DTS
          IF(APF.GT.0.0) PERIM=CPR*APF**EPR
          IF(APF.LE.0.0) PERIM=0.0
          QL=QL-PERIM*QINF(K1)/43200.0
313       ABF=AB+QL*DTS
          IF(ABF.LE.0.0) ABF=0.0
          IF(ABF.EQ.0.0) GO TO 305
          AAF=AA+QL*DTS
          IF(AAF.LE.0.0) AAF=0.0
          QBF=ALP*ABF**EXP
          QAF=ALP*AAF**EXP
          IF(QL.EQ.0.0) GO TO 314
          DEN=EXP1*(AB-AA)*QL
          PROD=ALP/DEN
          XS=PROD*(ABF**EXP1-AAF**EXP1-AB**EXP1+AA**EXP1)
          GO TO 322
314       XS=(QB-QA)*DTS/(AB-AA)
322       AB=ABF
          AA=AAF
          QB=QBF
          QA=QAF
          X=X+XS
          XSS=XSS+XS
          IF(X.GE.SLN) GO TO 323
C
C  SEDIMENT ROUTING
          QE=ALP*(((QB/ALP)**BET+(QA/ALP)**BET)/2.0)**EXP
          IF(XSS.GT.DX) CALL SROUT
```

```
              QP=QB
              AP=(AA+AB)/2.0
              K1=K1+1
              GO TO 311
       323    QB=QB-QL*(X-SLN)
              QA=QA-QL*(X-SLN)
              QC=ALP*((((QB/ALP)**BET+(QA/ALP)**BET)/2.0)**EXP
              IF(K1.EQ.KC) QC=(QC+Q(KC,KOUT))/2.0
              Q(K1,KOUT)=QC
       C
              QE=Q(K1,KOUT)
              CALL SROUT
              DO 390 L=1,NSOIL
       390    GS(K1,KOUT,L)=CP(L)*QE
              GO TO 324
       C
       C  FLOW CEASES
       C
       303    IF(K2.EQ.0) GO TO 325
              IF(K1.GT.KC) GO TO 326
              GO TO 327
       326    K2=0
       325    Q(K1,KOUT)=0.0
              DO 392 L=1,NSOIL
       392    GS(K1,KOUT,L)=0.0
       327    K1=KS+1
              GO TO 301
       C
       C  SOLUTION WITHOUT SHOCK
       305    IF(K1.GT.ITCOM) GO TO 312
              QL=QLAT(K1)
              IF(ITYPE.NE.3) GO TO 331
              APF=AP+QL*DTS
              IF(APF.GT.0.0) PERIM=CPR*APF**EPR
              IF(APF.LE.0.0) PERIM=0.0
              QL=QL-PERIM*QINF(K1)/43200.0
       331    AC=AP+QL*DTS
              IF(K1.EQ.KS.AND.K2.GT.0) AC=AP+QL*DTS/2.0
              IF(AC.LE.0.0) AC=0.0
              QC=ALP*AC**EXP
              IF(QL.EQ.0.0) GO TO 332
              XS=(QC-QP)/QL
              GO TO 333
       332    XS=TERM*AP**EXM1
       333    X=X+XS
              XSS=XSS+XS
              IF(X.GE.SLN.AND.K2.EQ.0) GO TO 351
              IF(X.GE.SLN) GO TO 334
              IF(K2.GT.0) GO TO 360
       C  INITIAL RISING PART OF HYDROGRAPH
              Q(K1,KOUT)=(QC+QP)/2.0
              QE=Q(K1,KOUT)
              CALL SROUT
              DO 393 L=1,NSOIL
       393    GS(K1,KOUT,L)=CP(L)*QE
              GO TO 362
       360    CONTINUE
       C
       C  SEDIMENT ROUTING
              QE=QC
```

```
         IF(XSS.GT.DX) CALL SROUT
362      QP=QC
         AP=AC
         K1=K1+1
         GO TO 305
334      Q(K1,KOUT)=QC-QL*(X-SLN)
C
         QE=Q(K1,KOUT)
         CALL SROUT
         DO 394 L=1,NSOIL
394      GS(K1,KOUT,L)=CP(L)*QE
C
C  INTERPOLATION OF FLOW AND SEDIMENT DISCHARGES AT THE SEGMENT OUTLET
324      K3=K1-KC
         IF(K3.LE.1) GO TO 351
         QD=Q(K1,KOUT)-Q(KC,KOUT)
         QAD=QD/FLOAT(K3)
         K3M=K3-1
         DO 352 J=1,K3M
         Q(KC+J,KOUT)=Q(KC,KOUT)+QAD*FLOAT(J)
352      CONTINUE
         DO 395 L=1,NSOIL
         GSD=GS(K1,KOUT,L)-GS(KC,KOUT,L)
         GSAD=GSD/FLOAT(K3)
         DO 396 J=1,K3M
396      GS(KC+J,KOUT,L)=GS(KC,KOUT,L)+GSAD*FLOAT(J)
395      CONTINUE
351      KC=K1
         IF(K2.EQ.0) KC=K1-1
         IF(KC.LT.1) KC=1
         K1=KS+1
         IF(K2.EQ.0) K1=KS
         K2=KS
         GO TO 301
C
C  EXTRAPOLATION OF OUTFLOWS AT END OF LAST TIME STEP
312      IF(KC.EQ.ITCOM) GO TO 391
         K3=ITCOM-KC
         QD=Q(KC,KOUT)-Q(KC-1,KOUT)
         QAD=QD/FLOAT(K3)
         DO 353 J=1,K3
         Q(KC+J,KOUT)=Q(KC,KOUT)+QAD*FLOAT(J)
353      CONTINUE
         DO 397 L=1,NSOIL
         GSD=GS(KC,KOUT,L)-GS(KC-1,KOUT,L)
         GSAD=GSD/FLOAT(K3)
         DO 398 J=1,K3
398      GS(KC+J,KOUT,L)=GS(KC,KOUT,L)+GSAD*FLOAT(J)
397      CONTINUE
391      RETURN
         END
C
         SUBROUTINE SROUT
C  THIS SUBROUTINE ROUTES ALL SEDIMENT FRACTIONS
         DIMENSION ADP(5),GLAT(5),CONC(5)
         COMMON /GEN/ ITMAX,ITCOM,ITPON,DT,DTS
         COMMON /COV/ CND,GCD,HLR,HIR
         COMMON /RAI/ DR(300),RNET(300),QINF(300)
         COMMON /FLO/ Q(300,5),ALP,EXP,K,ITYPE,SLN,SLP,CPR,EPR,
        $KOUT,QUP(300),QLAT(300)
```

```
          COMMON /SED/ GS(300,5,5),ZL(100),ZD(100,5),GDUP(300,5),
         $GDLAT(300,5),POR(5),CP(5),DSO(5),PC(5),VS(5),ERO(300),
         $BEG(100),END(100),ADF,SNU,EMV,HGC,SGC,QE,AP,K1,BRE,APS,ITS,X,
         $XS,XSS,NO,BET,DX,SUBW,SPGR,ACCLN,GAMA,K2,KS,GMAX,NSOIL
C
C   SOIL SURFACE ELEVATION AND DETACHED SOIL VOLUME AT THE START OF
C   THE CURRENT TIME STEP
          IF(K2.EQ.0.OR.K2.EQ.KS) GO TO 401
          DO 402 J=1,100
          IF(X.GE.BEG(J).AND.X.LE.END(J)) GO TO 403
          GO TO 402
403       Z=ZL(J)
          DO 490 L=1,NSOIL
490       ADP(L)=ZD(J,L)
          GO TO 480
402       CONTINUE
          GO TO 480
401       IF(K1.EQ.KS) Z=0.0
          IF(K1.GT.KS) Z=ZL(NO)
          DO 496 L=1,NSOIL
          IF(K1.EQ.KS) ADP(L)=0.0
496       IF(K1.GT.KS) ADP(L)=ZD(NO,L)
480       NO=NO+1
          BEG(NO)=X-XSS
          END(NO)=X
C   HYDRAULIC PARAMETERS
          IF(QE.LT.1.0E-5) GO TO 404
          AE=(QE/ALP)**BET
          VEL=QE/AE
          WEP=CPR*AE**EPR
          HYR=AE/WEP
          RN=QE/(SNU*WEP)
C   AVERAGE  LATERAL INFLOW AND POTENTIAL EROSION RATES DURING THE
C   CURRENT TIME STEP
          K4=K1-ITS+1
          DO 491 L=1,NSOIL
          TGLAT=0.0
          DO 405 J=ITS,K1
405       TGLAT=TGLAT+GDLAT(J,L)
491       GLAT(L)=TGLAT/FLOAT(K4)
          TERO=0.0
          DO 406 J=ITS,K1
406       TERO=TERO+ERO(J)
          AERO=TERO/FLOAT(K4)
          DTSS=DTS*FLOAT(K4)
          IF(X.GT.SLN) DTSS=DTS/(1.+(X-SLN)/(SLN-X+XS))
          DIB=BRE*AERO
C   COMPUTE EFFECTIVE TRACTIVE FORCE IN VEGETATED REACHES
          IF(ITYPE.EQ.1.OR.EMV.EQ.0.0) GO TO 408
          IF(Z.GT.EMV) GO TO 409
          RATIO=1.0-Z/EMV
          IF(RATIO.GT.1.0) RATIO=1.0
          EHT=HLR*RATIO
          ESC=SGC*RATIO
          EGC=1.0-HGC-ESC
          IF(HYR.GT.EHT) EGC=1.0-HGC-ESC*EHT/HYR
          GO TO 410
409       EGC=1.0-HGC
          GO TO 410
408       EGC=1.0-GCD
```

```
410      TAO=GAMA*HYR*SLP*EGC
         UST=SQRT(TAO*ACCLN/GAMA)
         DO 499 L=1,NSOIL
C   SEDIMENT CARRYING CAPACITY
         DFT=D50(L)
         DMM=DFT*304.8
         W=VS(L)
         IF(ITYPE.EQ.1)CALL YALIN(UST,DFT,SNU,SUBW,SPGR,ACCLN,VEL,HYR,
        $CEE)
         IF(ITYPE.GT.1.AND.DMM.GE.0.1) CALL YANG(DFT,UST,SNU,VEL,SLP,
        $W,SPGR,CEE)
         IF(ITYPE.GT.1.AND.DMM.LT.0.1) CALL LAURSN(DFT,UST,SPGR,VEL,
        $GAMA,SUBW,SNU,DFT,HYR,ACCLN,W,CEE)
         CONC(L)=CEE*PC(L)/100.0
C   POTENTIAL SEDIMENT EROSION(+VE)/DEPOSITION(-VE)
         GDPL=(AE*CONC(L)-APS*CP(L))/DTSS-GLAT(L)
         BT=W*DTSS/HYR
         IF(GDPL.GT.0.0)GO TO 407
         IF(BT.LT.1.0)GDPL=BT*GDPL
C   DEPTH OF DETACHED SOIL AT THE START OF THE CURRENT TIME STEP
407      ADC=ADP(L)
C   EROSION BY RAINDROP IMPACT
         RATIO=1.0-ADC/GMAX
         IF(RATIO.LE.0.0) RATIO=0.0
         IF(RN.LE.900.0) ADC=ADC+PC(L)/100.0*DIB*RATIO*DTSS
         RAD=ADC-CDPL/WEP*DTSS
C   EROSION BY SURFACE RUNOFF
         IF(RAD.GE.0.0) GO TO 411
         DGD=-ADF*RAD
         GD=WEP*(ADC+DGD)/DTSS
         AS=APS*CP(L)+(GD+GLAT(L))*DTSS
         CONC(L)=AS/AE
         ZD(NO,L)=0.0
         DZ=-DGD
         GO TO 413
C   DETACHED SOIL DEPTH AND SOIL SURFACE ELEVATION AT THE END OF THE
C   CURRENT TIME STEP
411      ZD(NO,L)=RAD
         DZ=(RAD-ADP(L))/EGC
413      ZL(NO)=Z+DZ/POR(L)
412      CP(L)=CONC(L)
499      CONTINUE
         GO TO 497
C   RUNOFF CEASED
404      AE=0.0
         QE=0.0
         DO 498 L=1,NSOIL
498      CP(L)=0.0
497      APS=AE
         ITS=K1+1
         XSS=0.0
         RETURN
         END
C
         SUBROUTINE YALIN(UST,DFT,SNU,SUBW,S,G,VEL,HYR,CEE)
C
C   THIS SUBROUTINE COMPUTES THE TRANSPORT RATE OF NON COHESIVE
C   SEDIMENTS USING THE BEDLOAD FORMULA DEVELOPED BY YALIN(1963)
C
         CALL SHIELD(UST,DFT,SNU,SUBW,TC)
```

```
        Y=UST*UST/((S-1.)*G*DFT)
        YC=TC/(SUBW*DFT)
        IF(Y-YC) 4,4,5
4       CEE=0.0
        GO TO 6
5       SEGMA=Y/YC-1.0
        A=2.45*SQRT(YC)/S**0.4
        X1=0.635*DFT*UST*S*SEGMA
        X2=1.-ALOG(1.+A*SEGMA)/(A*SEGMA)
        CEE=X1*X2/(VEL*HYR)
6       CONTINUE
        RETURN
        END
C
        SUBROUTINE YANG(DFT,UST,SNU,V,SLP,W,S,CEE)
C
C    THIS ROUTINE COMPUTES THE TRANSPORT RATE OF NONCOHESIVE SEDIMENTS
C    USING THE TOTAL LOAD FORMULA DEVELOPED BY YANG(1973)
        D=DFT
        A=UST*D/SNU
        IF(A.GE.70.0) GO TO 7
        VCW=2.5/(ALOG10(A)-0.06)+0.66
        GO TO 8
7       VCW=2.05
8       ESP=V*SLP/W-VCW*SLP
        IF(ESP) 9,9,10
9       CEE=0.0
        GO TO 11
10      F1=5.435-0.286*ALOG10(W*D/SNU)-0.457*ALOG10(UST/W)
        F2=1.799-0.409*ALOG10(W*D/SNU)-0.314*ALOG10(UST/W)
        F3=ALOG10(ESP)
        E=F1+F2*F3
        C=10.0**E
        CEE=C*S/(S-1.)*1.0E-6
11      CONTINUE
        RETURN
        END
C
        SUBROUTINE LAURSN(DFT,UST,S,V,GAMA,SUBW,SNU,DM,Y,G,W,CEE)
C
C    THIS SUBROUTINE USES THE TOTAL-LOAD FORMULA DEVELOPED BY
C    LAURSEN(1958)
        D=DFT
        DP=DM
        CALL SHIELD(UST,DFT,SNU,SUBW,TC)
        UU=ALOG10(UST/W)
        IF(UU.GE.0.40) GO TO 1
        FF=1./(12.32-10.5*EXP(0.047*(UU+2.)))
        GO TO 4
1       IF(UU.GT.1.5) GO TO 2
        FF=2.045*UU+0.942
        GO TO 4
2       IF(UU.GE.2.2) GO TO 3
        FF=3.38+SQRT(1.416-(UU-2.51)**2.)
        GO TO 4
3       FF=0.26*UU+3.953
4       FL=10.0**FF
        TO=((GAMA*V*V)/(G*58.))*(DP/Y)**0.3333333
        IF(TO.LT.TC) GO TO 5
        CEE=0.01*((TO/TC)-1.)*FL*(D/Y)**1.1666666
```

```
      GO TO 6
5     CEE=0.0
6     CONTINUE
      RETURN
      END
C
      SUBROUTINE SHIELD(UST,DFT,SNU,SUBW,TC)
C
C THIS SUBROUTINE COMPUTES THE CRITICAL BED SHEAR STRESS DERIVED
C FROM SHIELDS' FUNCTION
      REY=UST*DFT/SNU
      IF(REY.GT.10.0) GO TO 1
      TC=0.08*SUBW*DFT/REY**0.4
      GO TO 3
1     IF(REY.GT.500.0) GO TO 2
      TC=0.022*SUBW*DFT*REY**0.16
      GO TO 3
2     TC=0.06*SUBW*DFT
3     CONTINUE
      RETURN
      END
C
      SUBROUTINE SETVEL(D,T,S,W)
C
C THIS ROUTINE COMPUTES THE SETTLING VELOCITY OF SEDIMENT PARTICLES OF
C ANY DENSITY. THE ROUTINE ASSUMES A SHAPE FACTOR OF 0.7 AND INTERPOLATES
C THE VALUES TABULATED BY THE SUBCOMMITTEE ON SEDIMENTATION, INTER-
C AGENCY COMMITTEE ON WATER RESOURCES, 1957.
C
      DIMENSION A(6,11),Z(2)
      DATA A(1,1),A(1,2),A(1,3),A(1,4),A(1,5),A(1,6),A(1,7),A(1,8),
     $A(1,9),A(1,10),A(1,11)/
     $0.04,0.06,0.10,0.20,0.40,0.80,1.50,2.00,3.00,7.00,10.00/
      DATA A(2,1),A(2,2),A(2,3),A(2,4),A(2,5),A(2,6),A(2,7),A(2,8),
     $A(2,9),A(2,10),A(2,11)/
     $0.10,0.24,0.60,1.80,4.60,9.50,16.10,19.90,25.30,39.50,44.00/
      DATA A(3,1),A(3,2),A(3,3),A(3,4),A(3,5),A(3,6),A(3,7),A(3,8),
     $A(3,9),A(3,10),A(3,11)/
     $0.14,0.32,0.76,2.20,5.30,10.50,16.90,20.30,25.60,39.50,44.00/
      DATA A(4,1),A(4,2),A(4,3),A(4,4),A(4,5),A(4,6),A(4,7),A(4,8),
     $A(4,9),A(4,10),A(4,11)/
     $0.18,0.40,0.92,2.50,5.80,11.00,17.50,20.70,25.90,39.50,44.00/
      DATA A(5,1),A(5,2),A(5,3),A(5,4),A(5,5),A(5,6),A(5,7),A(5,8),
     $A(5,9),A(5,10),A(5,11)/
     $0.23,0.49,1.10,2.85,6.30,11.60,17.90,21.10,26.20,39.50,44.00/
      DATA A(6,1),A(6,2),A(6,3),A(6,4),A(6,5),A(6,6),A(6,7),A(6,8),
     $A(6,9),A(6,10),A(6,11)/
     $0.29,0.57,1.26,3.20,6.70,12.00,18.10,21.50,26.50,39.50,44.00/
      VSC(T)=1.41E-5 -3.48E-7*(T-10.) +5.00E-9*(T-10.)*(T-15.)
     $        +2.67E-11*(T-10.)*(T-15.)*(T-20.) -4.00E-12*(T-10.)*
     $        (T-15.)*(T-20.)*(T-25.)
C
      IF(D.GE.0.040) GO TO 2
      VISC=VSC(T)
      SS=0.0009669*D*D/VISC
      GO TO 18
C
C INTERPOLATION
2     CONTINUE
      Q=T/10.
```

```
      KT=Q+1.
      PT=Q-KT+1.
      DL=ALOG10(D)
      DO 10 J=1,10
      IF(D.LE.A(1,J)) GO TO 20
10    CONTINUE
20    J=J-1
      C=ALOG10(A(1,J))
      E=ALOG10(A(1,J+1))
      PD=(DL-C)/(E-C)
      DO 50 L=1,2
      I=L+KT
50    Z(L)=(1.-PD)*ALOG10(A(I,J))+PD*ALOG10(A(I,J+1))
      R=(1.-PT)*Z(1)+PT*Z(2)
      SS=10.**R
C  ADJUSTING SETTLING VELOCITY FOR SPECIFIC GRAVITY
18    W=SS*SQRT((S-1.0)/1.65)/30.5
      RETURN
      END
```